AN ANALYSIS OF CERTAIN LOCALIZED NONLINEAR DISPERSIVE WAVES

by

Edward Allen Overman II

A Dissertation Submitted to the Faculty of the

DEPARTMENT OF MATHEMATICS

In Partial Fulfillment of the Requirements
For the Degree of

DOCTOR OF PHILOSOPHY

In the Graduate College

THE UNIVERSITY OF ARIZONA

1 9 7 8

THE UNIVERSITY OF ARIZONA

GRADUATE COLLEGE

I hereby recommend that this dissertation prepared under my direction by Edward Allen Overman II

entitled An Analysis of Certain Localized Nonlinear Dispersive Waves

be accepted as fulfilling the dissertation requirement for the degree of Doctor of Philosophy

David W McLaughlin 7/13/78
Dissertation Director Date

As members of the Final Examination Committee, we certify that we have read this dissertation and agree that it may be presented for final defense.

Frederick A. Hopf	6/14/78
Herman Flaschka	7/13/78
Robert E O'Malley Jr	8/3/78
George H. Hamilton	8/14/78

Final approval and acceptance of this dissertation is contingent on the candidate's adequate performance and defense thereof at the final oral examination.

STATEMENT BY AUTHOR

This dissertation has been submitted in partial fulfillment of requirements for an advanced degree at The University of Arizona and is deposited in the University Library to be made available to borrowers under rules of the Library.

Brief quotations from this dissertation are allowable without special permission, provided that accurate acknowledgment of source is made. Requests for permission for extended quotation from or reproduction of this manuscript in whole or in part may be granted by the head of the major department or the Dean of the Graduate College when in his judgment the proposed use of the material is in the interests of scholarship. In all other instances, however, permission must be obtained from the author.

SIGNED: F O Brennan

To my wife, Linda, who put up with many nights and weekends and months of study and absence:

> Some glory in their birth, some in their skill,
> Some in their wealth, some in their body's force,
> Some in their garments, though newfangled ill,
> Some in their hawks and hounds, some in their horse.
> And every humor hath his adjunct pleasure,
> Wherein it finds a joy above the rest.
> But these particulars are not my measure,
> All these I better in one general best.
> Thy love is better than high birth to me,
> Richer than wealth, prouder than garments' cost,
> Of more delight than hawks or horses be.
> And having thee, of all men's pride I boast,
> Wretched in this alone, that thou mayst take
> All this away and me most wretched make.
>
> --Shakespeare, Sonnet 91

ACKNOWLEDGMENTS

I am grateful to my advisor, Professor David W. McLaughlin, for the time and assistance he has proveided me over the past few years. In particular I am indebted for his help in finding a thesis topic and also in obtaining financial support for me through the Army Research Office (Durham), grant DAAG29-78-G0059.

Also my thanks go out to Professor Frederic A. Hopf with whom I worked closely on this thesis topic. His patience and encouragement will not be forgotten.

Professor Warren E. Ferguson, Jr., has always been willing to spend time to help a novice learn the hows, whats, and whys of computer programming and numerical methods. He is a dedicated teacher and has been of invaluable assistance in furthering my development in this field. I know that I also speak for many others.

Two other professors, in particular, Hermann Flaschka and George L. Lamb, Jr., have always been willing to provide assistance (and, occasionally, answers).

Also a former roommate, Dr. Gerald Moore, read parts of this thesis and made helpful suggestions.

Finally, Mrs. Sarah Oordt has spent many late nights and early mornings typing this thesis. I apologize for the fact that terms and formulae which are clear to me can be unintelligible to everyone else.

TABLE OF CONTENTS

TABLE OF CONTENTS--Continued

LIST OF ILLUSTRATIONS

LIST OF ILLUSTRATIONS--Continued

ABSTRACT

Fluctuations in coherent steady-state pulses are investigated, theoretically, in the superradiant regime of a swept-gain laser amplifier. Spontaneous emission is modelled by letting the initial polarization be a complex stochastic variable. Energy fluctuations are found in the steady-state region. These fluctuations differ from peak power fluctuations in a laser oscillator in four ways:

(1) these energy fluctuations are macroscopic (∿10% of the classical value);

(2) they are unidirectional in that energies lower than the semiclassical value are always involved;

(3) they are episodic in character and clearly different from "random walk" processes about a classical mean;

(4) they are largely independent of the magnitude of the initial polarization.

It is shown, analytically as well as numerically, that these energy fluctuations arise from fluctuations in the phase of the initial polarization. An energy distribution is also derived, which is predicted to be observed in the output of this laser. It is also shown that these

fluctuations are fundamentally different from the macroscopic fluctuations in Dicke superradiance, which have been reported previously by Bonifacio, Schwendimann, and Haake and also by Degiorgio.

CHAPTER 1

INTRODUCTION

In this dissertation we investigate, theoretically, fluctuations in coherent steady-state pulses in the superradiant regime of a swept-gain laser amplifier. The mathematical model to be studied is the Maxwell-Bloch equations

$$\frac{\partial}{\partial \mu}\mathcal{P} = \mathcal{E} n - \frac{1}{T_2}\mathcal{P}$$

$$\frac{\partial}{\partial \mu} n = - \mathrm{Re}(\mathcal{E}\mathcal{P}^*) - \frac{1}{T_1} n \qquad \mu \geq 0, \qquad z \geq 0$$

$$\frac{\partial}{\partial z}\mathcal{E} = \alpha' \mathcal{P} - \kappa \mathcal{E} .$$

Here $\mathcal{P}$ is the complex amplitude of the atomic polarization, $\mathcal{E}$ is the complex amplitude of the envelope of the incident electric field, and n is the population inversion. T_1 is the decay time for the electrons to drop to other energy levels, and T_2 is the decay time for the atoms to depolarize. z is the distance into the amplifier and $\mu = t - z/c$ is the retarded time, where t is the time and c is the speed of light in the amplifier. The boundary conditions are $\mathcal{E}(\mu, z = 0)$, $\mu \geq 0$ and $\mathcal{P}(\mu = 0, z)$, $n(\mu = 0, z)$, $z \geq 0$.

Here, we set $T_1 = \infty$ so we are in the superradiant regime, $\mathscr{E}(\mu,0) = 0$ so that the pulse builds up from spontaneous emission, and $n(0,z) = +1$ since initially all the electrons are in the excited state. We model spontaneous emission by letting $\mathscr{P}(0,z)$ be a complex stochastic variable.

We find energy fluctuations in the steady-state region which differ from peak power fluctuations in a laser oscillator in four ways:

(1) these energy fluctuations are macroscopic;

(2) they are unidirectional;

(3) they are episodic;

(4) they are largely independent of the magnitude of the initial polarization.

We show, analytically as well as numerically, that these energy fluctuations arise from fluctuations in the phase of $\mathscr{P}(0,z)$. We also derive an energy distribution that we predict would be observed in the output of this laser.

We begin, in Chapter 2, with a brief introduction designed for the reader unfamiliar with the basic facts about lasers. In Chapter 3 we describe the steady-state pulses which arise in this amplifier. Having introduced the necessary background information, Chapter 4 describes the problem at hand. Then, in Chapter 5, we present our

numerical data to provide the intuitive understanding for the analysis to follow. In Chapter 6 we discuss, analytically, the physical process which causes these energy fluctuations. In Chapter 7 we discuss, analytically, the stochastics, including the energy distribution which we predict would be observed experimentally in the output of a real laser amplifier. Finally, in Chapter 8 we summarize our results.

CHAPTER 2

INTRODUCTION TO COHERENT RADIATION AND RESONANT MEDIA

This introduction is designed to provide some general background material on lasers. The first half will describe the physical behavior of a laser from a semiclassical point of view, and the second half will introduce the mathematical equations for the particular model which we will study in the remainder of this dissertation.

Physical Preliminaries

To begin, we review some basic facts about light. When an electron, which is in an excited state of an atom, drops into a lower energy state, electromagnetic radiation (a photon) is created. This radiation travels away from the atom at the speed of light, c, which in free space is 3×10^{10} cm/sec. The energy given up by the atom in this decay process, $\mathscr{T}_e$, and the angular frequency of the emitted radiation, ω, are related by $\mathscr{T}_e = \hbar\omega$ where $\hbar$, Planck's constant, is 1.05×10^{-27} gram cm^2/sec. In a typical laser the frequency of the radiation is $\sim 4 \times 10^{15}$ sec^{-1} with a wavelength, $\lambda = 2\pi c/\omega$, of $\sim 5 \times 10^{-5}$ cm, which is visible light. The lifetime for this electron transition is defined

as the time it would take, in a large sample, for a fraction $1 - 1/e$, $\sim.63$, of the sample to emit photons by this transition. The length of the light pulse (a photon wave packet) is proportional to this lifetime. In a typical laser the length of a photon wave packet is $\sim 10^2$ cm. Such a pulse of radiation passes a fixed point in $\sim 10^{-8}$ sec. With these numbers one can show that laser radiation can be considered as monochromatic (of a single frequency) even though the pulse actually consists of a range of frequencies. To verify this assertion, use the Heisenberg uncertainty principle $\Delta z \Delta\omega \sim c$, where Δz is the length of the pulse and $\Delta\omega$ is its frequency range. With the numbers given above, $\Delta\omega \sim 10^8$ sec^{-1} which is certainly negligable compared to $\omega \sim 4 \times 10^{15}$ sec^{-1}. (In fact, the actual value of $\Delta\omega$ in a laser is orders of magnitude less than this. The value given here is more appropriate to electron decay through spontaneous emission which is defined below.)

Normally, when a burst of light is created by a large number of atoms decaying in this way, most of the atoms emit photons spontaneously (i.e., independently of the photons being created by other atoms in the system). The photons created by this process, called <u>spontaneous emission</u>, travel away from the system in all directions. Since the photons are created independently, their phases are independent and,

when many photons are averaged to obtain light on a macroscopic scale, no phase structure remains. However, there is another process which creates unidirectional, coherent (of the same wavelength and phase) light. This process is called stimulated emission.

For simplicity, let us consider an idealistic two-level atom, that is, an atom with only one electron which can be either of two energy levels, a or b. Let the energies of these two states be $\mathscr{T}_a$ and $\mathscr{T}_b$ with $\mathscr{T}_a > \mathscr{T}_b$. Let the electron be in the lower energy state, state b, and let a beam of light pass by with frequency $(\mathscr{T}_a - \mathscr{T}_b)/\hbar$, which is the frequency difference between the two states. Then there is a certain probability that a photon in the light beam will be absorbed by the atom and excite the electron to state a. This process is called stimulated absorption. Conversely, once this electron is in the excited state, there is a certain probability that a photon will cause the electron to drop back into the lower level and emit another photon of the same frequency, $(\mathscr{T}_a - \mathscr{T}_b)/\hbar$. This process is called stimulated emission The newly created photon has the remarkable property (because of the resonant process of its creation) that it travels in the same direction and with the same phase as the incident photon.

Although classical mechanics is unable to completely explain either of these two stimulated processes, there are special circumstances under which it can give comparable results. For example, in Sargent, Scully, and Lamb (1974), it is shown that a monochromatic plane wave which impinges upon an infinite sheet of classical oscillators (charges fixed in position by springs) will cause similar processes. This occurs because the incident plane wave sets up oscillations in the sheet which are 90° out of phase with the plane wave; in turn the oscillating charges in the sheet set up their own electric field, which, for large distances from the sheet, is 90° out of phase with the sheet. Thus the resulting electric field is either in phase with or 180° out of phase with the incident plane wave. In this classical model, stimulated absorption results when the electric field which has been created by the oscillating charges is 180° out of phase with the incident plane wave, for then we have destructive interference between the incident and created fields and energy has been lost to the oscillators. However, if the two electric fields are in phase we have stimulated emission since the energy is being resonantly returned to the plane wave.

To obtain coherent radiation, it is necessary that stimulated emission dominate stimulated absorption. Since

the probabilities for the two processes are equal, this means that more electrons must be in the excited state than in the lower state. Thus in a laser atoms are excited (pumped) to the upper energy level and photons are created by spontaneous emission. Initially most of these photons travel out the sides of the medium and their energy is lost. However a few travel down the medium creating more photons with the same frequency and phase by stimulated emission and so causing still more stimulated emission. This cascade effect continues and greatly increases the intensity of the beam. (For example, in a ruby laser a light pulse can be produced with a peak power (energy per unit time) of 10^9 watts which contains $\sim 10^{18}$ photons and which passes a fixed point in $\sim 10^{-7}$ sec.) As the electrons drop into the lower level, the probability for stimulated absorption increases and becomes important. This is detrimental to the laser pulse because some of the pulse energy is used to reexcite the electrons and thus return energy to the medium. Generally lasers avoid this problem by continually reexciting electrons by methods which do not interfere with the pulse itself.

In this dissertation, we are concerned with particular lasers where the halflife for spontaneous emission is very short. (One example is a laser with its electron transition in the far ultra-violet region, i.e., $\lambda \sim 10^{-8}$ to

10^{-7} cm.) If all the electrons in the medium were excited at the same time, most would have decayed to the lower state by spontaneous emission long before the pulse arrived; then, by stimulated absorption, the pulse would die out. To avoid this difficulty, the electrons in the medium are excited at the speed of light in the medium so that the pulse always sees excited atoms directly in front of it. This process, called swept-gain excitation, can be caused by a second laser which sweeps its beam along the side of the medium at the speed of light and causes the excitation of the medium.

Before introducing the mathematical model, let us discuss in more detail the resonant interaction of a single atom with an electromagnetic field. The electron in a two-level atom has a certain probability density to be at any point in the atom. In the absence of outside forces, this probability density is symmetric about the nucleus, and so, on the average, the negative charge is at the nucleus. However, in an external electric field, the probability density will no longer be at the nucleus. This charge asymmetry makes the atom into a small dipole which generates an electric field, which in turn reacts back on the initial electric field. A dipole is described by a vector quantity, called a dipole moment, whose magnitude is the charge of the electron times the effective distance between the center of

the electron charge and the nucleus and whose direction is from the negative to the positive charge. The polarization, $\bar{p}$, is defined as the net dipole moment per unit volume.

Thus, the physical model of a laser involves a resonant interaction between the incident radiation and the atoms in the medium. The atoms are initially excited. Then, from the quantum mechanical viewpoint, the incident pulse causes stimulated emission of photons which travel in the same direction and in phase with the incident pulse. Classically, we say that the incident radiation stimulates the excited atoms to emit radiation which constructively adds to the incident radiation. In either model a cascade effect occurs so that the output of the laser is an intense, coherent, unidirectional pulse. In the next section we model these points mathematically. We close with a schematic, Figure 2.1, of the swept-gain laser.

Mathematical Model

The semiclassical description of a laser can be found in many sources including Allen and Eberly (1975) and Icsevgi and Lamb (1969). The results are summarized here.

In the semiclassical model, we treat the electromagnetic field classically and obtain the equation governing the interaction between the field and the atoms, called the Maxwell wave equation,

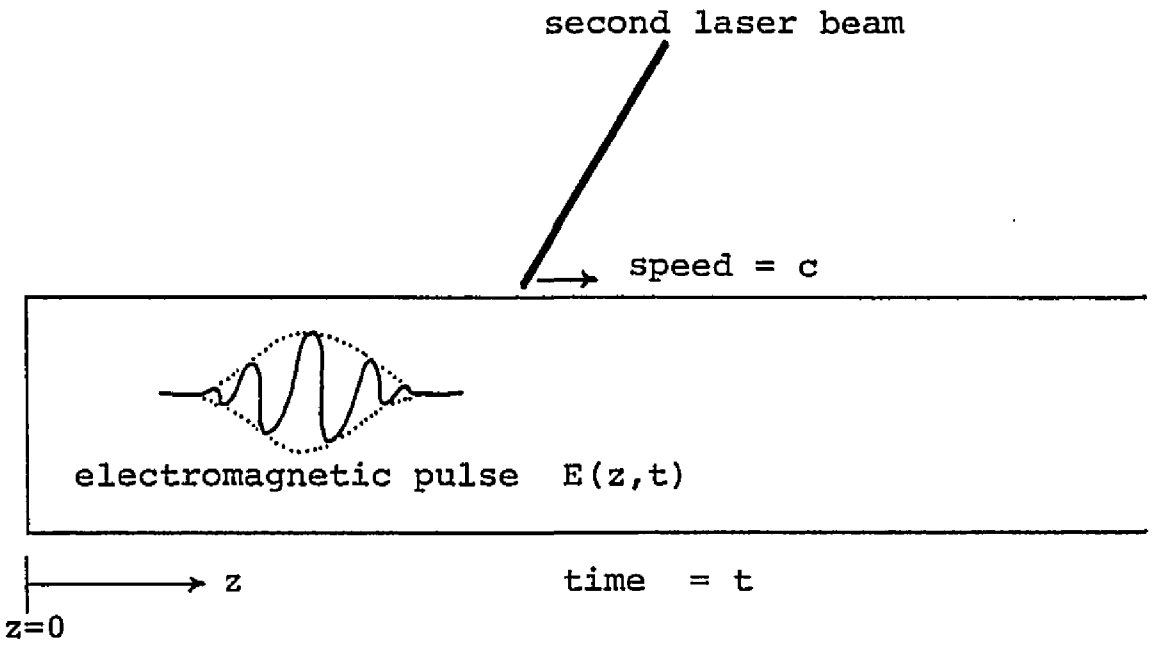

Figure 2.1. Schematic of the swept-gain laser.

$$\left(\frac{\partial^2}{\partial z^2} - \frac{1}{c^2}\frac{\partial^2}{\partial t^2}\right)E = \frac{4\pi}{c^2}\frac{\partial^2}{\partial t^2}p. \tag{2.1}$$

Here $E(z,t)$ denotes the electromagnetic field and $p(z,t)$ the macroscopic polarization.

The dynamics of a two-level atom are treated quantum mechanically by a two-component Schroedinger equation

$$i\frac{\partial}{\partial t}\begin{pmatrix}\alpha\\ \beta\end{pmatrix} = \frac{1}{2}\begin{pmatrix}\omega & -qE\\ -qE & -\omega\end{pmatrix}\begin{pmatrix}\alpha\\ \beta\end{pmatrix}. \tag{2.2}$$

Here ω is the frequency difference between the two energy levels, $\alpha(z,t,\omega)$ and $\beta(z,t,\omega)$ denote the probability

amplitudes for the upper and lower states respectively, and q is a parameter describing the strength of the dipole. To describe the polarization of a two-level atom, P_a, in terms of α and β, we introduce new variables

$$T = |\alpha|^2 + |\beta|^2 \qquad n = |\alpha|^2 - |\beta|^2$$
$$P_+ = \alpha\beta^* + \alpha^*\beta \qquad P_- = i(\alpha\beta^* - \alpha^*\beta). \tag{2.3}$$

Then $P_a = qP_+$. In terms of these variables equation (2.2) becomes

$$\frac{\partial}{\partial t}T = 0$$
$$\frac{\partial}{\partial t}n = -qEP_-$$
$$\frac{\partial}{\partial t}P_+ = -\omega P_- \tag{2.4}$$
$$\frac{\partial}{\partial t}P_- = \omega P_+ + qEn,$$

which are called the Bloch equations.

The variable $T = |\alpha|^2 + |\beta|^2$ is the probability that the electron is in one of the two energy states and is initially one. From equation (2.4a) we see that T remains

one, so that the electron remains for all time in our two-level system. The variable $n = |\alpha|^2 - |\beta|^2$ is the population difference between the upper and lower states. Thus $n = +1$ if the electron is in the excited state and $n = -1$ if it is in the lower state. The variables P_+ and P_- are polarization variables.

To relate the classical part of the model, equation (2.1), (the macroscopic part) to the quantum mechanical part, equation (2.4), (the microscopic part) we need a map which converts the microscopic polarizations, P_a, of many atoms to a macroscopic polarization, p. We denote this map by $\langle \cdot \rangle$ so

$$p(z,t) = \langle P_a(z,t,\omega) \rangle .$$

Typically, this mapping process can include many physical effects. For example, the atoms can have slightly different transition frequencies due to effects such as collisions. It is common to include this frequency spread in the definition of the micro to macro map. However, for our purposes here it is sufficient to assume that all the atoms have the same transition frequency as the frequency of the pulse and to let the mapping be simply given by

$$p(z,t) = \langle P_a(z,t,\omega) \rangle = n_0 P_a(z,t,\omega_0) \qquad (2.5)$$

where n_0 is the density of atoms in the medium. Equations (2.1) and (2.4), together with the definition (2.5) of the micro to macro map, constitute an idealized model of the system.

We now simplify these equations. First, we introduce the monochromatic nature of the pulse by setting

$$E(z,t) = \tilde{\mathcal{E}}(z,t)\cos(k_0 z - \omega_0 t + \phi(x,t))$$

where the pulse envelope, $\tilde{\mathcal{E}}$, and the phase function, ϕ, vary slowly on the length and time scales of the system, i.e.,

$$\frac{\partial \tilde{\mathcal{E}}}{\partial z} << k_0 \tilde{\mathcal{E}}, \qquad \frac{\partial \tilde{\mathcal{E}}}{\partial t} << \omega_0 \tilde{\mathcal{E}}$$

with similar equations for ϕ. Second, we introduce this same monochromatic nature into the polarization by a similar ansatz:

$$P_+(z,t) = u(z,t)\sin(k_0 z - \omega_0 t + \phi(z,t))$$

$$+ v(z,t)\cos(k_0 z - \omega_0 t + \phi(z,t)).$$

Again, the envelopes u and v are to be slowly varying. Finally, we introduce the complex amplitudes

$$\mathcal{E}(z,t) = \mathcal{E}(z,t)e^{i\phi(z,t)},$$

$$\mathcal{P}(z,t) = (u(z,t) + iv(z,t))e^{i\phi(z,t)}.$$

Then our equations become, with the inclusion of the slowly varying envelope approximation (α' is a positive constant),

$$\frac{\partial}{\partial t}\mathcal{P} = \mathcal{E}n$$

$$\frac{\partial}{\partial t}n = -\mathrm{Re}(\mathcal{E}\mathcal{P}^*) \qquad (2.6)$$

$$\left(\frac{\partial}{\partial z} + \frac{1}{c}\frac{\partial}{\partial t}\right)\mathcal{E} = \alpha'\mathcal{P}.$$

This model is quite accurate once decays are included. There is a decay process, with lifetime T_1, which describes the electron decay by, among other processes, spontaneous emission (from the excited state to the lower state as well as from both states to other states which we are not considering) and which enters in equation (2.6b) for $\frac{\partial n}{\partial t}$. A second decay process, with lifetime T_2, describes the randomization of the phases of the individual atoms. This randomization causes interference between the electric fields

created by the polarizations and so decreases the energy available to the pulse. It enters in equation (2.6a) for $\frac{\partial \mathscr{P}}{\partial t}$. Finally, the pulse itself would decay away, on a length scale of $1/\kappa$, due to nonresonant losses (such as radiation leaking out the sides of the medium and also into other modes of radiation). This enters in equation (2.6c). In this phenomenological manner, we introduce these decay processes to obtain the coupled system

$$\frac{\partial}{\partial t}\mathscr{P} = \mathscr{E} n - \frac{1}{T_2}\mathscr{P}$$

$$\frac{\partial}{\partial t} n = -\mathrm{Re}(\mathscr{E}\mathscr{P}^*) - \frac{1}{T_1} n \qquad (2.7)$$

$$\left(\frac{\partial}{\partial z} + \frac{1}{c}\frac{\partial}{\partial t}\right)\mathscr{E} = \alpha'\mathscr{P} - \kappa\mathscr{E}$$

This system is called the Maxwell-Bloch equations.

It is natural to introduce a retarded time, μ, where $\mu = t - z/c$, in equation (2.7) both because of the particular form of the derivatives in equation (2.7c) and because our swept-gain excitation causes the "sweep" to arrive at the point z at the time $t = cz$ (i.e., at $\mu = 0$). Then we obtain

$$\frac{\partial}{\partial \mu}\mathcal{P} = \mathcal{E} n - \frac{1}{T_2}\mathcal{P}$$

$$\frac{\partial}{\partial \mu} n = -\mathrm{Re}(\mathcal{E}\mathcal{P}^*) - \frac{1}{T_1} n \qquad (2.8)$$

$$\frac{\partial}{\partial z}\mathcal{E} = \alpha'\mathcal{P} - \kappa\mathcal{E}$$

where our boundary conditions are $\mathcal{E}(\mu, z = 0)$, $\mathcal{P}(\mu = 0, z)$, and $n(\mu = 0, z)$. All of the atoms are excited by the "sweep" at $\mu = t - z/c = 0$; thus, $n(0,z) \equiv +1$. Since the pulse will be formed by spontaneous emission, we assume no pulse is sent into the medium; thus $\mathcal{E}(\mu, 0) \equiv 0$. The boundary condition on the polarization $\mathcal{P}(0,z)$ is more complicated and will be discussed in some detail at the end of the next chapter. These boundary conditions are shown in Figure 2.2.

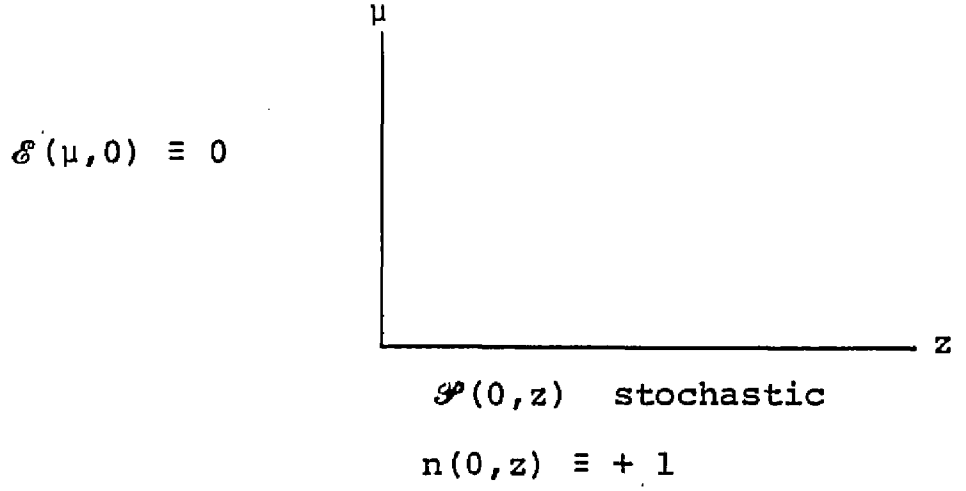

Figure 2.2. Boundary conditions for the Maxwell-Bloch equations, equations (2.8).

CHAPTER 3

STEADY-STATE PULSES

To better understand the Maxwell-Bloch equations, we first rescale equation (2.8) to depend on a single parameter. Then we discuss the travelling waves, or steady-state pulses (SSPs), which arise from the reduced equations. And finally we discuss the boundary condition $\mathcal{P}(0,z)$.

If we rescale the variables in equation (2.8) to be μ/T_2, κz, and $T_2\mathcal{E}$, we obtain

$$\frac{\partial}{\partial(\mu/T_2)}\mathcal{P} = (T_2\mathcal{E})n - \mathcal{P}$$

$$\frac{\partial}{\partial(\mu/T_2)}n = -\mathrm{Re}((T_2\mathcal{E})\mathcal{P}^*) - \frac{T_2}{T_1}n \qquad (3.1)$$

$$\frac{\partial}{\partial(\kappa z)}(T_2\mathcal{E}) = \frac{\alpha' T_2}{\kappa}\mathcal{P} - (T_2\mathcal{E}).$$

For this dissertation we neglect the term $\frac{T_2}{T_1}n$ in equation (3.1b) by setting $T_1 = \infty$. The rationale for this will be discussed later in this chapter. Then the only parameter in the equations is $\alpha' T_2/\kappa$, which is the ratio of the gain to the loss and must be greater than one for the amplification process to dominate. This rescaling shows that, without

loss of generality, we can simplify equation (3.1) by setting $\kappa = T_2 = 1$. Then our equations become

$$\frac{\partial}{\partial \mu} \mathscr{P} = \mathscr{E} n - \mathscr{P}$$

$$\frac{\partial}{\partial \mu} n = -\mathrm{Re}(\mathscr{E}\mathscr{P}^*) \tag{3.2}$$

$$\frac{\partial}{\partial z} \mathscr{E} = \alpha' \mathscr{P} - \mathscr{E} \ .$$

These are the equations to be studied henceforth.

We begin this study by discussing the steady-state pulses (SSPs) which arise as $z \to \infty$ and we follow the discussion in Arecchi and Bonifacio (1965). To see that SSPs are indeed formed in this limit, we concentrate on equation (3.2c), which can be integrated to give

$$\mathscr{E}(\mu,z) = e^{-z}\, \mathscr{E}(\mu,0) + \alpha' e^{-z} \int_0^z e^{x}\, \mathscr{P}(\mu,x)\, dx. \tag{3.3}$$

We assume that

$$\left| \int_0^z e^{x}\, \mathscr{P}(\mu,x)\, dx \right| \to \infty \quad \text{as} \quad z \to \infty. \tag{3.4}$$

Then

$$\lim_{z\to\infty} \mathcal{E}(\mu,z) = \lim_{z\to\infty} \alpha' e^{-z}\int_0^z e^{x}\, \mathcal{P}(\mu,x)dx = \alpha'\, \mathcal{P}(\mu,z) \qquad (3.5)$$

by L'Hospital's rule. Thus

$$\frac{\partial}{\partial z}\, \mathcal{E}(\mu,z) \to 0 \quad \text{as} \quad z \to \infty \quad \text{for all} \quad \mu \geq 0$$

and so z-independent SSPs form.

To obtain an analytical expression for these SSPs, set $\frac{\partial \mathcal{E}}{\partial z} = 0$ in equation (3.2c) so that $\mathcal{E} = \alpha'\mathcal{P}$. Substitute this into equations (3.2a) and (3.2b) and solve these equations with boundary conditions

$$n(0,z) = +1$$

$$\mathcal{P}_o(z) \equiv \mathcal{P}(0,z) = \mathcal{P}_o = |\mathcal{P}_o| \exp(i\theta_{\mathcal{P}_o})$$

to obtain

$$n = \frac{1}{\alpha'} - \varepsilon \tanh\left(\frac{\mu-\tau_d}{\tau_p}\right)$$

$$\mathcal{P} = \varepsilon \exp(i\theta_{\mathcal{P}_o})\, \mathrm{sech}\left(\frac{\mu-\tau_d}{\tau_p}\right) \qquad (3.6)$$

$$\mathcal{E} = \frac{1}{\tau_p} \exp(i\theta_{\mathcal{P}_o})\, \mathrm{sech}\left(\frac{\mu-\tau_d}{\tau_p}\right)$$

where

$$\varepsilon = \sqrt{(1 - \frac{1}{\alpha'})^2 + |\mathscr{P}_o|^2},$$

$$\tau_p = \frac{1}{\alpha'\varepsilon}, \qquad \tau_d = \frac{1}{2}\tau_p \ell n\left(\frac{1+(\alpha'-1)\tau_p}{1-(\alpha'-1)\tau_p}\right).$$

(Notice that our assumption, equation (3.4), is consistent with this SSP.) In this dissertation we always take $|\mathscr{P}_o| \sim 10^{-8}$ to 10^{-4} so $\alpha' - 1 >> |\mathscr{P}_o|$ and so the parameters reduce to

$$\tau_p \sim \frac{1}{\alpha'-1}, \qquad \tau_d \sim \tau_p \ell n\left(2\frac{1-1/\alpha'}{|\mathscr{P}_o|}\right) \tag{3.7}$$

This SSP is graphed in Figure 3.1.

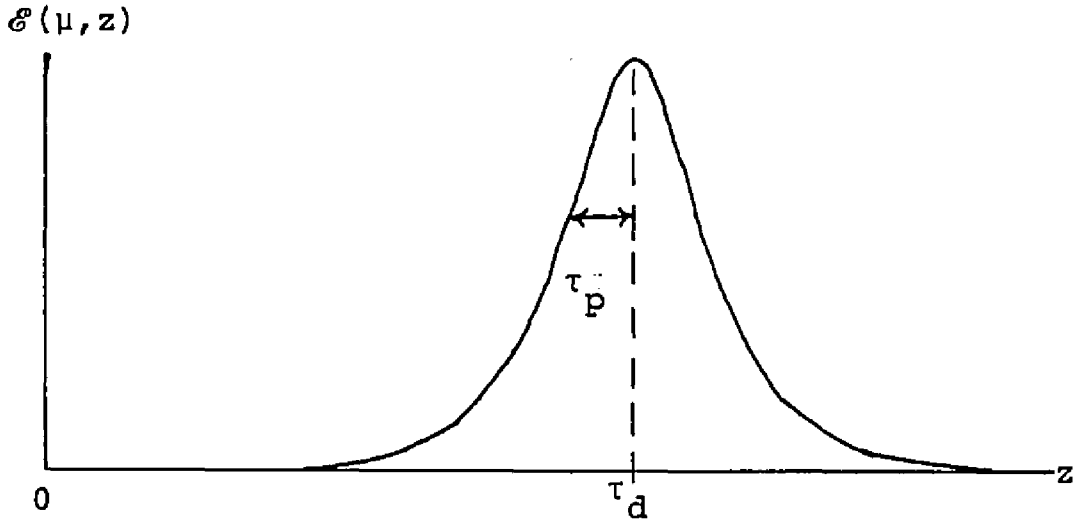

Figure 3.1. A steady-state pulse.

Let us clarify one feature of this SSP which is unusual. Normally SSPs are functions of distance and are independent of time. Here, however, we have SSP which is a function of time and independent of position. Thus, at any point in the laser, z, we graph in Figure 3.1 the SSP shape as a function of the retarded time, $\mu = t - z/c$ (so that the swept-gain excitation arrives at the time of zero). For example, τ_d is the time difference, at a fixed point, between seeing the "sweep" and seeing the peak of the SSP.

The quantity which we will most often use to describe the pulse is its energy, $\mathcal{T}$, which is defined as[1]

$$\mathcal{T}(z) = \int_0^\infty |\mathcal{E}(\mu,z)|^2 d\mu. \tag{3.8}$$

For the SSP the energy is

$$\mathcal{T}_{sc} \sim 2(\alpha' - 1). \tag{3.9}$$

(The subscript "sc" stands for "semiclassical".)

Notice that the SSP which arises in our equations is a power-balance solution. That is, the pulse is losing energy due to nonresonant losses (the κ term in the Maxwell-Bloch equations) and gaining energy from the medium.

---

[1]We absorb the ratio of dipole matrix element over $\hbar$ into the definition of $\mathcal{E}$. The field has dimensions of frequency and $\mathcal{P}$ and n are dimensionless. Energies and powers have dimensions of frequency and frequency squared, respectively.

When these two energies balance the SSP forms. The shape of the SSP, determined by τ_p, depends only on the gain, α', (see equation (3.7)) which is fixed by the Maxwell-Bloch equations, that is, by the physical system itself. The center of the pulse, determined by τ_d, on the other hand, is fixed by the boundary conditions and not by the system itself. Thus the location is the only "free" parameter in the problem.

Now let us return to our discussion of T_1 in equation (3.1). Recall that we set $T_1 = \infty$ and thus neglected the decay of the electrons from the excited state. The purpose of this paragraph is to describe the physical problem of interest in this dissertation and show that neglecting this decay is appropriate. We are interested in the superradiant regime of the laser, that is, where the maximum height of the SSP is approximately proportional to the gain[1] α', the width to $1/\alpha'$, and thus the peak power (energy per unit time) to $(\alpha')^2$ and the energy to α'. (Normally in a laser the pulse width is independent of α' and the peak power and energy are approximately proportional to α'.) Thus, in the superradiant regime, the pulse width can be much shortened and the peak power greatly increased by increasing the gain. Since T_1 is the lifetime for the electrons to

---

[1] To be precise the gain referred to here is the small-signal gain and not the saturated gain.

be in the excited state, we want the center and width of the pulse, τ_d and τ_p respectively, to be much less than T_1 so that all of the energy given to the atoms by the "sweep" will be available to create and amplify the pulse and cause superradiance. There are two ranges of parameters which will satisfy this criterion (i.e., τ_d, $\tau_p << T_1$). The first is to fix T_1 and T_2 and pick α' large enough (since τ_d, $\tau_p \to 0$ as $\alpha' \to \infty$). The second is to fix α' and T_2 and let T_1 be large enough. We choose the second range and let $T_1 = \infty$ but we note that this approximation also gives the correct answer in the first range (Bonifacio, Hopf, Meystre, and Scully 1975).

To close this chapter, we describe various choices of the boundary condition of the polarization $\mathscr{P}(0,z) \equiv \mathscr{P}_o(z)$. Quantum mechanical fluctuations in spontaneous emission enter the Maxwell-Bloch equations only through $\mathscr{P}_o(z)$. The classical approach ignores such fluctuations, and sets $\mathscr{P}_o(z) \equiv 0$, in which case no photons will be created to start stimulated emission; hence, no pulse will form. Still worse, even if an incident pulse is sent into the medium (i.e., $\mathscr{E}(\mu,0) \neq 0$), it will eventually disappear. The semiclassical method of handling spontaneous emission is by setting $\mathscr{P}_o(z)$ equal to a non-zero constant as we have done in this chapter. This is why we used

the term "semiclassical" for the energy of the SSP, equation (3.9). Finally, we can quantum mechanically model the random nature of spontaneous emission by letting $\mathcal{P}_o(z)$ be a stochastic variable. Of course in this case there is no SSP since condition (3.4) for their existence is violated.

This concludes our general background discussion of lasers and the Maxwell-Bloch equations. In this dissertation we model spontaneous emission in the superradiant regime quantum mechanically by letting $\mathcal{P}_o(z)$ be stochastic. Our problem is to understand how this stochastic nature of the boundary condition affects the behavior of the steady-state (i.e., the power-balance) pulse.

CHAPTER 4

ENERGY AND POWER FLUCTUATIONS

In this chapter we summarize the results of our study of the behavior of steady-state (i.e., power-balance) pulses in the superradiant regime of a swept-gain laser amplifier, modelling spontaneous emission by a stochastic $\mathscr{P}_o(z)$. In order to visualize the actual behavior of the SSPs,[1] we open with the original computer simulation which shows large-scale fluctuations in the SSPs. To underscore the unusual behavior of these fluctuations, we contrast them to fluctuations observed in other laser models. Finally, we discuss the physical origin of our fluctuations in the Maxwell-Bloch equations to bring out the causes of their unusual behavior. This discussion of the physical origin can be read either as presenting the physical reasons for the fluctuations or as presenting, intuitively, the nature of the fluctuations in preparation for the analysis to follow. With either viewpoint, the mathematical analysis which corroborates our claims is presented in the next two chapters.

---

[1] In the stochastic case, we use the term "SSP" to denote power-balance pulses whose shapes are slowly varying.

History of SSPs

Before beginning our study of SSP behavior, we summarize some historical background material on SSPs that we refer to in this dissertation. Coherent pulse amplification in an inverted laser medium, as discussed in Chapters 2 and 3, was first studied analytically by Arecchi and Bonifacio (1965), who discovered the SSP solution (see also Armstrong and Courtens 1968 and 1969) for the case of a homogeneously broadened (T_1 and T_2 finite) amplifier with a linear loss ($\kappa > 0$). Subsequently, a number of authors extended this analysis to cover inhomogeneous broadening (i.e., to cover that case in which the atoms have a range of transition frequencies centered around the frequency of the pulse) (Hopf 1968) and lossless ($\kappa = 0$) operation (Hopf and Scully 1969). All these treatments were semiclassical in that the input pulse was taken to be a classical field. In the latter two papers, spontaneous emission was neglected ($\mathcal{P}_o(z) \equiv 0$). Recall from the last chapter that in this case the pulse will eventually disappear; however, this decay is rather slow and the pulse still can be studied numerically for a long time. The coherent pusle amplification problem was reinvestigated further in the context of a swept-gain travelling wave amplifier (Hopf, Meystre, and McLaughlin 1976; Bonifacio, Hopf, Meystre, and Scully 1975; Hopf, Meystre, Scully, and Seely 1975; Hopf and Meystre 1975). It was found that, in the

presence of a linear loss ($\kappa > 0$), semiclassical approximations (treating the pulse classically) were inadequate (Hopf et al. 1976); however, as discussed in Chapter 3, one could circumvent some of these difficulties by letting the boundary condition $\mathscr{P}_o(z)$ be a non-zero constant (Bonifacio et al. 1975).

Next, the effects of spontaneous emission in a swept-gain amplifier were studied by letting $\mathscr{P}_o(z)$ be a stochastic variable and studying the Maxwell-Bloch equations, equation (2.7), with $T_1 = T_2$. In Hopf and Meystre (1975) the equations were studied numerically at the leading edge of the pulse (i.e., μ small) where $|\mathscr{E}\mathscr{P}| << 1$, so $n \approx +1$ and the equations become linear. (This is called the linear region of the laser.) Next, Hopf et al. (1976) studied the Maxwell-Bloch equations analytically in this same linear region. And finally Bonifacio et al. (1975) studied the equation numerically in the nonlinear region (i.e., for all $\mu \geq 0$). These latter authors found that, in the $T_1 = T_2$ regime, SSPs would form and that the energies of these SSPs would have Gaussian fluctuations about the semiclassical value.

In this dissertation we reexamine the effect of spontaneous emission in the superradiant regime of the

amplifier. We discover large-scale fluctuations which, as will be discussed shortly, are quite unlike the Gaussian fluctuations found previously.

Computer Simulation

Before discussing the results of the computer simulation, we first fix the stochastic boundary conditions. Hopf et al. (1976) used the fully quantum mechanical version of the Maxwell-Bloch equations to show that the quantum amplification process in the linear region could be simulated exactly by replacing the spontaneous emission operator of quantum theory by a Gaussian stochastic variable. While this is not a valid procedure in the nonlinear region of the pulse, it is intuitively obvious that any large effects in the nonlinear region, due to spontaneous emission, will be visible in the linear region. Indeed, the large fluctuations to be studied here originate from spontaneous emission effects in the linear region, and the stochastic representation is justified.

We thus take $\mathscr{P}_o(z)$ to be a bivariate Gaussian stochastic variable with mean zero and delta correlation, that is,

$$\langle \mathscr{P}_o(z) \rangle = 0$$

$$\langle \mathscr{P}_o(z)\, \mathscr{P}_o(z') \rangle = \overline{\mathscr{P}_o}^2 \delta(z - z'). \tag{4.1}$$

The value of the standard deviation, $\overline{\mathscr{P}}_o$, is fundamentally related (Hopf et al. 1976) to the gain α', to the lifetime, T_1, for the excited atoms to decay, and to the population in the upper state; in addition, it contains a somewhat arbitrary geometric factor. For that reason, we find it convenient to regard $\overline{\mathscr{P}}_o$ as an extra free parameter in the problem.

To study the SSP behavior, it is convenient to use two quantities which are fundamental to the pulses, namely, their energy, $\mathscr{T}$, (recall

$$\mathscr{T}(z) = \int_0^\infty |\mathscr{E}(\mu,z)|^2 d\mu$$

from Chapter 3), and their peak power, $I_p(z)$, which is the square of the maximum height of the pulse,

$$I_p(z) = \max_{\mu \geq 0} |\mathscr{E}(\mu,z)|^2. \qquad (4.2)$$

As fixed reference values for these quantities, we will use their semiclassical values, that is, the energy and peak power of the corresponding semiclassical SSP, denoted by $\mathscr{T}_{sc}$ and I_{sc} respectively. This corresponding semiclassical SSP is found by replacing the stochastic boundary condition, $\mathscr{P}_o(z)$, as defined in equation (4.1), by the

semiclassical boundary condition, $\mathscr{P}_o(z) \equiv \mathscr{P}_o$, discussed in Chapter 3, where for $\mathscr{P}_o$ we use the standard deviation of the stochastic $\mathscr{P}_o(z)$, namely $\overline{\mathscr{P}}_o$. We find, from Chapter 3, that

$$\mathscr{T}_{sc} \sim 2(\alpha' - 1) \quad \text{and} \quad I_{sc} \sim \frac{1}{\alpha'-1}.$$

In Figure 4.1 we plot the results of the original numerical solution of the Maxwell-Bloch equations, equation (3.2), with stochastic boundary data $\mathscr{P}_o(z)$, as described in equation (4.1). We restrict our attention to the steady-state region (i.e., where the power-balance has formed). (Recall that we always take $n(0,z) \equiv +1$ and $\mathscr{E}(\mu,0) \equiv 0$.) Note that for simplicity we are taking the ratio of the stochastic quantities to their semiclassical values so that the value 1.0 on the ordinate refers to the semiclassical value. In this example the parameters are $\alpha' = 2$ and $\overline{\mathscr{P}}_o = 10^{-6}$. (Although the numerical code was accurate to a few percent, only a few values of $\mathscr{E}$ were printed out so that Figure 4.1 is only accurate to $\sim$10%, i.e., $1 - \mathscr{T}(z)/\mathscr{T}_{sc}$ is accurate to $\sim$10%.)

In Figure 4.1a, the plot of the pulse energy, there are four properties to which we focus the reader's attention. Each will be discussed in some detail later. First, the

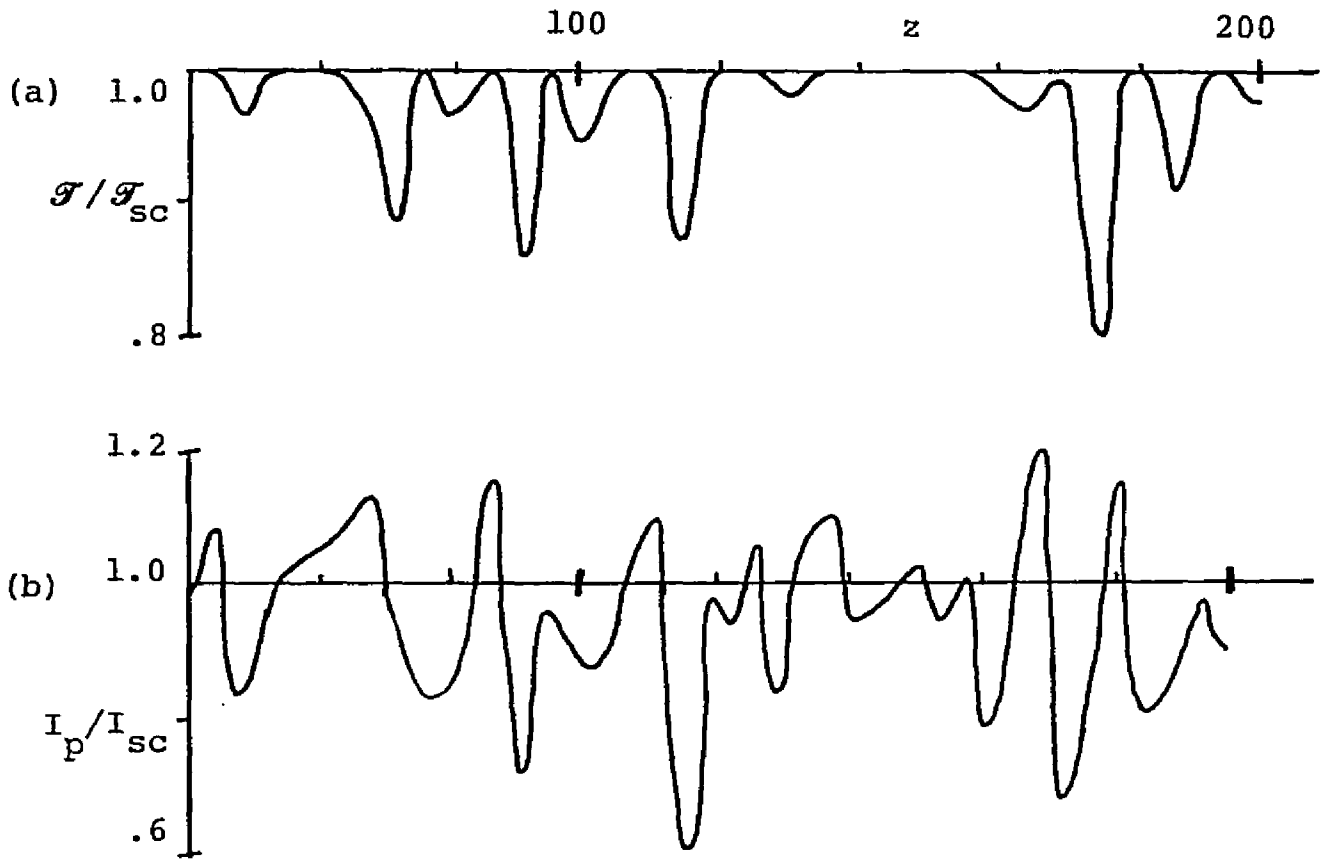

Figure 4.1. Energy and peak power for a stochastic $\mathscr{P}_o(z)$ ($\alpha' = 2$, $\overline{\mathscr{P}}_o = 10^{-6}$).

fluctuations are "large" (about 10% of the classical value). Second, the fluctuations are unidirectional in that energies lower than the semiclassical value are always involved. Third, they are episodic in character (i.e., they occur "once in awhile"). Finally, the fluctuations are largely independent of the standard deviation $\overline{\mathcal{P}}_o$ of the boundary data $\mathcal{P}_o(z)$. In fact, when we reduced $\overline{\mathcal{P}}_o$ by a factor of 100 but chose the same set of random numbers to generate $\mathcal{P}_o(z)$, the fluctuations remained the same within the limits of the numerical analysis.

Comparison with Other Fluctuations

To see the unusual character of these properties, let us contrast them to the behavior in a normal laser oscillator.[1] (The comparison is sensible because the formula for the pulse energy, given in equation (3.9), is closely analogous to the expression for the peak power in a single mode laser. It is simply necessary to replace the saturation energy T_2^{-1} in equation (3.9) by the saturation power

---

[1] In physics terminology the term "laser" or "laser oscillator" refers to an amplifying medium in which the pulse is reflected back through the medium many times before it attains enough energy to be emitted from the medium. The term "laser amplifier" or "amplifier" refers to an amplifying medium in which the pulse passes down the medium only once and is then emitted. To be precise, in this dissertation we are studying a "swept-gain laser amplifier". Beginning in this chapter we have been adhering to these definitions.

$(T_1T_2)^{-1}$.) (Harvey 1970, Chapter 24, has an exhaustive reference list on laser fluctuations.) First, in a laser, the power fluctuations are many orders of magnitude smaller than the energy fluctuations in Figure 4.1a. We note that our fluctuations do not become laser-like as the gain is further increased. While the fluctuations typically decrease as the gain α' increases, they are still $\sim$5% for $\alpha' = 20$. Second, in a laser the power fluctuations are Gaussian and centered about a mean as opposed to the unidirectional energy fluctuations observed here. Third, laser fluctuations are "random walk" processes (i.e., Brownian motion) and not episodic. Finally, laser fluctuations are strongly dependent on the standard deviation of the noise (spontaneous emission) while, as mentioned earlier, when we reduced $\overline{\mathcal{P}}_o$ by a factor of 100 the fluctuations remained the same within $\sim$10%.

Physical Intuition about the Origin and Characteristics of Amplifier Fluctuations

To study the physical origin of laser amplifier fluctuations, let us begin with the $T_1 = T_2$ regime. Recall that T_1 is the lifetime for the excited atoms to decay and so, in this case, the excited atoms are decaying on a time comparable to the location of the center of the SSP, τ_d. (Recall that τ_d is the time difference between

the swept-gain excitation and the peak of the SSP passing a fixed point.) Thus, the farther a pulse lags behind the swept-gain excitation, the less energy there is in the atoms to be transferred to the pulse. And so the energy of the SSP depends crucially on τ_d. The stochastic nature of the magnitude of $\mathscr{P}_o(z)$ causes the center of the SSP to jiggle about a central point, which is the semiclassical (i.e., $\mathscr{P}_o(z) \equiv \overline{\mathscr{P}}_o$) center of the SSP. Thus the energy of the SSP also jiggles about the semiclassical energy.

However, in the superradiant regime (where we set $T_1 = \infty$) fluctuations in the magnitude of $\mathscr{P}_o(z)$ do not cause significant energy fluctuations. We present here a very simple argument for this fact. After we have discussed the actual origin of the fluctuations in Figure 4.1a we will be able to present more convincing arguments. And, finally, in the next chapter we will present numerical data to support our claims.

The simple argument is as follows: The energy of the semiclassical SSP in the superradiant regime is $2(\alpha' - 1)$ which is independent of the initial polarization $\mathscr{P}_o(z)$. Thus in the stochastic case, even though fluctuations in $\mathscr{P}_o(z)$ cause a jitter in the location of the center of the SSP, the energy of the SSP is independent of the centering and should remain constant. Thus the

magnitude of $\mathscr{P}_o(z)$ cannot be the source of the macroscopic fluctuations observed in Figure 4.1a.

To understand the physical origin of the fluctuations in Figure 4.1a, we write $\mathscr{E} = |\mathscr{E}|\exp(i\theta_{\mathscr{E}})$ with a similar definition for $\mathscr{P}$ and combine equations (3.2c) and (3.8) to obtain an equation for the pulse energy, $\mathscr{T}$,

$$\frac{\partial \mathscr{T}}{\partial z} = 2\alpha' \int_0^\infty |\mathscr{E}||\mathscr{P}|\cos(\theta_{\mathscr{P}} - \theta_{\mathscr{E}})d\mu - 2\mathscr{T} . \qquad (4.3)$$

The first term on the right hand side of equation (4.3) represents the energy extracted from the inverted medium which sustains the SSP against the dissipative losses in the second term. For convenience, we define a relative phase angle $\phi \equiv \theta_{\mathscr{P}} - \theta_{\mathscr{E}}$. ϕ is the term that appears in the cosine and dominates the physics of this problem. The semi-classical pulse is given by $\phi = 0$, but in the stochastic case, because $\mathscr{P}_o(z)$ changes randomly, the phase difference is non-zero. Since this makes the cosine term smaller, the extracted energy is less than that given by classical results. For the most part, $\phi \approx 0$, which means that the fluctuations are too weak to be seen in the numerical results. Occasionally, however, one finds ϕ to be large, and, since as we shall see, this phase quantity is not attenuated significantly as it passes through the main portion

of the pulse, the extracted energy drops suddenly, and the pulse energy is dissipated in the losses. After this "phase wave" has passed through the pulse, ϕ reverts to being near zero and the pulse quickly recovers. These events occur rather frequently and lead to episodes of pulse destruction whose duration (in the z-direction) is characterized by the gain α'. The correlation of the phase waves with energy destruction is very evident in our numerical calculations. We do not show it here.

Now let us return to our argument about the independence of fluctuations in the magnitude of $\mathscr{P}_o(z)$ and fluctuations in energy. As we have just seen, fluctuations in the phase of $\mathscr{P}_o(z)$ occasionally cause a phase wave to form at the leading edge of the pulse (small μ). This phase wave then travels back through the pulse creating a condition under which the medium cannot give its energy as efficiently to the pulse. (In fact, occasionally the phase wave causes the pulse to return energy to the medium.) Thus the pulse loses energy due to nonresonant losses (the κ term).

Fluctuations in the magnitude of $\mathscr{P}_o(z)$ can only affect the energy of the pulse if they influence strongly some element of the above chain if events. However, the magnitude of $\mathscr{P}_o(z)$ does not influence the creation of

phase waves as will be shown analytically in Chapter 6. Fluctuations in the magnitude of $\mathscr{P}_o(z)$ do, as mentioned previously, shift, logarithmically, the average location of the peak of the pulse. However this shift only affects the energy fluctuation weakly as can be seen from the following argument. Once a large, and potentially destructive, phase wave is launched, it dies away quite slowly, but moves rapidly back through the pulse with a constant speed which is dependent only the the gain α' (as we shall see later). Thus, fluctuations in the magnitude of $\mathscr{P}_o(z)$ will not affect the speed of the phase wave but only cause the phase wave to travel different distances before encountering the peak of the pulse. Now, $\mathscr{P}_o(z)$ only affects the location of the center of the pulse, τ_d, logarithmically so large changes in $\mathscr{P}_o(z)$ will give rise to small changes in τ_d. And, in addition, the phase wave dies away slowly so changes in τ_d will only affect the phase wave slightly. It is the combination of the weak influence of $\mathscr{P}_o(z)$ on τ_d and the weak influence of τ_d on the phase wave which makes the energy fluctuations insensitive to changes in $\mathscr{P}_o(z)$.

A similar argument shows why changes in the standard deviation of $\mathscr{P}_o(z)$, $\overline{\mathscr{P}}_o$, only affect the size of the energy fluctuation weakly. (This is one of the unusual

properties of our fluctuations that was commented on previously.) Simply repeat the above argument, replacing the term "fluctuations in the magnitude of $\mathscr{P}_o(z)$" by "changing $\overline{\mathscr{P}}_o$".

Power Fluctuations

In addition to energy fluctuations in the SSPs, there are also fluctuations in power. There are two distinct powers which can be studied, namely the power of the pulse at the point (μ,z), $I(\mu,z)$, which is defined as

$$I(\mu,z) = |\ \mathscr{E}(\mu,z)|^2$$

and also the peak power of the pulse, $I_p(z)$, which, as we have already defined in equation (4.2), is

$$I_p(z) = \max_{\mu \geq 0} |\ \mathscr{E}(\mu,z)|^2.$$

The power at a point, $I(\mu,z)$, is not particularly useful for discussing SSP destruction because, as just mentioned, the peak of the pulse shifts back and forth under the influence of the magnitude of $\mathscr{P}_o(z)$. This shifting will give rise to large variations in the power at the point although the peak power will be hardly affected. Thus, in Figure 4.1b we have plotted the peak power of the pulse.

Notice that in the interval $140 \leq z \leq 160$ in Figure 4.1 that the energy is constant but the peak power is varying by $\sim 5\%$. As we will show numerically in the next chapter, in this interval the fluctuations are due to changes in the magnitude of $\mathscr{P}_o(z)$ and not changes in its phase. All the other fluctuations in the figure are due to changes in the phase of $\mathscr{P}_o(z)$. From other numerical calculations, the maximum power fluctuations when $\alpha' = 2$ are $\sim 10\%$ from amplitude modulations in $\mathscr{P}_o(z)$ and $\sim 70\%$ from phase modulations. When $\alpha' = 10$ the respective numbers are $\sim 2\%$ and $\sim 50\%$. Thus the fluctuations in peak power are also fundamentally different from those in the $T_1 = T_2$ regime, which, like the energy fluctuations, are due to location jitter.

Finally, for those acquainted with Dicke superradiance (Dicke 1954; Banfi and Bonifacio 1974; Rehler and Eberly 1971), in which all the atoms are excited at the same time and the model is a more complicated version of the Maxwell-Bloch equations, equation (2.7) (Bonifacio, Kim, and Scully 1969; Bonifacio et al. 1971), we contrast the theoretical predictions of fluctuations in Dicke superradiance (Degiorgio 1971; Bonifacio, Schwendimann, and Haake 1971) with our fluctuations. In Dicke superradiance, the quantum problem is analyzed taking the ensemble average of the power

at a point (μ,z), i.e., $\langle I(\mu,z)\rangle$, and then comparing this average with the semiclassical prediction of the power of the SSP at (μ,z). Since the location jitter of the peak of the pulse, which occurs in the Dicke case in a manner identical to ours, is of the order of the pulse width, this procedure leads to a large difference between the quantum and semiclassical powers. Hence, one finds "macroscopic fluctuations" (Bonifacio et al. 1971) in the power. Using peak power, however, it is shown in Degiorgio (1971) that there are no fluctuations in the Dicke case of the type shown in Figure 4.1. In other words, the analysis of the Dicke problem predicts that one should observe the semiclassical peak power and energy for every pulse emitted by the laser. The conclusion results direction from imposing "mean field" conditions (i.e., spatial homogeneity) on the problem and hence eliminating from the beginning the phase waves that cause the fluctuations in Figure 4.1. We note that swept-gain and Dicke superradiance have very different geometries, so it is not clear whether our fluctuations should be present in the Dicke case. However our method of analysis should be applicable, although with greater difficulty in the numerical portion. Since the experimental state of the art (Bowden, Howgate, and Robl 1977 has a recent compendium on the experiments in Dicke and swept-gain superradiance) is far more

advanced in the Dicke case than for swept-gain amplifiers, it will be worthwhile to investigate this question in detail.

In the next two chapters we analyze the fluctuations in the nonlinear region of the SSP. This study can be broken up into three issues:

(1) how the phase waves are started;

(2) how they propagate through the pulse; and

(3) how they affect the energy and power.

Of these, only the first is quantum mechanical (i.e., stochastic), and the first two, together, can be treated analytically by the methods used in Hopf et al. (1976). The third issue is treated deterministically using numerical solutions to show how phase waves of different magnitudes affect the waveform. Since the parameter $\overline{\mathscr{P}}_o$ affects the fluctuation weakly, the problem reduces to a single parameter (α') study. We deal with the nonlinear question (the second and third issues) first in Chapter 5. This allows us to give a qualitative description of the behavior of the phase waves. The analytical discussion of the phase waves, including probability distributions, is contained in Chapters 6 and 7. The analytical formulae are somewhat impenetrable so we rely on the numerical work for intuition.

CHAPTER 5

NUMERICAL COMPUTATIONS

Since the fluctuations in Figure 4.1 are episodic in nature and rarely overlap, we can study them as individual entities. In this chapter the boundary condition $\mathscr{P}_o(z)$ is given deterministically and we solve, numerically, the fully nonlinear Maxwell-Bloch equations, equation (3.2), to study the behavior of an individual phase wave. (The details of the numerical code are in Appendix A.) Our results will show that such a phase wave will indeed generate a fluctuation in energy and power which has the general characteristics of a single fluctuation in Figure 4.1.

First, we discuss what choices of $\mathscr{P}_o(z)$ give rise to large fluctuations. Second, we describe the destruction process and clarify the nature of the phase wave, $\phi = \theta_{\mathscr{P}} - \theta_{\mathscr{E}}$. Third, we correlate the properties of the phase wave with changes in energy and power. Finally, we describe the physical process by which the phase wave is constrained to lie within a range of $360°$ (so we choose $|\phi| \leq 180°$).

As discussed in the last chapter, letting the magnitude of $\mathscr{P}_o(z)$ fluctuate causes no visible fluctuations in energy and only slight variations in peak power. To see

these slight fluctuations numerically, we graph, in Figure 5.1, the electic field, $\mathcal{E}$, and the peak power, $I_p(z)$, for $\alpha' = 2$ with the boundary condition

$$\mathcal{P}_o(z) = \begin{cases} 10^{-4} & \text{for } z \leq z_o \\ -(10^{-4} - 10^{-5})(z - z_0) + 10^{-4} & \text{for } z_o < z < z_o + 1 \\ 10^{-5} & \text{for } z \geq z_o + 1 \end{cases}$$

where z_o is large enough that an SSP will have formed. This linear change in $\mathcal{P}_o(z)$ was picked for simplicity. In Figure 5.1b we plot the peak power of the pulse. Notice that while $\mathcal{P}_o(z)$ changes by a factor of 10, the peak power only fluctuates by .1. (The peak power levels of at .994 because the analytical shape of the SSP, equation (3.6c), is weakly dependent on $\mathcal{P}_o(z)$ through the parameters τ_d and τ_p.) The energy is not plotted here because it only decreased to .993 and quickly returned to its SSP value of 1.000. Thus we see that the fluctuation shown here is similar to the fluctuations in Figure 4.1 in the interval $140 \leq z \leq 160$ where the peak power fluctuated by $\sim$5% and the energy remained constant.

To understand the cause of this minor power fluctuation, we plot the electric field, $\mathcal{E}$, in Figure 5.1a. At $z = z_o$ (the solid line) the SSP has formed. At $z - z_o = 24$

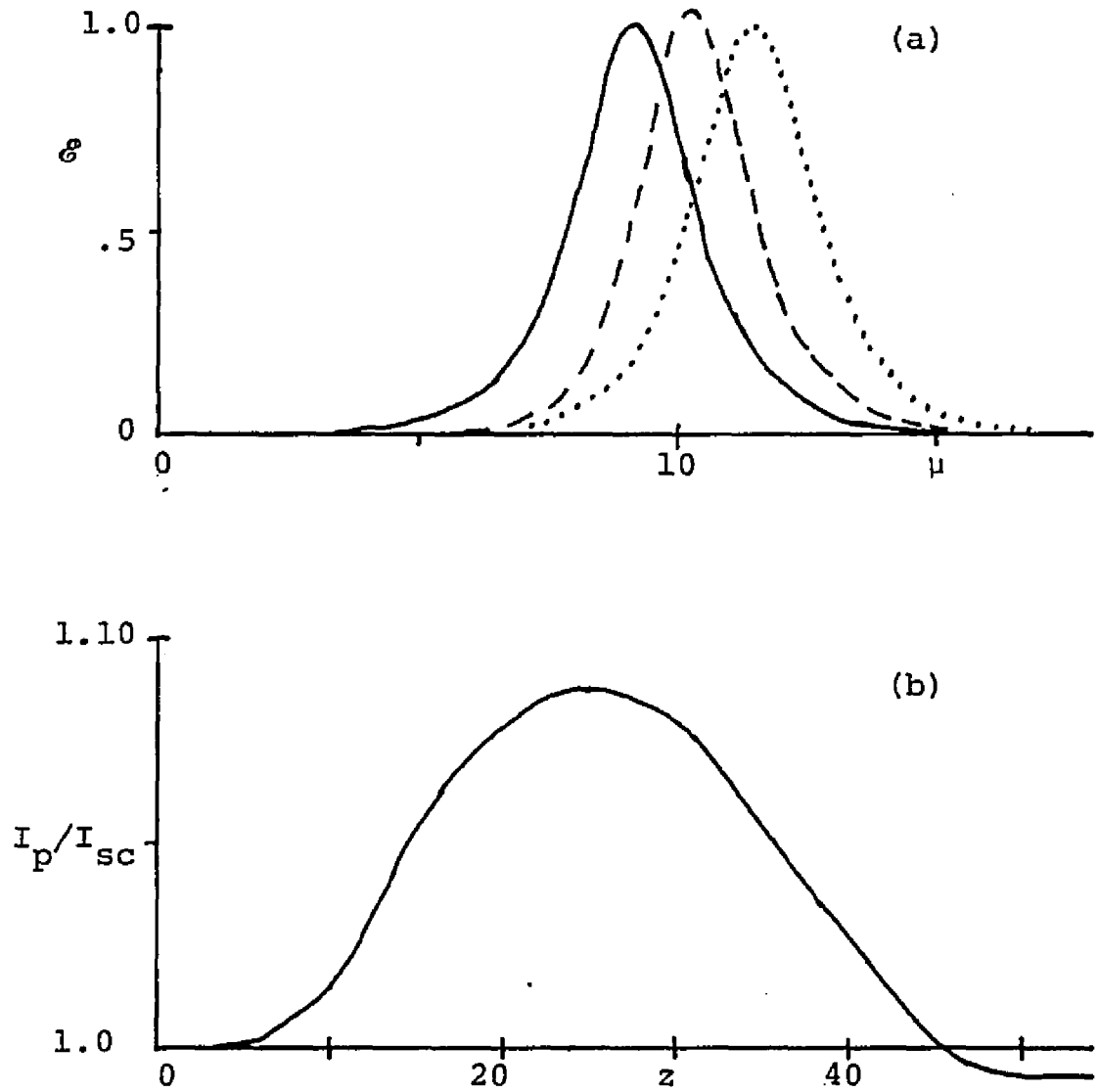

Figure 5.1. Changing the magnitude of $\mathscr{P}_o(z)$ ($\alpha' = 2$). $\mathscr{P}_o(z)$ is initially 10^{-4}, changes linearly to 10^{-5} for $z_o \leq z \leq z_o + 1$ and remains at 10^{-5}. $z - z_o = 0$ is the solid line, $= 24$ is the dashed line, $= 48$ is the dotted line. The gain, α', is 2.

(the dashed line) the pulse is shifting to the right. (Recall that as $\mathscr{P}_o(z)$ decreases, the location of the center of the SSP shifts to the right, and as $\mathscr{P}_o(z)$ increases the location of the center shifts to the left.) At $z - z_o = 48$ (the dotted line) the pulse has reformed an SSP.

The increase in power occurs because the leading edge of the pulse (small μ) begins moving to the right before the trailing edge. This causes the pulse to narrow and increase in height. In Figure 5.1a it is just possible to observe that the dashed curve is indeed narrower and higher. However, as can be seen, the increase in peak power is due to a minor, barely visible, deformation of the SSP.

Thus we see that fluctuations in the magnitude of $\mathscr{P}_o(z)$ do, indeed, cause no macroscopic fluctuations in energy and only minor fluctuations in peak power. However, as discussed previously, fluctuations in the phase of $\mathscr{P}_o(z)$ can lead to large-scale fluctuations in both quantities. To observe this behavior, we let the phase of $\mathscr{P}_o(z)$ be initially zero. We then change it as follows:

$$\mathscr{P}_o(z) = \begin{cases} \mathscr{P}_o & \text{for } z \leq z_0 \\ \mathscr{P}_o e^{i\beta\frac{z-z_0}{r}} & \text{for } z_o < z \leq z_o + r \\ \mathscr{P}_o e^{i\beta} & \text{for } z_o + r < z \end{cases} \tag{5.1}$$

Here again z_o is large enough so that an SSP will have formed, and $\mathscr{P}_o$ is real and positive. The linear increase in the phase is chosen for simplicity in the analysis to be presented in Chapter 6. We note that this linearity seems to give a good approximation to typical cases involving the stochastic boundary condition. For each choice of β and r, one observes a fluctuation in energy and power as the SSP attempts to change its phase from 0 to β (see equation (3.6c)). (We allow $r = 0$ in equation (5.1) in which case the phase shifts by β at $z = z_o$.)

Representative examples, which show the major features we have been discussing in the previous chapters, are shown in Figures 5.2-5.9. (We caution the reader to check the scales before comparing graphs, since, for ease in viewing, the graphs must all be about the same size.) We focus our attention, first, on the energy $(\mathscr{T}(z)/\mathscr{T}_{sc})$ and peak power $(I_p(z)/I_{sc})$ curves in Figure 5.2, where the parameters are $\alpha' = 2$, $\beta = 160°$, $r = 1$, and $\mathscr{P}_o = 10^{-4}$. Notice that the energy fluctuation shown here bears a striking resemblance to the energy fluctuations in Figure 4.1a and the same remark holds for the power fluctuations, even down to the initial increase in peak power before it drops off suddenly. Thus we see that the fluctuations in Figure 4.1 are, indeed, caused by phase waves.

Figure 5.2. Changing the phase of $\mathscr{P}_o(z)$ ($\alpha' = 2, \beta = 160°$, $r = 1$, $\mathscr{P}_o = 10^{-4}$).

In Figures 5.2-5.9 the magnitude of $\mathscr{P}_o(z)$, $\mathscr{P}_o$, remains constant, the phase of $\mathscr{P}_o(z)$ is initially 0 for $z \leq z_o$ and is β for $z > z_o + r$. If $r > 0$ the phase changes linearly between 0 and β. If $r = 0$ the phase changes discontinuously. In Figure 5.2 $z - z_o = 4$ is the solid line, $= 10$ is the dashed line, $= 16$ is the dotted line.

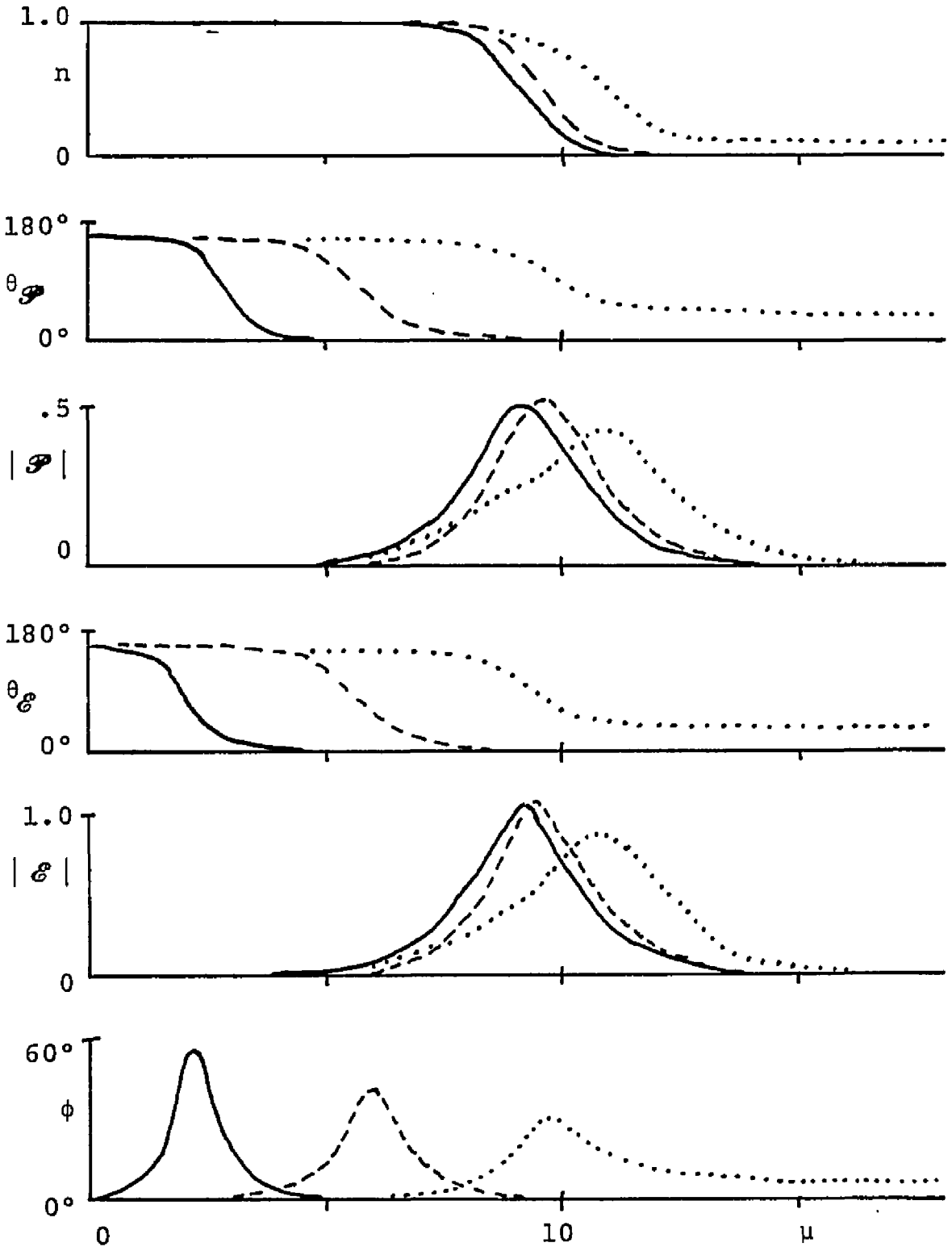

Figure 5.2. Changing the phase of $\mathscr{P}_o(z)$ ($\alpha' = 2, \beta = 160°$, $r = 1$, $\mathscr{P}_o = 10^{-4}$).

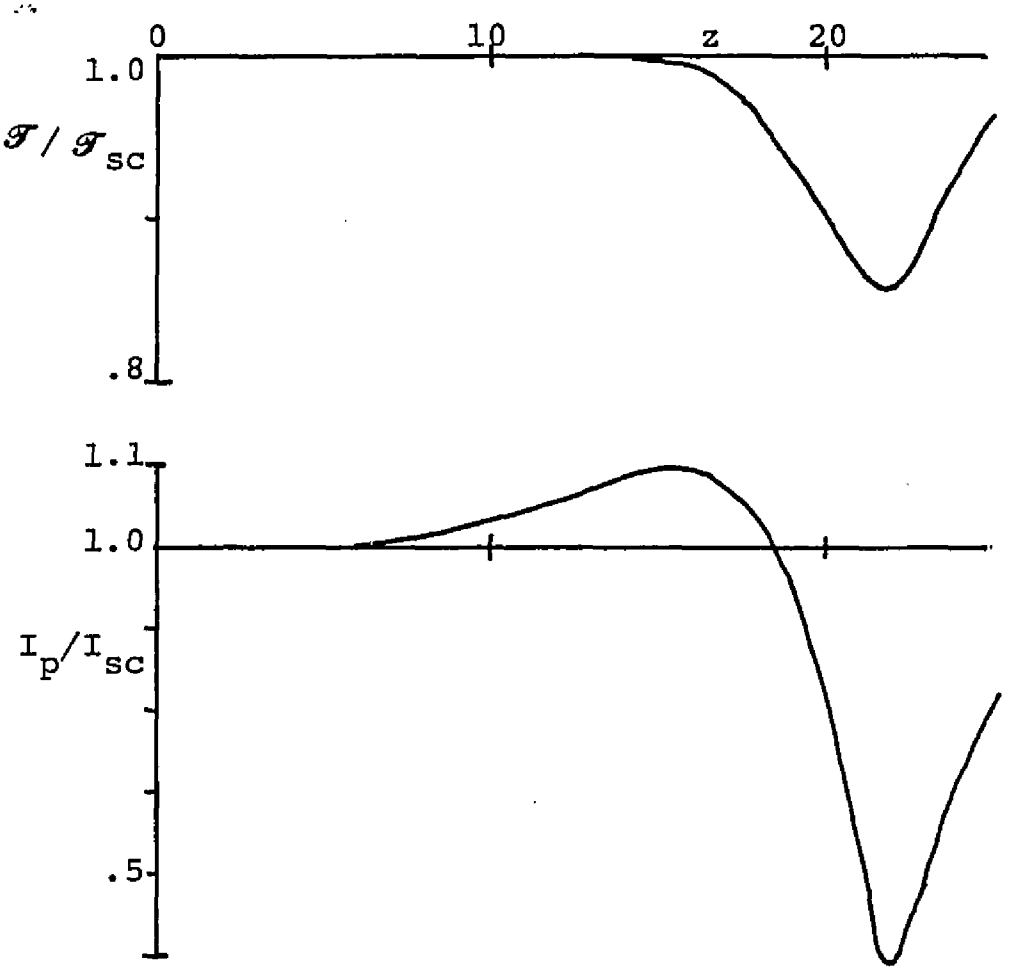

Figure 5.2 (continued).

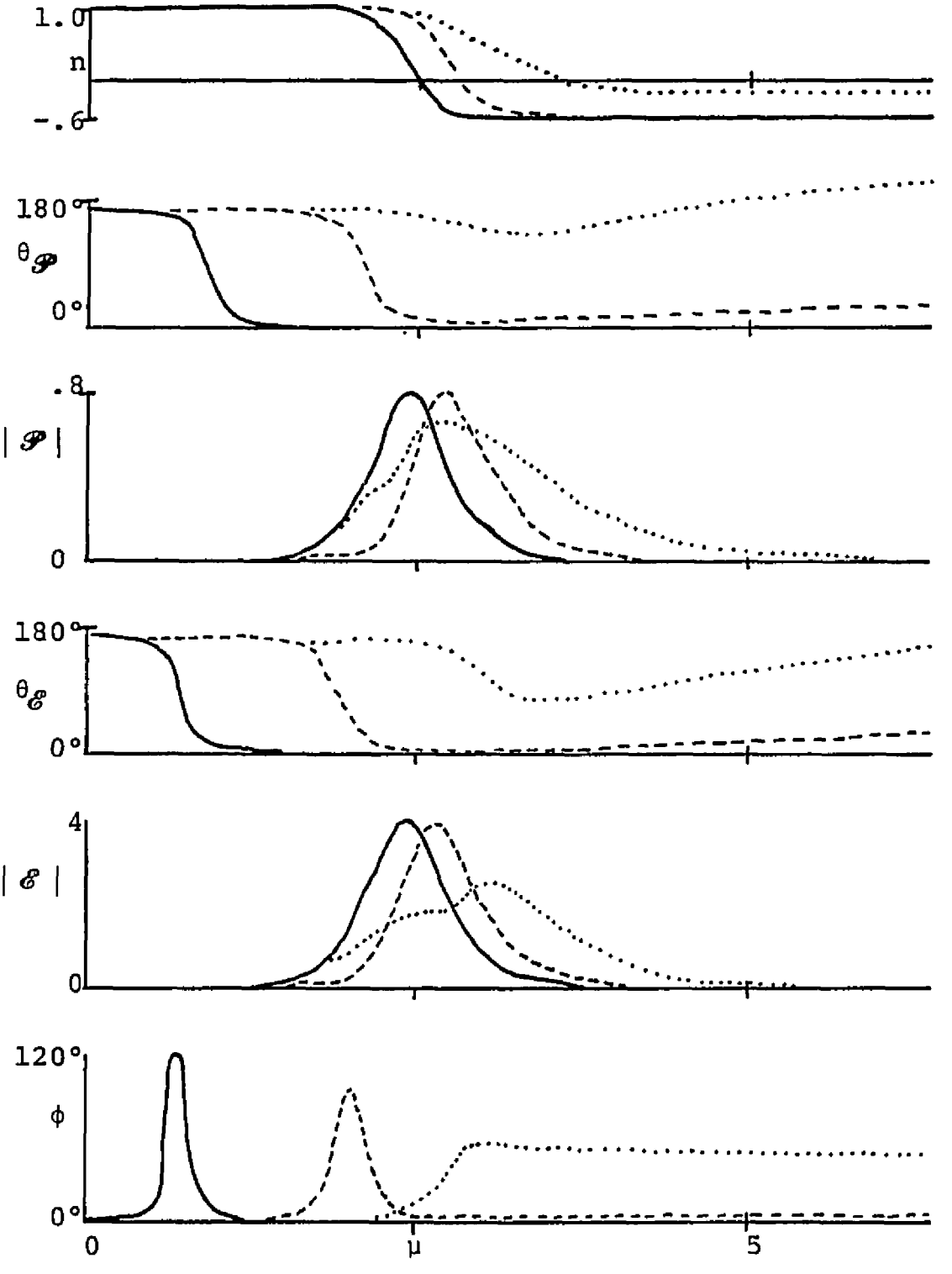

Figure 5.3. Changing the phase of $\mathscr{P}_o(z)$ ($\alpha' = 5, \beta = 170°$, $r = 0$, $\mathscr{P}_o = 10^{-4}$).

$z - z_o = 4$ (solid line), 10 (dashed line), 14 (dotted line).

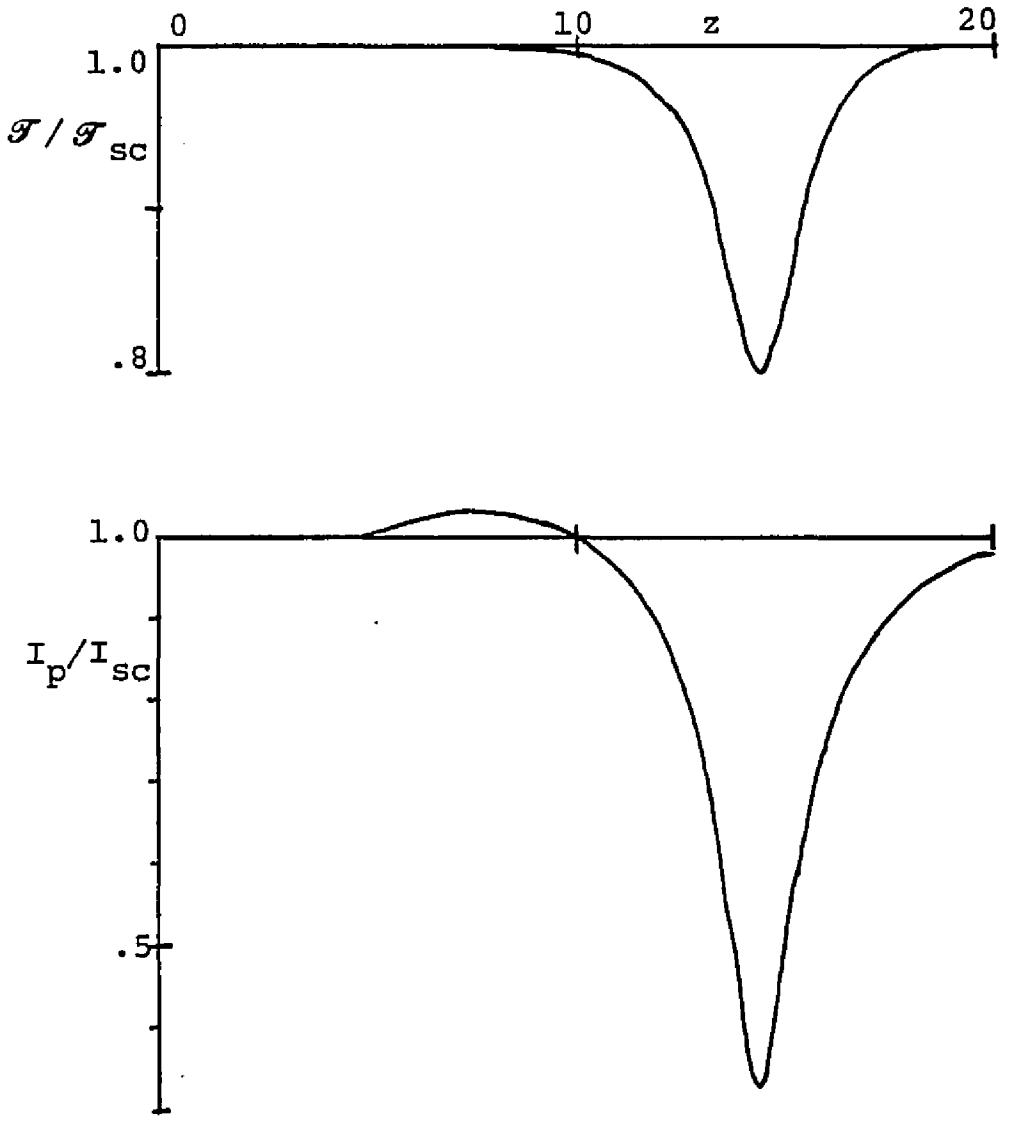

Figure 5.3 (continued).

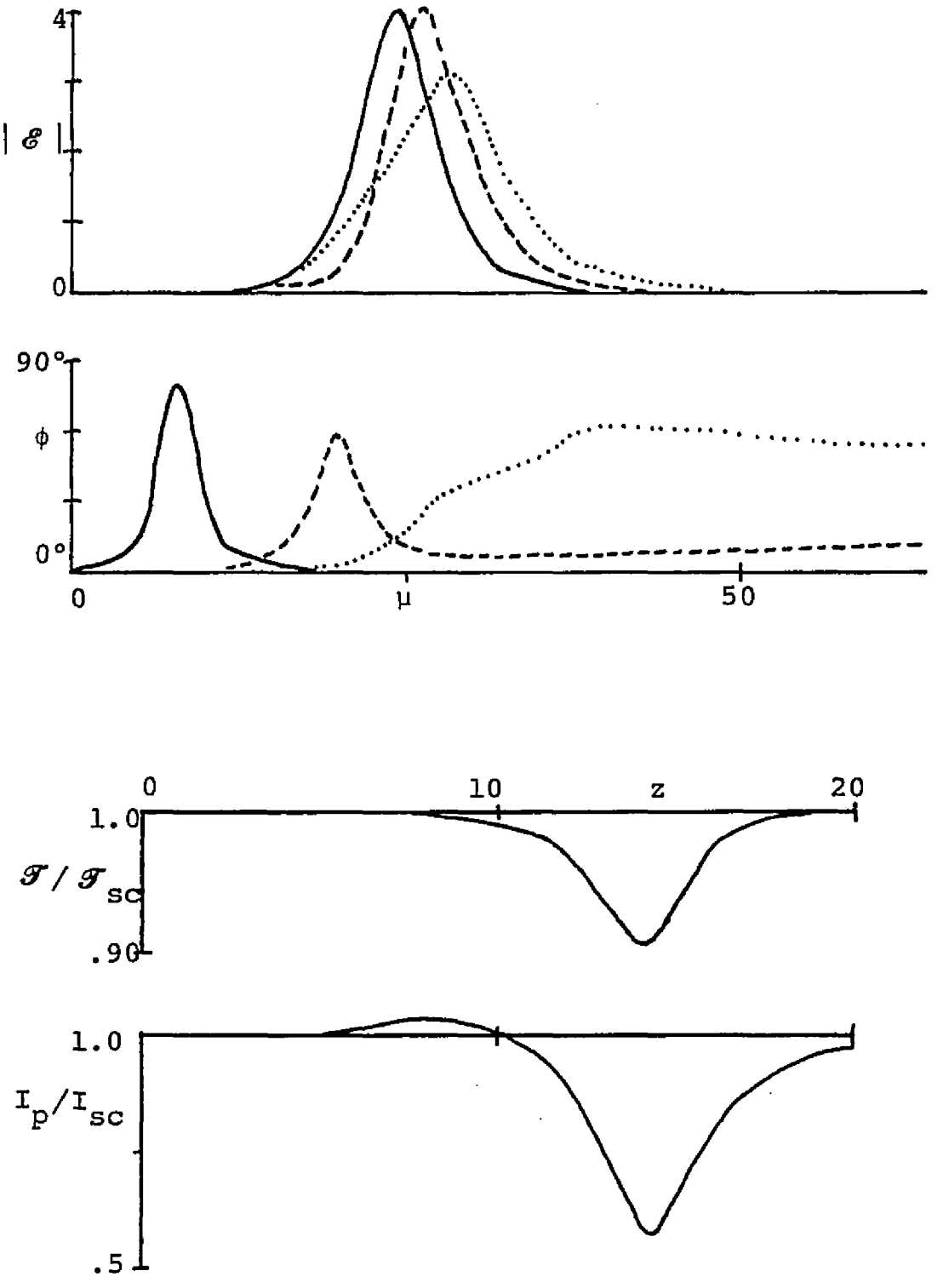

Figure 5.4. Changing the phase of $\mathscr{P}_o(z)$ ($\alpha' = 5, \beta = 160°$, $r = 0$, $\mathscr{P}_o = 10^{-4}$).
$z - z_o = 4$ (solid line), 10 (dashed line), 14 (dotted line).

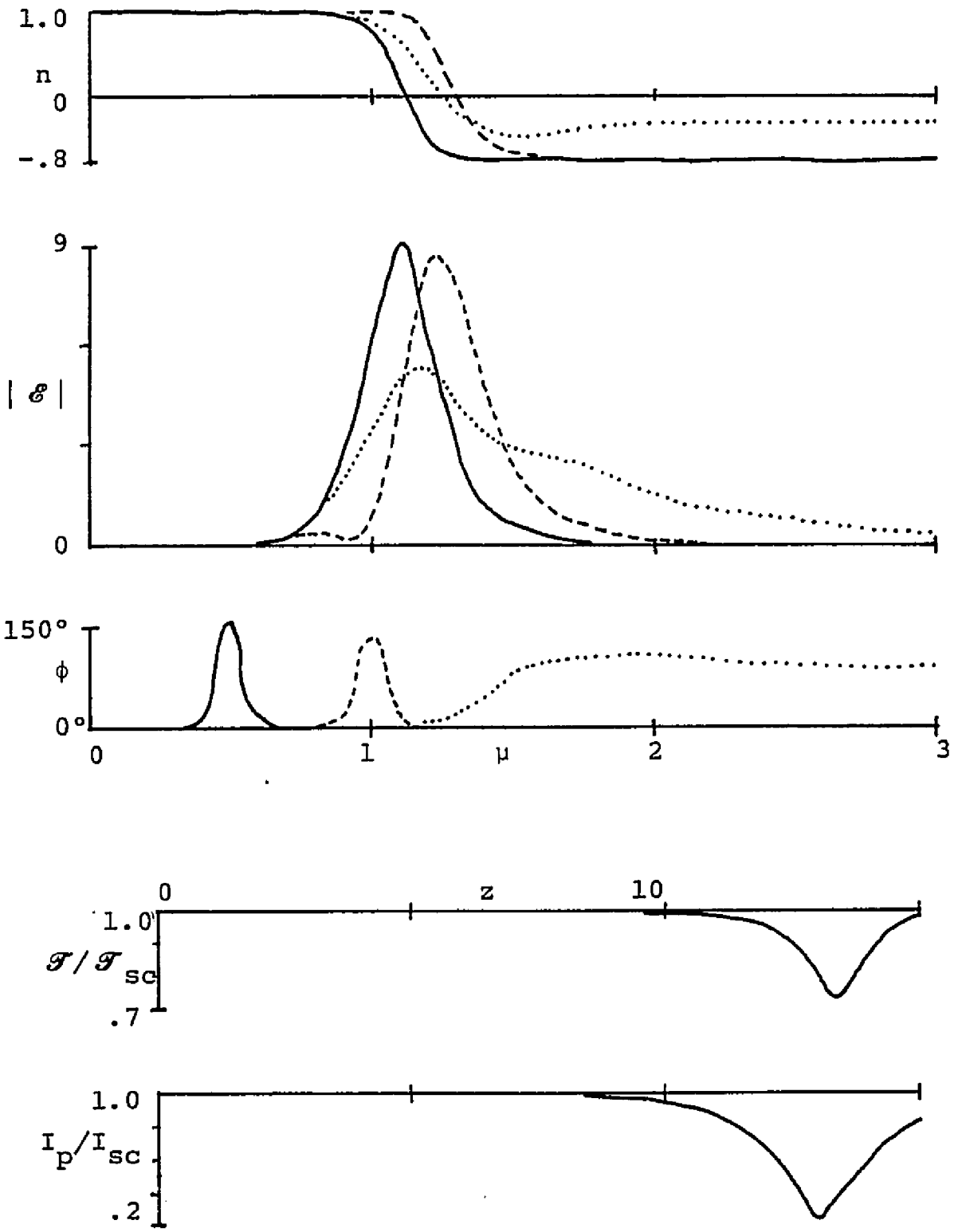

Figure 5.5. Changing the phase of $\mathscr{P}_o(z)$ ($\alpha' = 10, \beta = 176°$, $r = 0$, $\mathscr{P}_o = 10^{-4}$).
$z - z_o = 5$ (solid line), 10 (dashed line), 13 (dotted line).

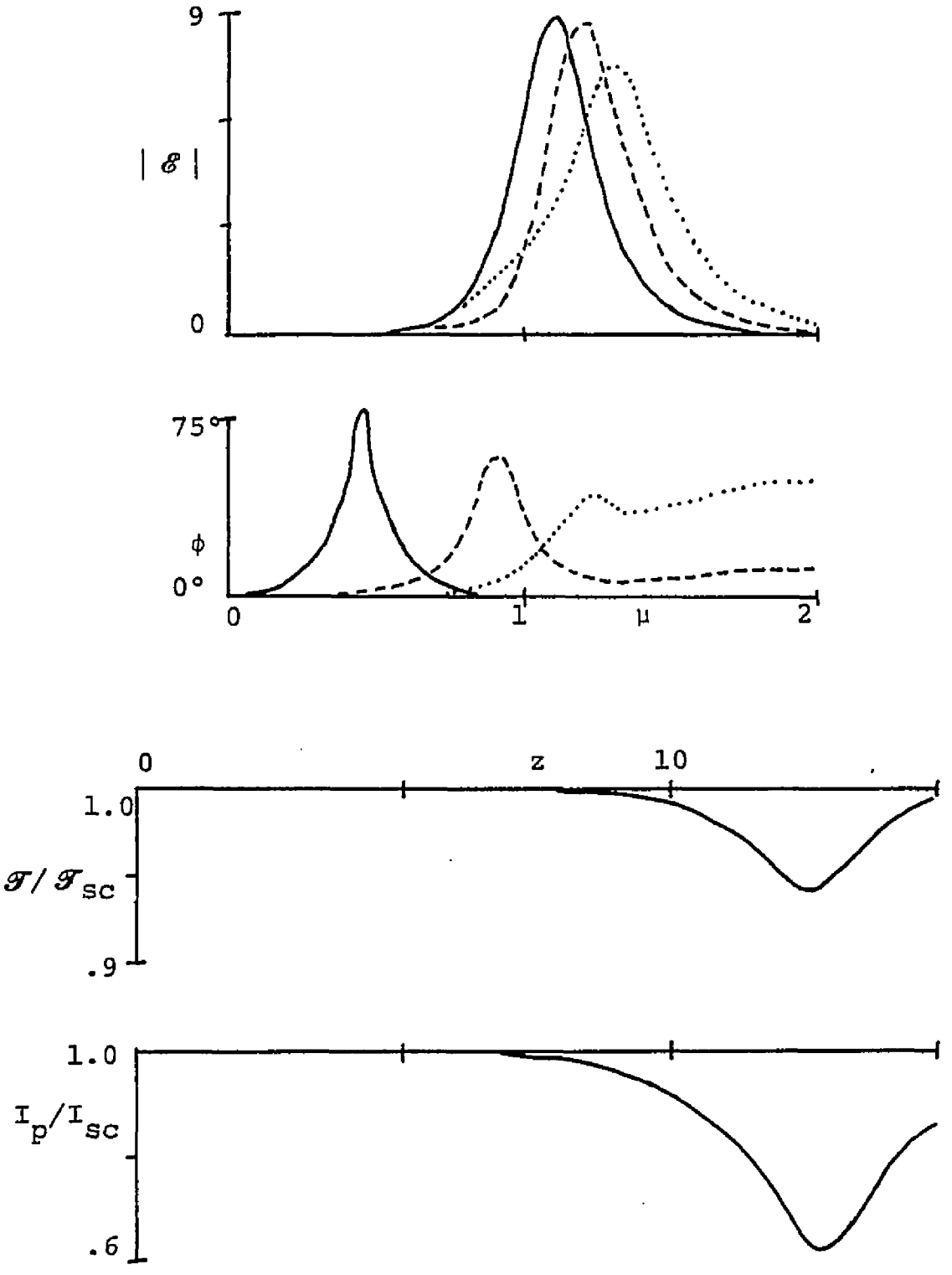

Figure 5.6. Changing the phase of $\mathscr{P}_o(z)$ ($\alpha' = 10, \beta = 160°$, $r = 0$, $\mathscr{P}_o = 10^{-4}$).
$z - z_o = 4.5$ (solid line), 9 (dashed line), 12 (dotted line).

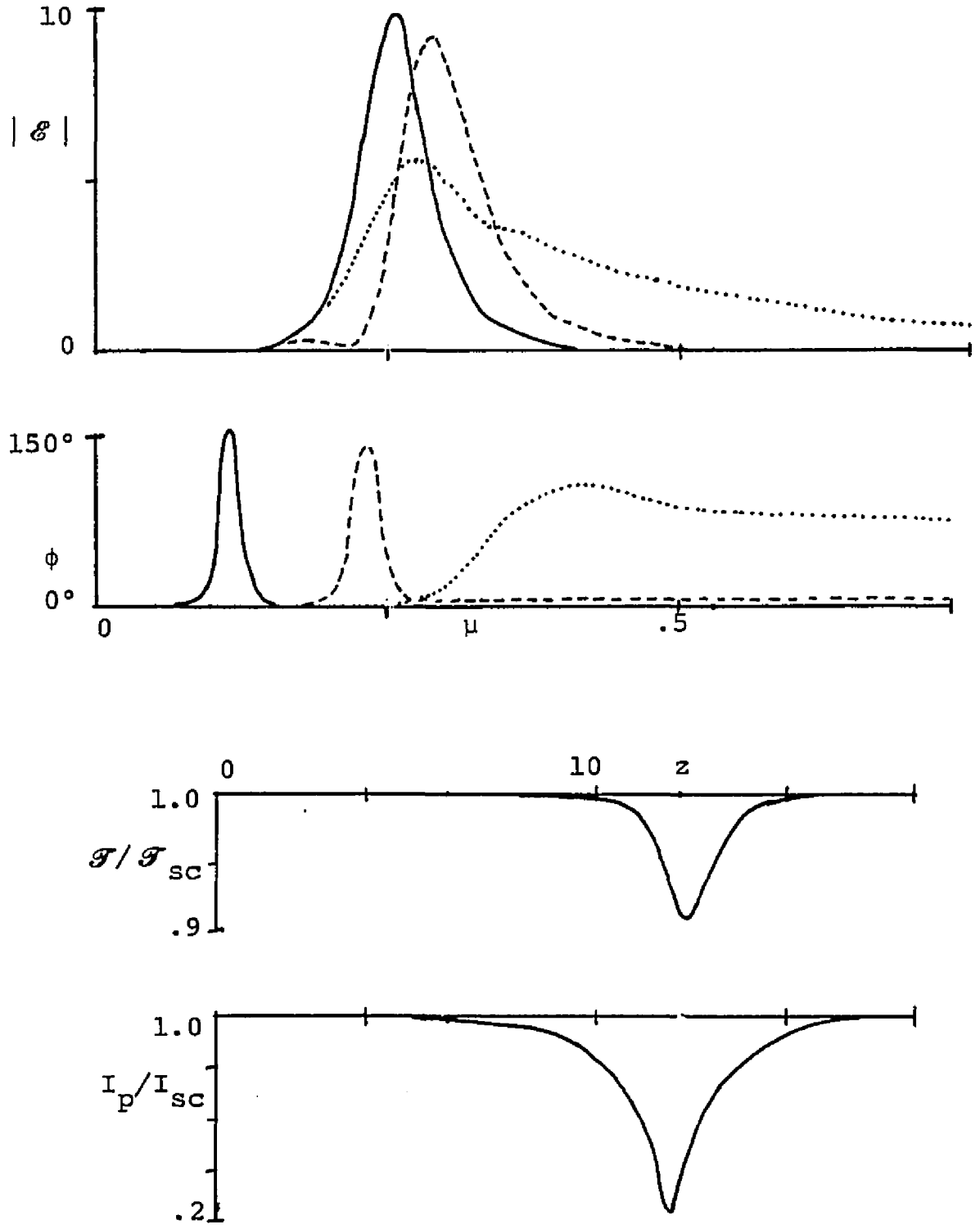

Figure 5.7. Changing the phase of $\mathscr{P}_o(z)$ ($\alpha' = 40, \beta = 176°$ $r = 0$, $\mathscr{P}_o = 10^{-4}$).
$z - z_o = 4.6$ (solid line), 9.2 (dashed line), 12.3 (dotted line).

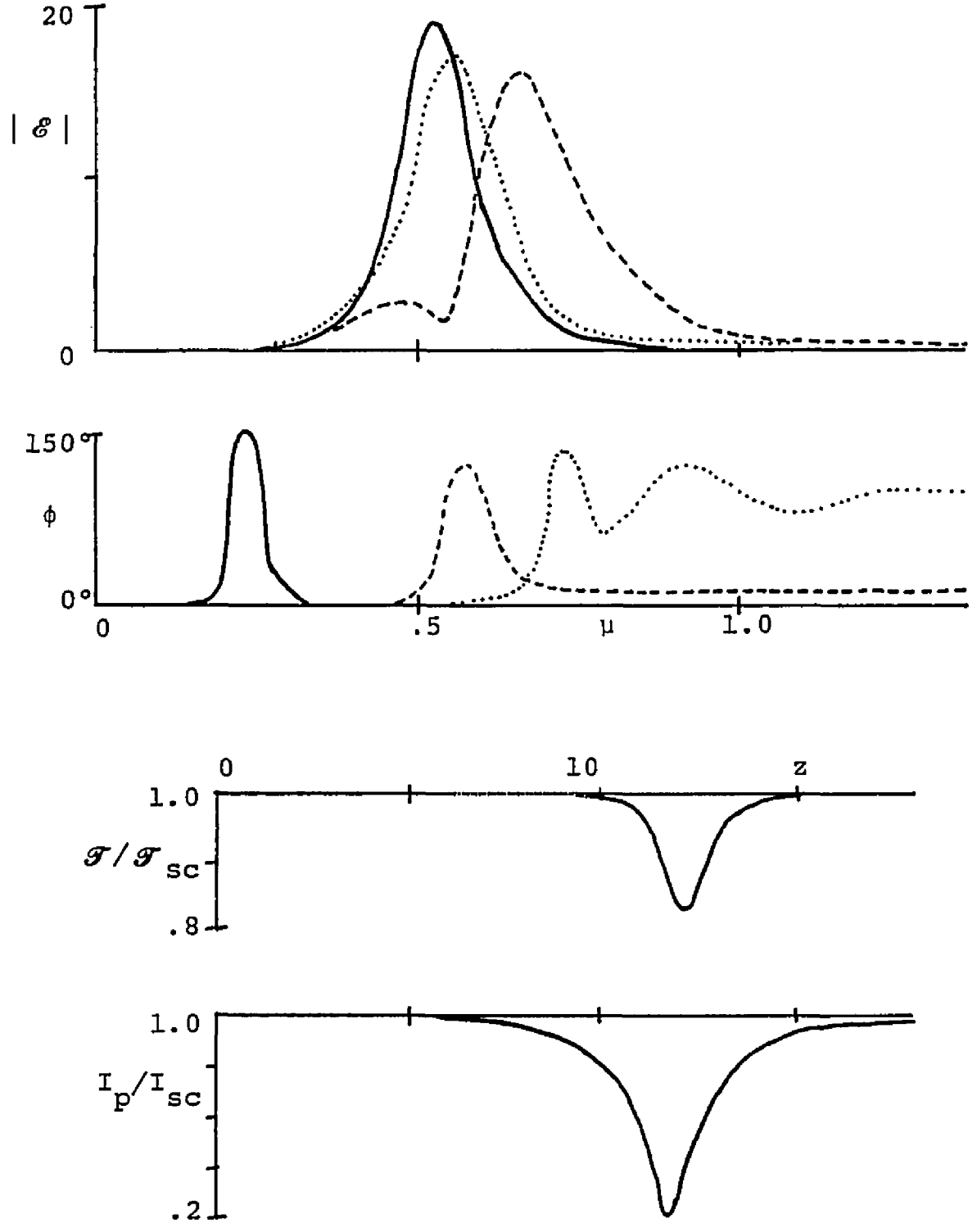

Figure 5.8. Changing the phase of $\mathscr{P}_o(z)$ ($\alpha' = 20, \beta = 176°$, $r = 0$, $\mathscr{P}_o = 10^{-4}$).

$z - z_o = 4.7$ (solid line), 11 (dashed line), 14.2 (dotted line).

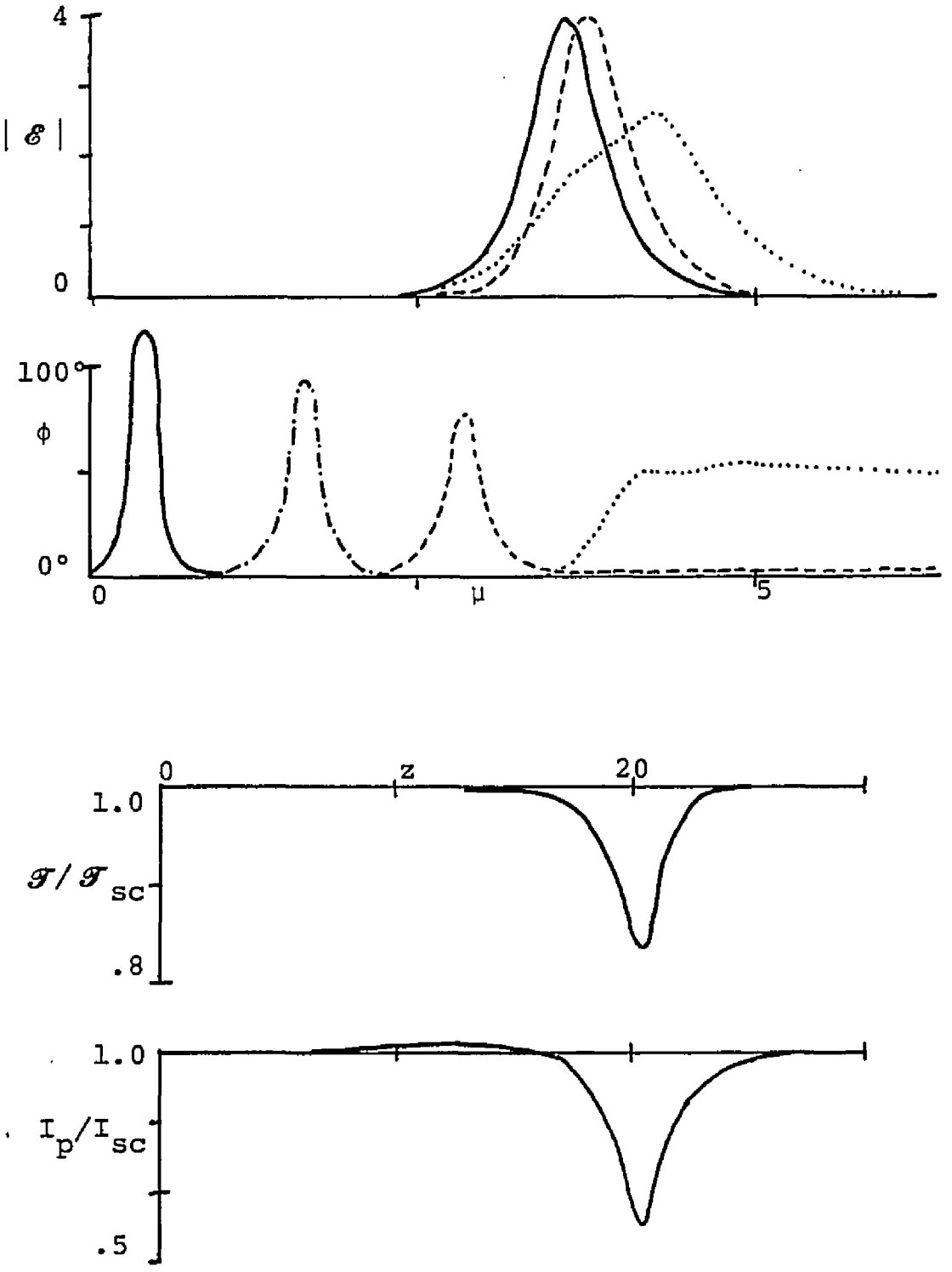

Figure 5.9. Changing the phase of $\mathscr{P}_o(z)$ ($\alpha' = 5, \beta = 170°$, $r = 0$, $\mathscr{P}_o = 10^{-6}$).
$z - z_o = 2$ (solid line), 8 (solid line in $|\mathscr{E}|$, dashed-dotted line in ϕ), 14 (dashed line), 20 (dotted line).

To see the effect of the phase wave in more detail, we also graph in Figure 5.2 the phase wave, ϕ, and all the internal variables in the Maxwell-Bloch equations, namely $|\mathscr{E}|$, $\theta_{\mathscr{E}}$, $|\mathscr{P}|$, $\theta_{\mathscr{P}}$, and n. (Recall that n is the population difference between the two energy states, so n = +1 if all the electrons are in the excited state and n = -1 if all the electrons are in the lower state.) At $z = z_o$ the SSP has formed and also n and $|\mathscr{P}|$ have formed their steady-state shapes (see equation (3.6)). These steady-state shapes are the solid lines in the graphs of $|\mathscr{E}|$, $|\mathscr{P}|$, and n. When $z - z_o = 4$ (the solid line) the pulse has not yet changed shape, but $\theta_{\mathscr{E}}$ now follows the phase shift in $\mathscr{P}$ and a phase wave has formed. When $z - z_o = 10$ (the dashed line) the pulse is moving to the right. This is because the pulse is not obtaining much energy from the medium near the phase wave and so it can only obtain this energy at a little later time when the phase wave is small. This time delay can be seen in the plot of n where the population of excited atoms decreases at a slightly later time than before, but still the same fraction of atoms eventually gives their energy to the pulse. When $z - z_o = 16$ (the dotted line) the phase wave has nearly reached the peak of the pulse, which has now lost its characteristic shape (in later figures we will see the pulse undergo much

more of a collapse). Notice from the plot of n that the energy transfer from the excited atoms to the pulse has been greatly delayed and many more atoms are left in the excited state. For slightly larger z, the phase wave will reach the peak of the pulse and cause the greatest change in the pulse shape. Then the pulse will quickly move back to the left and regain its former shape.

Let us now return to the energy and peak power graphs. In the energy plot we see the energy decrease rapidly once the phase wave reaches the main body of the pulse. Notice that the minimum energy occurs at $z \sim 17.3$, which is when the phase wave reaches the peak of the pulse. As will be discussed at length later, the decrease in the energy is governed by the size of the phase wave. Thus, phase waves whose maxima are near $180°$ at the peak of the pulse cause the largest energy fluctuations. The peak power also decreases rapidly in this region, reaching its minimum at the same point as does the energy. It also quickly recovers its former value once the phase wave has passed by. The initial increase in power has the same cause as in Figure 5.1, namely the leading edge moves back before the trailing edge and so the pulse narrows and increases in height. Although this initial increase in peak power occurs in all the figures to follow, its size decreases with increasing gain until it can no longer be seen for $\alpha' = 20$ and 40.

Figures 5.3-5.9 all show essentially the same features just seen in Figure 5.2, although certain features show up better in one figure than another. The rest of the figures do show the quantitative differences in the pulse shape, as well as the energy and power fluctuations for different values of the parameters.

In Figure 5.3 we plot the same variables as in the last figure and choose our parameters to be $\alpha' = 5$, $\beta = 170°$, $r = 0$, and $\mathscr{P}_o = 10^{-4}$. (As we shall see later, letting $r = 0$, so that $\mathscr{P}_o(z)$ is discontinuous, does not cause any qualitative differences in the variables.) As in all the figures in this chapter, the SSP shape is the solid line in the $|\mathscr{E}|$ plot. Also in this figure the steady-state shapes for $|\mathscr{P}|$ and n are the solid lines in their respective plots. The only noticeable difference in behavior from Figure 5.2 is that the phases of $\mathscr{E}$ and $\mathscr{P}$ do not return to zero for large μ. The cause can be seen when the Maxwell-Bloch equations are rewritten in polar coordinates:

$$\frac{\partial}{\partial\mu}|\mathscr{P}| = |\mathscr{E}|n\cos\phi - |\mathscr{P}| \tag{5.2}$$

$$|\mathscr{P}|\frac{\partial}{\partial\mu}\theta_{\mathscr{P}} = -|\mathscr{E}|n\sin\phi$$

$$\frac{\partial}{\partial \mu} n = -|\mathscr{E}||\mathscr{P}|\cos\phi$$

$$\frac{\partial}{\partial z}|\mathscr{E}| = \alpha'|\mathscr{P}|\cos\phi - |\mathscr{E}|$$

$$|\mathscr{E}|\frac{\partial}{\partial z}\theta_{\mathscr{E}} = \alpha'|\mathscr{P}|\sin\phi.$$

Concentrating on equation (5.2b), we see that $\frac{\partial}{\partial \mu}\theta_{\mathscr{P}}$ changes sign when n changes sign. From the equation for n in the SSP, equation (3.6a), we see that n will become negative for large μ if $\alpha' \gtrsim 2$. As can be seen from Figure 5.3, $\phi < \pi$ so $\sin\phi$ is positive. Thus $\frac{\partial}{\partial \mu}\theta_{\mathscr{P}}$ changes from negative to positive when n passes through zero ($\mu \sim 3.5$) and so the phase of $\mathscr{P}$ increases for $\mu \gtrsim 3.5$. As can be seen from all the figures to follow, the phase of $\mathscr{E}$ also begins increasing at about this value and the phase wave levels off at some value. This effect is not significant in our discussion.

Another observation which can be seen more clearly in this figure than the last is that the pulse shape flattens out in the vicinity of the phase wave. As mentioned previously, this is because the pulse cannot extract as much energy due to the presence of the phase wave, and so the dissipative losses (the κ term) can be as large or larger

than the energy extracted from the medium. Notice in the differential equation for the pulse energy, equation (4.3), the energy decreases most rapidly for ϕ near $180°$.

In later figures we dispense with the plots of n, $|\mathscr{P}|$, $\theta_{\mathscr{P}}$, and $\theta_{\mathscr{E}}$ since they have the same behavior as in Figures 5.2 and 5.3. Thus in Figure 5.4 we only plot $|\mathscr{E}|$, ϕ; the energy, and the peak power. The parameters are $\alpha' = 5$, $\beta = 160°$, $r = 0$, and $\mathscr{P}_o = 10^{-4}$. Thus, this figure can be compared to the last to see how crucial the magnitude of the phase wave is to the pulse destruction.

In Figures 5.5 and 5.6 we again compare the size of the phase wave. The parameters are $\alpha' = 10$, $r = 0$, and $\mathscr{P}_o = 10^{-4}$ for both figures. In addition, in Figure 5.5 $\beta = 176°$ and in Figure 5.6 $\beta = 160°$. In Figure 5.5 we again plot n to show a case where the pulse returns energy to the medium (the dotted line).

In Figure 5.7 the parameters are $\alpha' = 40$, $\beta = 176°$, $r = 0$, and $\mathscr{P}_o = 10^{-4}$. Note that the graphs are quite similar to Figure 5.5. In Figure 5.8 the parameters are $\alpha' = 20$, $\beta = 176°$, $r = 0$, $\mathscr{P}_o = 10^{-4}$. If we had chosen $z - z_o = 9.45$ and 12.6 we would have shapes quite similar to the dashed and dotted, respectively, Figures 5.6 and 5.7. However we have graphed these curves at slightly larger distances to show how quickly the pulse regains its former

shape once the phase wave has passed by. If we had chosen $z - z_o = 12.6$ we would see the pulse trailing off slowly as in Figures 5.5 and 5.7 (the dotted lines). Thus we see how quickly this tail forms and then disappears.

Finally in Figure 5.9 the parameters are $\alpha' = 5$, $\beta = 170°$, $r = 0$, and $\mathscr{P}_o = 10^{-6}$. Thus this figure can be compared with Figure 5.3 to see the effect of a change in the magnitude of $\mathscr{P}_o$. Comparing the two figures we see that a change in $\mathscr{P}_o$ by a factor of 100 causes the size of the energy fluctuation to decrease by a factor of $\sim.1$ and the size of the peak power fluctuation to decrease by a factor of $\sim.05$.

The figures shown so far have brought out all the essential features of the pulse behavior which were described in previous chapters. Figure 5.1 has shown the weak influence of the magnitude of $\mathscr{P}_o(z)$ on energy and power fluctuations as well as upon pulse destruction, while Figures 5.2-5.9 have shown the strong influence of the phase of $\mathscr{P}_o(z)$. The weak influence of the magnitude of $\mathscr{P}_o(z)$ on a phase wave, and thus on the energy and power fluctuations can be seen in Figures 5.2 and 5.9. Also the slow decay of the phase waves and their travelling at a constant speed can be seen in all of Figures 5.2-5.9.

The reason for the catastrophic collapse of the pulse due to the phase wave can be clearly understood with an instantaneous phase shift of 180° in $\mathscr{P}_o(z)$ (i.e., $\beta = 180°$ and $r = 0$). Since $\mathscr{P}_o(z)$ is real and so is $\mathscr{E}(\mu,0)$ (since it is zero), it follows from the Maxwell-Bloch equations that $\mathscr{P}$ and $\mathscr{E}$ remain real with the phase shift occurring as a change in sign (Hopf and Scully 1969, Icsevgi and Lamb 1969). The phase shift must propogate through the pulse and change $\mathscr{E}$ from positive ($\theta_{\mathscr{E}} = 0°$) to negative ($\theta_{\mathscr{E}} = 180°$). Moreover, $\mathscr{E}(\mu,z)$ is a continuous variable in μ and z (see equation (3.3)) so that at the point at which $\mathscr{E}$ changes sign, (i.e., $\theta_{\mathscr{E}}$ changes from 0° to 180°), the electric field is zero. The phase shifts in $\mathscr{E}$ and $\mathscr{P}$ look like shock fronts propogating through the pulse, while the phase wave, ϕ, looks like a square wave. When the phase shift of the field reaches the peak of the pulse, the field is zero at the point, and so one necessarily finds large changes in the waveform with corresponding fluctuations in energy and power. A representative example is given in Figure 5.10 where $\alpha' = 2$, and $\mathscr{P}_o = 10^{-4}$. Note that since $\mathscr{E}$ is real, we plot $\mathscr{E}$ and not $|\mathscr{E}|$.

Now that we have shown how the phase waves propagate through the pulse we will discuss, numerically, the

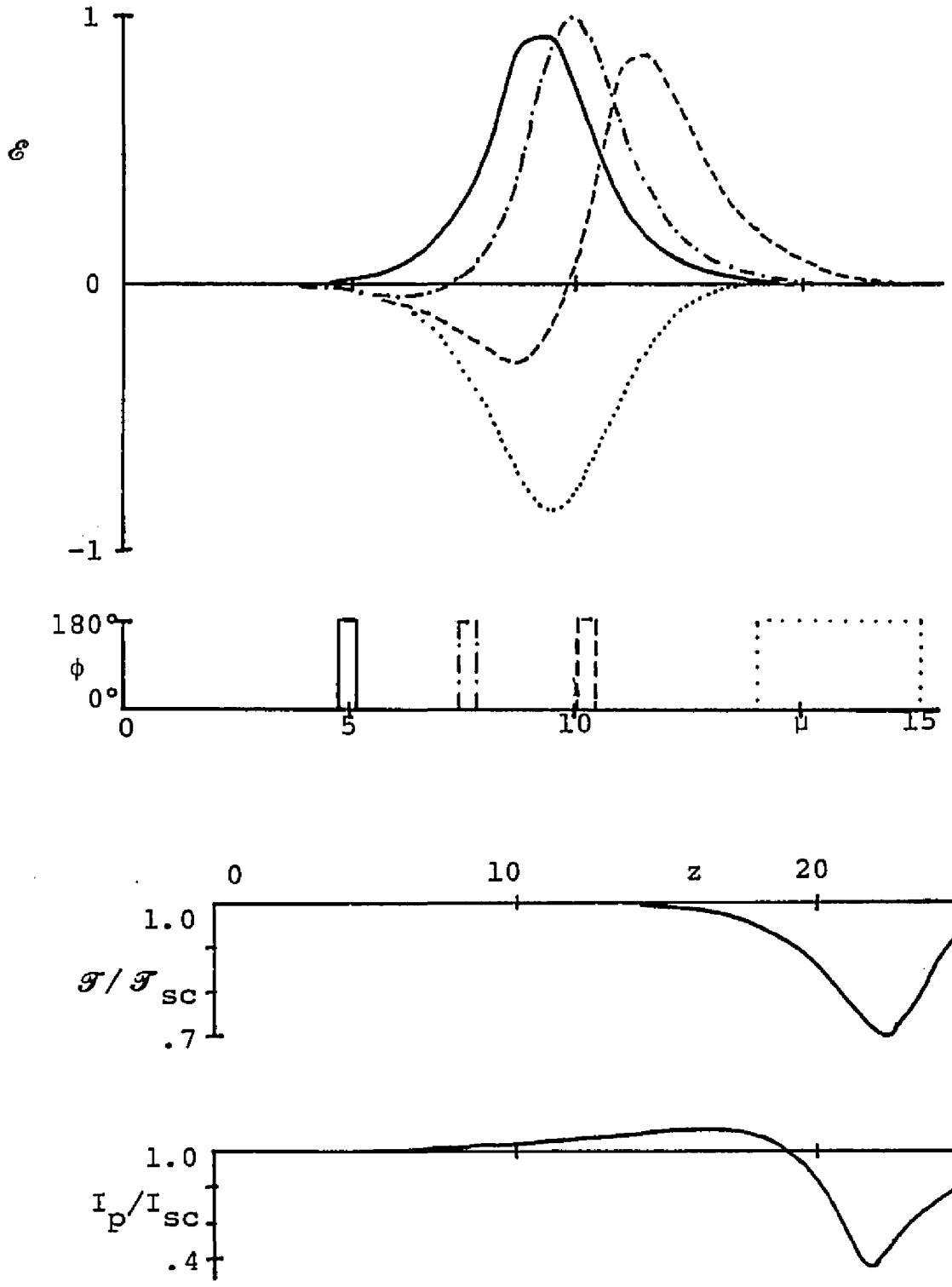

Figure 5.10. Changing the sign of $\mathscr{P}_o(z)$ ($\alpha' = 2, \beta = 180°$, $r = 0$, $\mathscr{P}_o = 10^{-4}$).

$z - z_o = 10$ (solid line), 15 (dashed-dotted line), 20 dashed line), 25 (dotted line). NOTE: $\mathscr{E}$ is graphed and not $|\mathscr{E}|$.

relationship between the phase wave and the energy and peak power fluctuations. The point of maximum energy and power decrease in any episode occurs when the maximum of the phase wave reaches the peak of the pulse. Because of the central role of the maximum value of the phase wave at the peak of the pulse, we denote it with the special symbol Φ_{max}, where

$$\Phi_{max} = \max_{z} |\phi(\mu \sim \tau_d, z)| . \tag{5.3}$$

Here the range of z goes over the duration of an individual phase wave, which is normally well resolved. In equation (5.3) we indicate that the peak of the phase wave is not well resolved as the phase wave approaches, by writing "$\mu \sim \tau_d$". This can be seen from the figures in this chapter, where the peak of the phase wave shifts back by 20% to 50% when a large phase wave approaches. This creates no problem because, as can be seen from the figures, the phase wave is slowly varying near the peak of this pulse. We note that some care must be taken in using this definition for Φ_{max}, equation (5.3), since the phase wave loses its characteristic shape as it passes the peak of the pulse. This problem can be avoided by considering the maximum over z only for z up until the phase wave begins losing its characteristic shape.

We also define new symbols $\mathscr{T}_{min}$ and I_{min} as the minimum energy and peak power, respectively, in one excursion. We find, empirically, that the phase waves have basically the same shape at the peak of the pulse so that we can quantify to within 10% (which is satisfactory for our purposes) the energy and power fluctuations with the single variable Φ_{max} rather than with the more fundamental variables, r and β. We show in Figure 5.11 how the energy and peak power vary with this parameter and with the gain α' by plotting the curves for $\alpha' = 2, 5, 10, 20,$ and 40. This figure will be used in the next chapter and may be of experimental interest.

The gradual diminishing of the energy fluctuations with increasing gain is obvious in Figure 5.11a. As the gain increases, the phase waves move faster and the pulse width becomes narrower. The interaction time between the phase wave and the pulse is therefore reduced and the destruction is less marked. Of course, for Φ_{max} near 180° the phase wave is nearly a square wave with amplitude $\sim$180° and so large energy fluctuations ($\sim$30%) still occur.

Later on, we will use a fortuitous property of the energy (as opposed to the power) fluctuations, namely, that they can be treated as if they follow adiabatically the instantaneous magnitude of the phase wave at the peak of

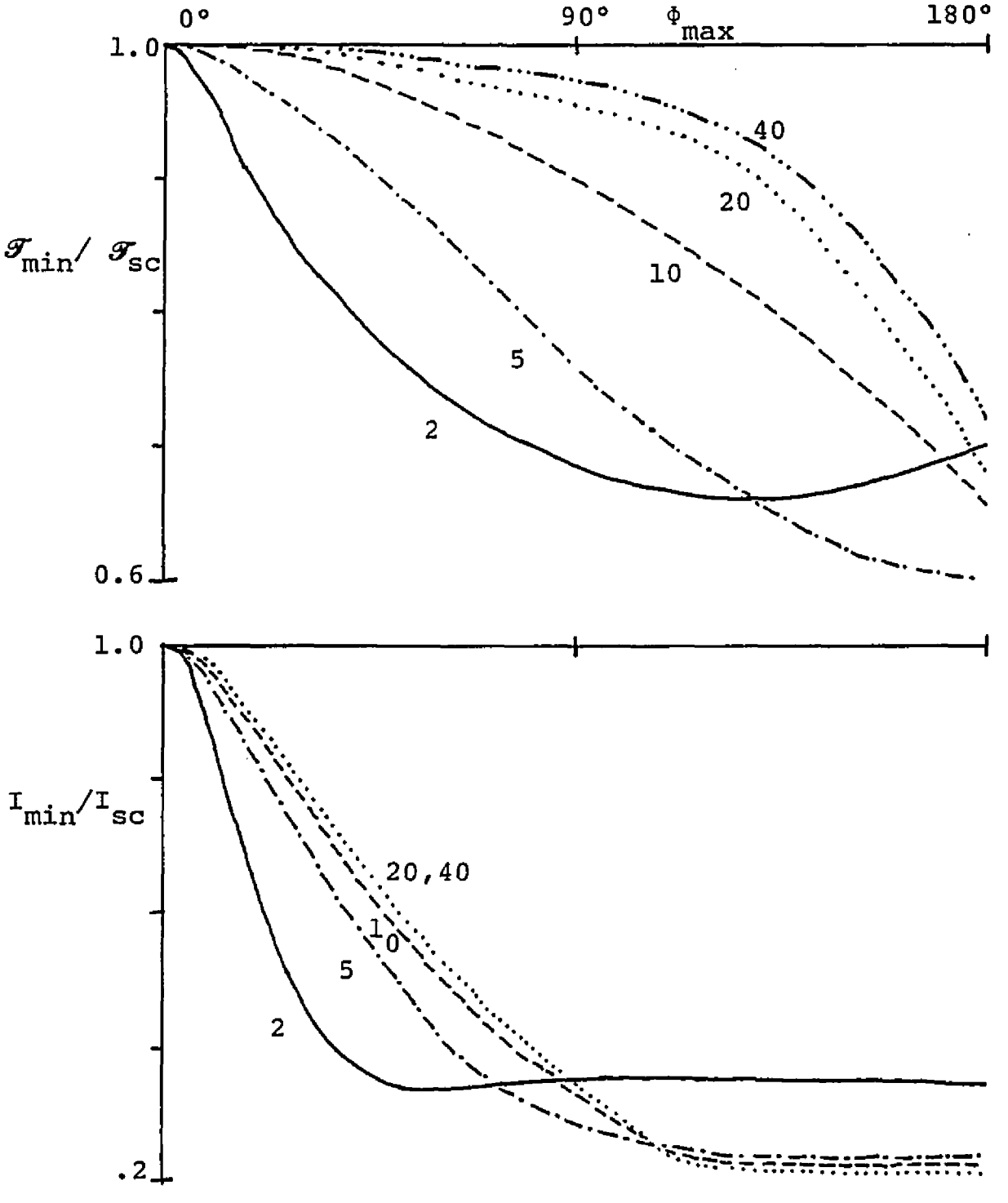

Figure 5.11. Minimum energy and peak power vs. Φ_{max}. $\alpha' = 2$ (solid line), 5 (dashed-dotted line), 10 (dashed line), 20 (dotted line), 40 (dot-dot-dotted-dashed line in the energy graph, dotted line in power graph).

the pulse, which is $|\phi(\mu \sim \tau_d, z)|$ (recall that the peak of the pulse is not well defined). This adiabatic property is physically correct (to within the 10% uncertainty in Figure 5.11) for the destructive half of the episodes. The recovery of the waves, however, is a complicated process in which the peak shifts forward in time quite rapidly, separating away from the phase wave. If one continues to view the phase wave at the same value of μ where it caused the maximum destruction, one finds that it dies away at almost the same rate as the wave recovers. We thus make no additional error by the useful fiction that the interaction is adiabatic throughout the entire interaction. Hence, the energy curve in Figure 5.11a can be taken to define the instantaneous value of the fluctuation $\mathscr{T}(z)/\mathscr{T}_{sc}$, as a function of $|\phi(\mu \sim \tau_d, z)|$. We will use this in Chapter 7 to predict the energy distribution function. Since the peak power is not adiabatic (note the initial increase in power in the figures), we do not attempt to compute that distribution function.

To close this chapter, we discuss numerically some important dynamical effects that enter into the determination of Φ_{max} from the fundamental parameters β and r. This discussion will be repeated analytically in the next chapter. When $r = 0$ (which is, of course, not physical

when $\mathscr{P}_o(z)$ is stochastic), β enters the equation for $\mathscr{P}_o(z)$, equation (5.1), only in the term $\exp(i\beta)$. Thus we need only consider β for $|\beta| \leq 180°$. However this is no longer true when $r > 0$ since then β does not occur modulo 360°. If $0 < \beta < 180°$, the phase wave behaves as in Figures 5.2-5.9, namely, it spreads out and decays in height. However if $180° < \beta < 360°$ the phase wave initially varies in exactly the opposite fashion, namely it narrows and increases in height. When Φ_{max} reaches 180°, the phase wave becomes discontinuous. When the phase wave again settles down, it has "flip-flopped" and becomes negative (i.e., $\theta_{\mathscr{P}} < \theta_{\mathscr{E}}$ so $\phi = \theta_{\mathscr{P}} - \theta_{\mathscr{E}} < 0$).

In order to explain this strange behavior in some detail, let us begin with an example. In Figure 5.12a, b, c, and d we plot $|\mathscr{E}|$, $\theta_{\mathscr{E}}$, $|\mathscr{P}|$, $\theta_{\mathscr{P}}$, and ϕ before (a and b), during (c), and after (d) this "flip-flop" has occurred. The parameters are $\alpha' = 2$, $\beta = 200°$, $r = 2$, and $\mathscr{P}_o = 10^{-4}$. In Figure 5.12a (where $z - z_o = 4.5$) we see that $\theta_{\mathscr{P}}$ and $\theta_{\mathscr{E}}$ have steep negative slopes corresponding to the points where $|\mathscr{P}|$ and $|\mathscr{E}|$ are near zero. In Figure 5.12b ($z - z_o = 5.5$) we see that the slopes of $\theta_{\mathscr{P}}$ and $\theta_{\mathscr{E}}$ have decreased further and become even steeper negative. Again this steepening corresponds to the points where $|\mathscr{P}|$ and $|\mathscr{E}|$ are now even closer to zero. This steepening occurs because, in the neighborhood where $|\mathscr{P}|$

Figure 5.12. A "flip-flop" of the phase wave ($\alpha' = 2$, $\beta = 200°, r = 2$, $\mathscr{P}_o = 10^{-4}$).

Figures 5.12a, b, c, d: In the graph of the phase, $\theta_{\mathscr{E}}$ is the solid line, $\theta_{\mathscr{P}}$ is the dashed line, and ϕ is the dotted line. In the graph of the magnitude $|\mathscr{E}|$ is the solid line and $|\mathscr{P}|$ is the dashed line. $z - z_o = 4.5$ is (a), 5.5 is (b), 6.5 is (c), 7.5 is (d).
Figure 5.12e: The graph of $\mathscr{P}(\mu, z)$ for $z = 5.5$ (the solid line) and 6.5 (the dashed line)
Figure 5.12f: The complete graph of the phase wave. $z - z_o = 4$ (the solid line), 12 (the dashed line), 20 (the dotted line).

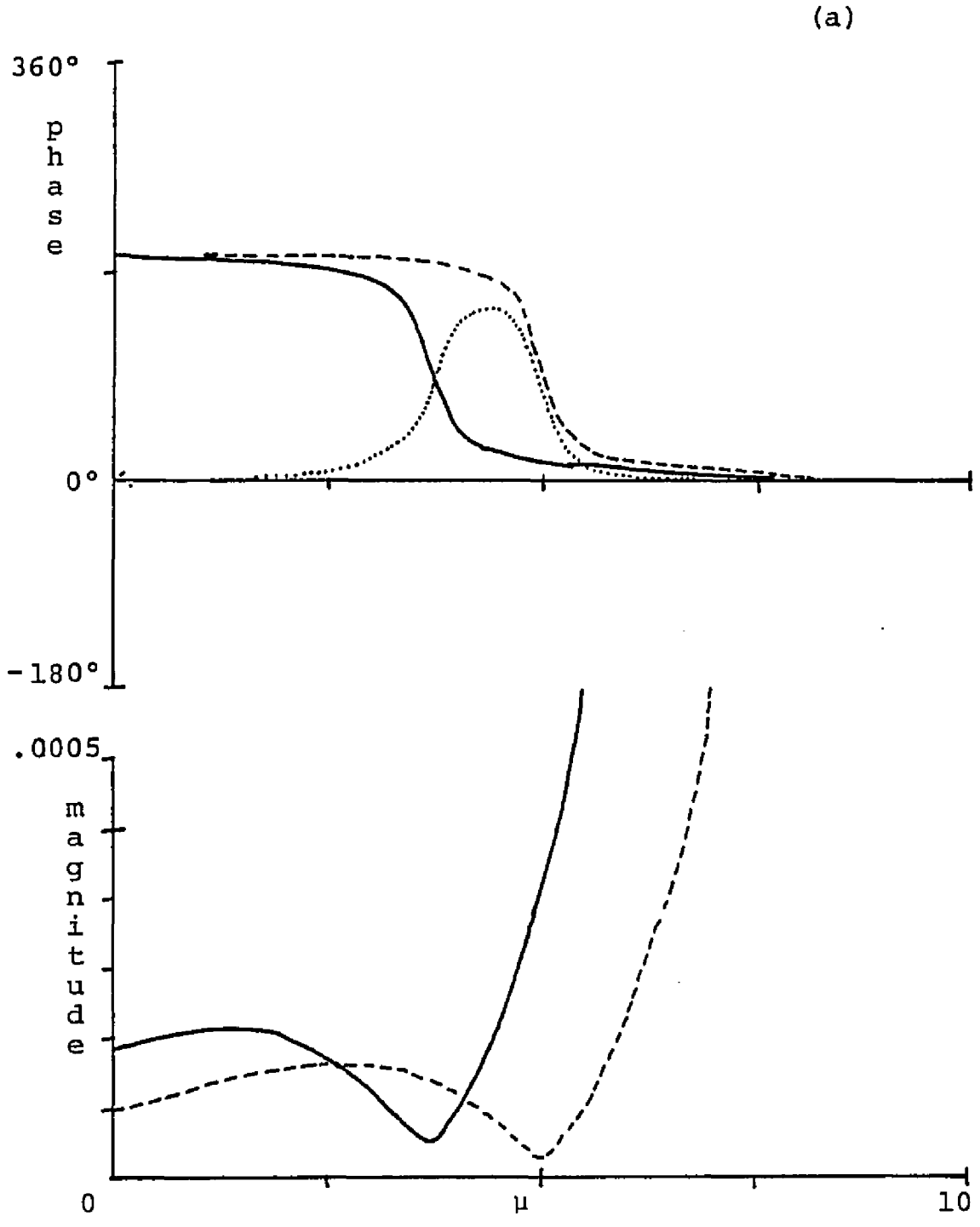

Figure 5.12. A "flip-flop" of the phase wave ($\alpha' = 2$, $\beta = 200°, r = 2$, $\mathcal{P}_o = 10^{-4}$).

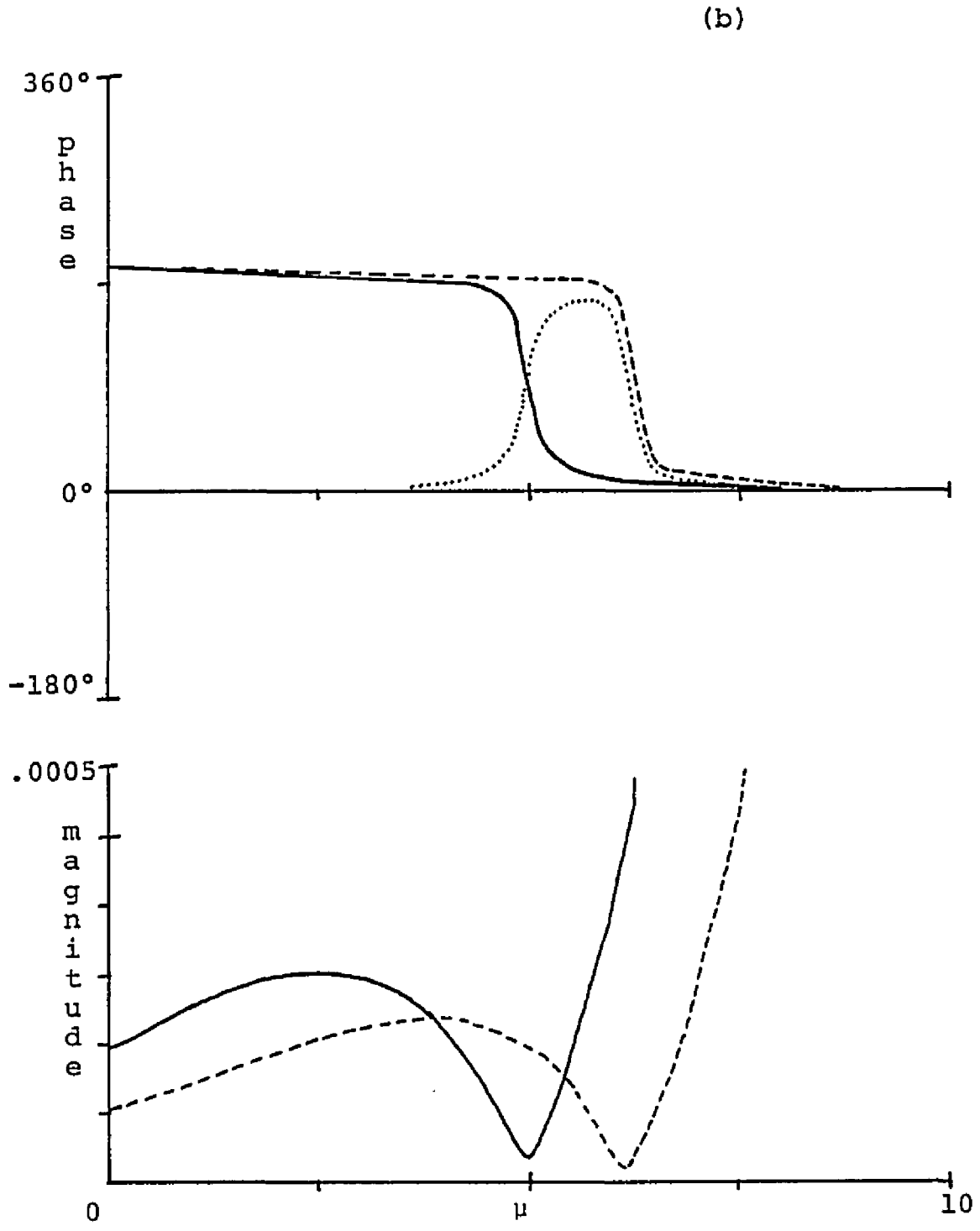

Figure 5.12 (continued). A "flip-flop" of the phase wave ($\alpha' = 2, \beta = 200°, r = 2, \mathcal{P}_o = 10^{-4}$).

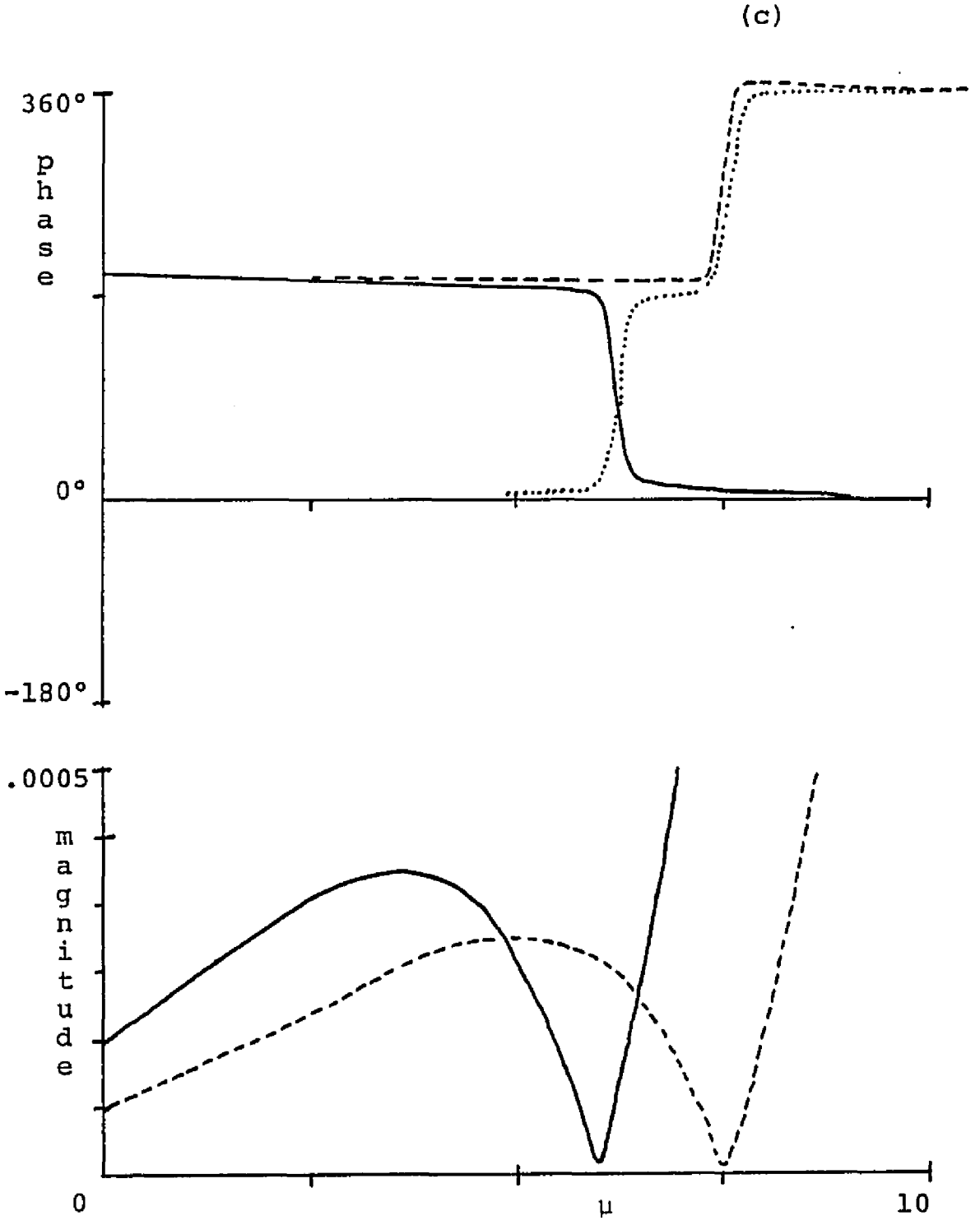

Figure 5.12 (continued). A "flip-flop" of the phase wave ($\alpha' = 2, \beta = 200°, r = 2, \mathscr{P}_o = 10^{-4}$).

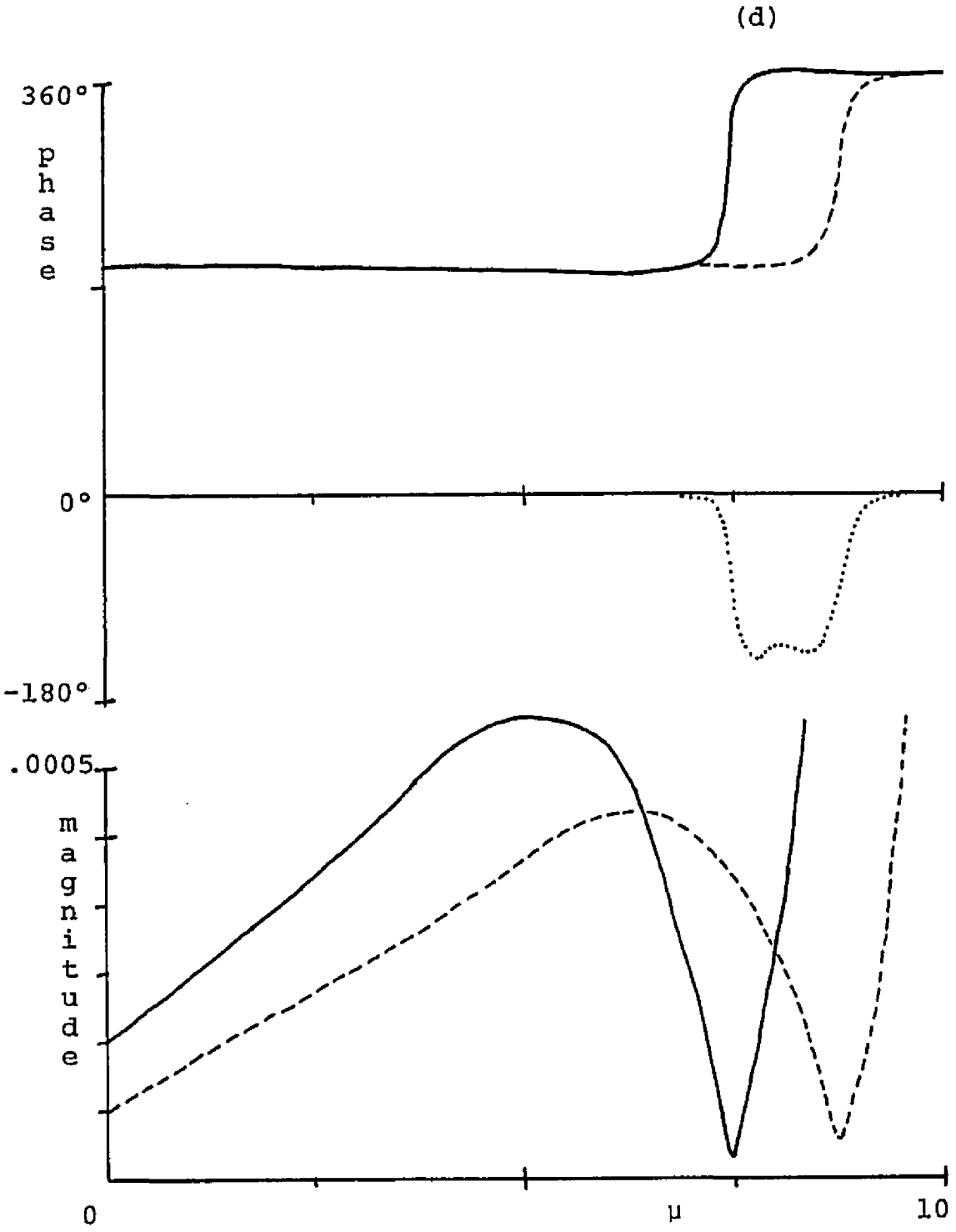

Figure 5.12 (continued). A "flip-flop" of the phase wave ($\alpha' = 2, \beta = 200°, r = 2, \quad \mathscr{P}_o = 10^{-4}$).

(e)

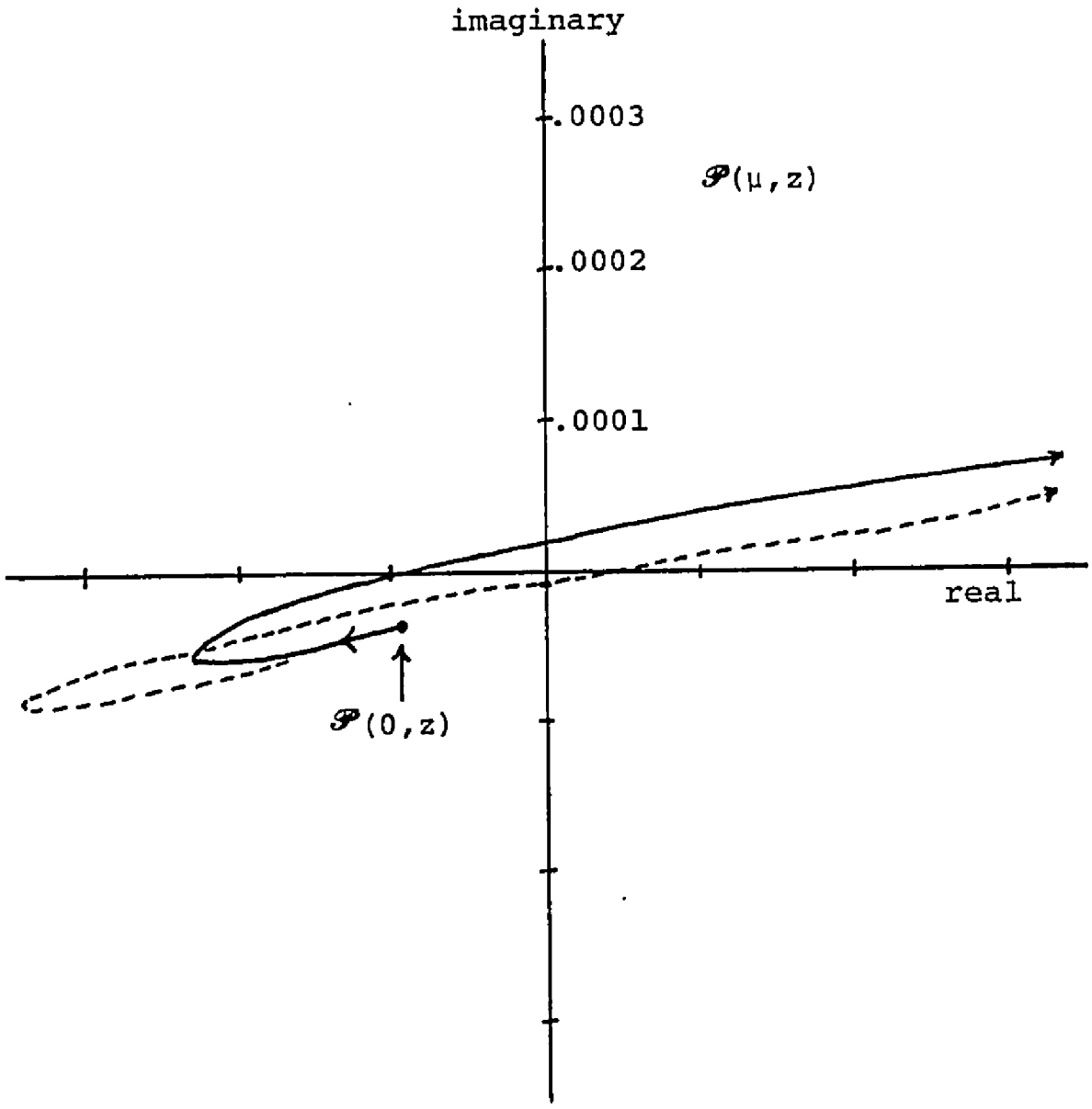

Figure 5.12 (continued). A "flip-flop" of the phase wave ($\alpha' = 2, \beta = 200°, r = 2, \quad \mathscr{P}_o = 10^{-4}$).

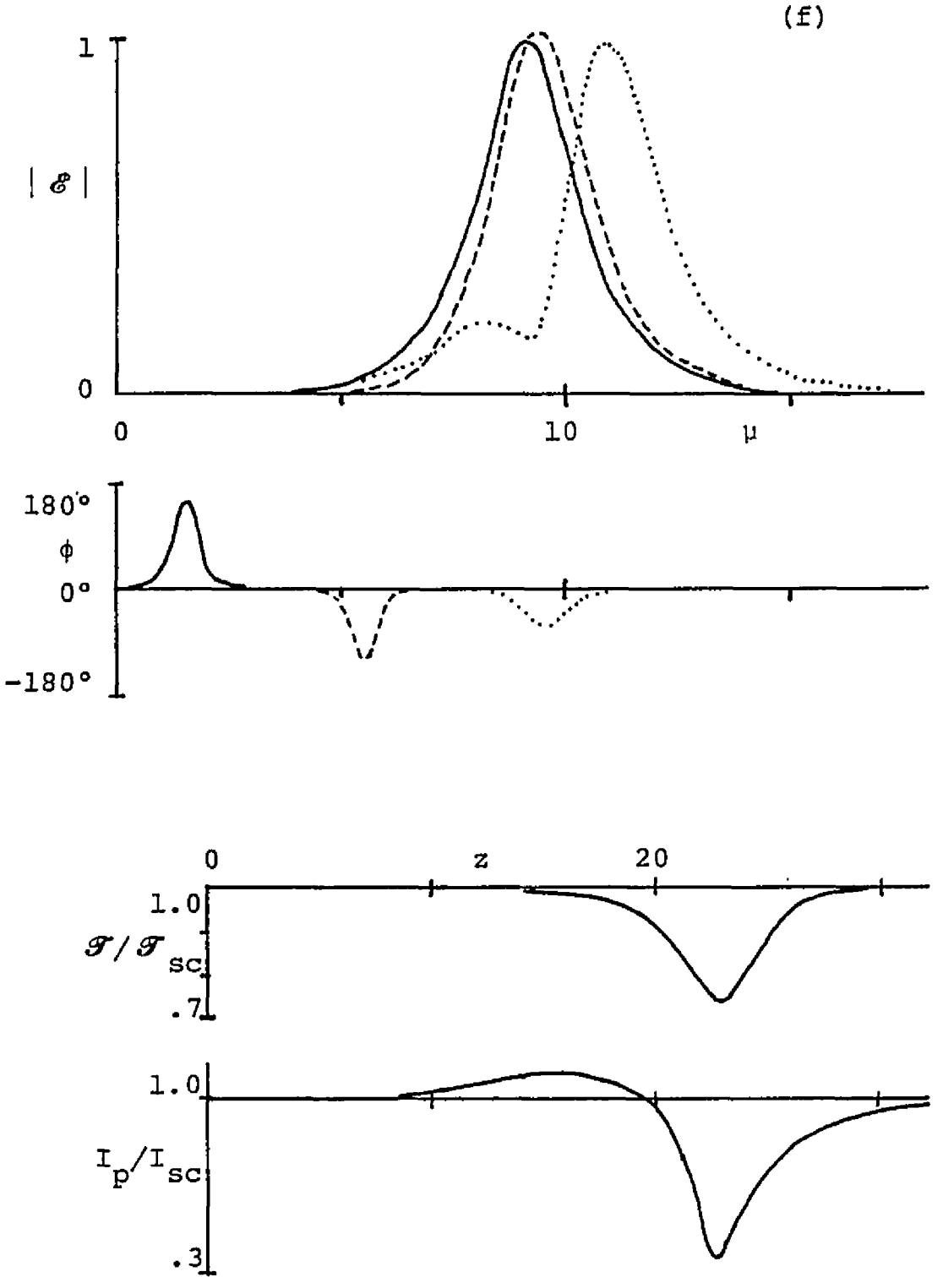

Fighre 5.12 (continued). A "flip-flop" of the phase wave ($\alpha' = 2, \beta = 200°, r = 2, \quad \mathscr{P}_o = 10^{-4}$).

is small, $\theta_{\mathscr{P}}$ can change rapidly. At the point where $|\mathscr{P}|$ becomes zero, $\theta_{\mathscr{P}}$ indeed becomes discontinuous and changes by 180°. In Figure 5.12c ($z - z_o = 6.5$) we plot the curves right after $|\mathscr{P}|$ has reached zero and begun to increase again. The phase of $\theta_{\mathscr{P}}$ now increases to 360°.

The reason for this "flip-flop" can be understood by considering $\mathscr{P}(\mu,z)$, which is a differentiable function of μ. Consider $z - z_o = 5.5$ (Figure 5.12b). Then $\mathscr{P}(0,z)$ has a magnitude of $\sim.0001$ and phase of $\sim 200°$, while for $\mu \gtrsim 30$, $\mathscr{P}(\mu,z)$ has large magnitude and phase near 0. Graphing $\mathscr{P}(\mu,z)$, in Figure 5.12e for $z - z_o = 5.5$ (the solid line), we see that the curve goes above the origin so the phase goes from 200° to 0°. However this curve is moving downward with increasing z and so for $z - z_o = 6.5$ (the dashed line) the curve has passed through the origin and so the phase goes from 200° to 360°.

Referring back to Figure 5.12d ($z - z_o = 7.5$) we see that $|\mathscr{E}|$ has also passed through zero and so the phase wave is returning to its usual shape.

To see that this "flip-flop" takes place when $\phi = 180°$ we need to consider the Maxwell-Bloch equations in polar coordinates, equation (5.2). Concentrating on equation (5.2b) $|\mathscr{P}|\frac{\partial}{\partial\mu}\theta_{\mathscr{P}} = -|\mathscr{E}|n \sin\phi$, we see that the slope of $\theta_{\mathscr{P}}$ changes sign when $\phi = 180°$ (recall $n \approx +1$). Recall

that in Figure 5.12a the phase wave is narrowing and increasing in height before the "flip-flop". Thus, just as ϕ reaches $180°$ the slope of $\theta_{\mathscr{P}}$ switches from negative to positive. Thus, except for the very short interval between $|\mathscr{P}|$ passing through zero and $|\mathscr{E}|$ passing through zero, we have $|\phi| \leq 180°$ or $\Phi_{max} \leq 180°$.

Waves that change in this way cause the most violent episodes of pulse destruction (e.g., causing the pulse to split into two peaks), since the initial increase in the peak of the phase wave delays the process of attenuation. Thus, comparing Figure 5.12f, where the entire curve is plotted, to Figure 5.2 we see that this "flip-flop" effect has created a larger energy and power fluctuation when $\beta = 200°$ than occurred when $\beta = 160°$, because Φ_{max} is larger in Figure 5.12. However, if β is too close to $360°$, the phase wave decays away rapidly since, once the "flip-flop" has occurred, the phase wave behaves as if the initial change in angle had been $\beta - 360°$, which is small. Thus the maximum pulse destruction occurs for β near $180°$. (Values of $\beta > 360°$ are statistically insignificant, but we mention that they also will perform this "flip-flop" and afterwards $\theta_{\mathscr{E}}$ and $\theta_{\mathscr{P}}$ will start at β and go to the nearest multiple of $360°$.)

CHAPTER 6

ANALYTICAL EXPRESSION FOR THE PHASE WAVE

In this chapter we find an analytical expression for the phase wave at the leading edge of the pulse, where the Maxwell-Bloch equations are linear. Comparing this analytical expression with our numerical computations, we find that this expression remains valid, to within $\sim$10%, even in the nonlinear region of the pulse. Thus, we can find the speed and the attenuation of the phase wave as it passes through the pulse. Finally, we will use this analytical expression to discuss the "flip-flop" of the phase wave.

To find the analytical expression for the phase wave, we let the initial polarization, $\mathcal{P}_o(z)$, be deterministic and given by equation (5.1). Then, at the leading edge of the pulse (μ small), $|\mathcal{E}\mathcal{P}| << 1$ and $n \approx +1$. Thus, the Maxwell-Bloch equations, equation (3.2), reduce to

$$\frac{\partial}{\partial \mu} \mathcal{P} = \mathcal{E} - \mathcal{P}$$

$$\frac{\partial}{\partial z} \mathcal{E} = \alpha' \mathcal{P} - \mathcal{E} \ . \tag{6.1}$$

The equation for the phase wave is then found (in Appendix B) to be

$$\phi(\mu,z) \approx \operatorname{arccot}\left[\frac{S^2 + (\tan^2\beta/2)(T^2 - \frac{1}{4})}{S \tan \beta/2}\right] \qquad (6.2)$$

where

$$S = \sqrt{\pi(z-z_0)} + \frac{r}{2}\left(\frac{\tan \beta/2}{\beta/2} - 1\right)$$

$$T = \alpha'\mu - (z - z_o) + \frac{r}{2}.$$

We fix $r \lesssim 1$, and assume that $z - z_o >> r$, and that S is not too near zero. The range of the arccotangent is $(0,\pi)$ when the denominator of the argument of equation (6.2) is positive and $(-\pi,0)$ when it is negative.

The derivation of equation (6.2) presented in Appendix B shows that our formula for $\phi(\mu,z)$ is valid at the leading edge of the pulse. In addition, the numerical computations show that equation (6.2) remains valid, to within $\sim$10%, in the main body of the pulse until the phase wave reaches the peak of the pulse. A typical computation is graphed in Figure 6.1 where we compare the analytical expression (the solid line) with the numerical computation (the dashed line). The parameters are the same as in

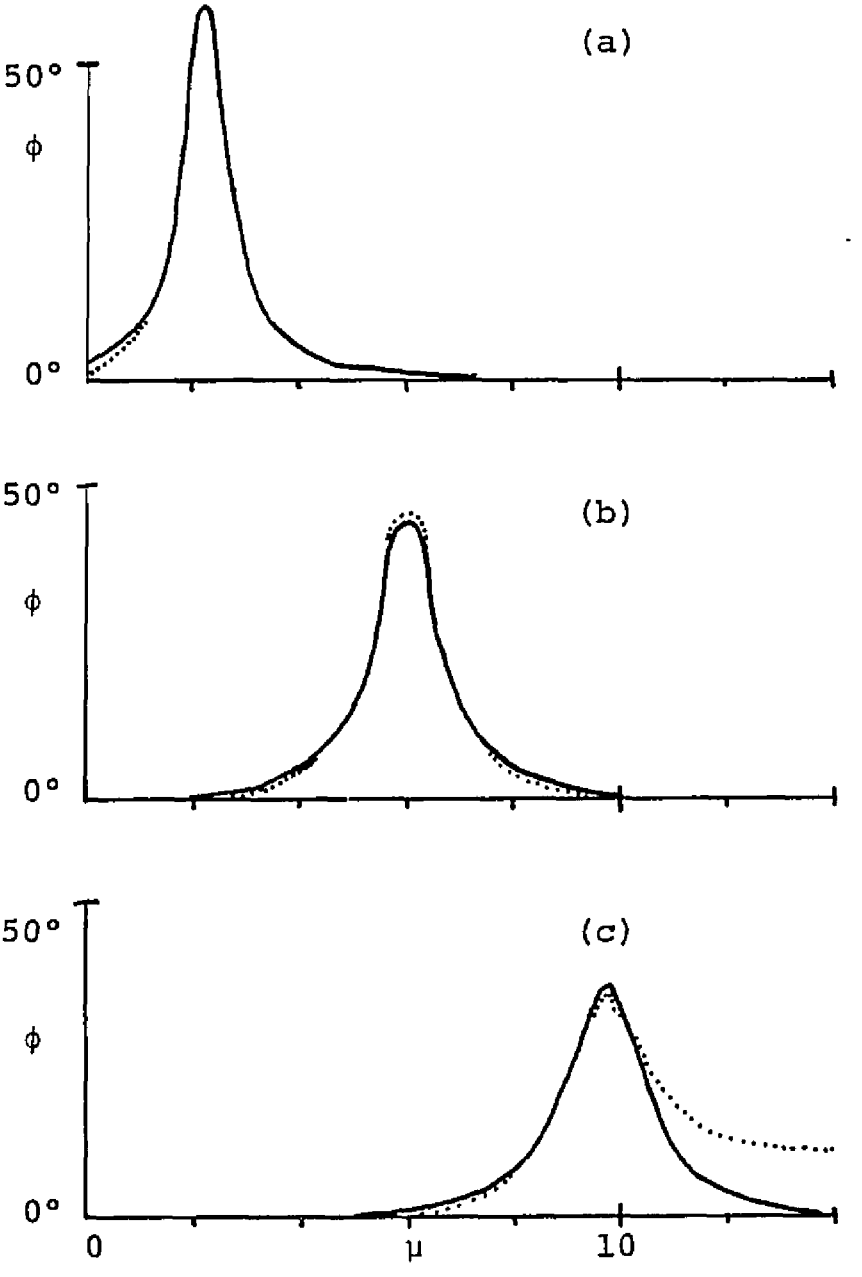

Figure 6.1. A comparison between the analytic expression (the solid line) and the numerical computation for the phase wave.

($\alpha' = 2, \beta = 160°, r = 1, \mathscr{P}_o = 10^{-4}$) $z - z_o = 4$ is (a), 10 is (b), 16 is (c).

Figure 5.2, namely $\alpha' = 2$, $\beta = 160°$, $r = 1$, and $\mathscr{P}_o = 10^{-4}$. The curves are plotted at the same values of $z - z_o$ as Figure 5.2, namely $z - z_o = 4$ (a), $= 10$ (b), and $= 16$ (c). The analytical expression can be seen to be extremely accurate until the phase wave reaches the peak of the pulse (in Figure 6.1c). This accuracy would be maintained if we had used any of the other figures in Chapter 5.

Now we return to the analytical expression for $\phi(\mu,z)$, equation (6.2), and find the speed and the attenuation of the phase wave. For fixed z, the maximum value of $|\phi|$ occurs when

$$T = \alpha'\mu - (z - z_o) + \frac{r}{2} = 0 \qquad (6.3)$$

which shows that the speed of the phase wave is the gain α', i.e.,

$$\frac{\Delta z}{\Delta \mu} = \alpha'.$$

Similarly, near the peak of the phase wave, the first term in the numerator of the argument of equation (6.2) (i.e., S) dominates the second. To obtain a rough estimate for the attenuation of a phase wave, we use the first order Taylor series expansion for the arccotangent and obtain

$$\max_{\mu \geq 0} |\phi(\mu,z)| \propto [\sqrt{\pi(z-z_o)} + \frac{r}{2}(\frac{\tan \beta/2}{\beta/2} - 1)]^{-1}. \qquad (6.5)$$

This shows that the peak of the phase wave is roughly proportional to $(z - z_o)^{-1/2}$. These expressions for the speed and the attenuation of the phase wave agree with all the figures in Chapter 5.

As we have discussed in the last chapter, the magnitude of the fluctuations in energy and peak power are functions of the gain and Φ_{max}, the maximum value of the phase wave at the peak of the pulse. Using equation (6.2) we can now relate Φ_{max} to the parameters β and r, which enter into the boundary condition for $\mathscr{P}_o(z)$, equation (5.1). The absolute value of the phase wave at the peak of the pulse, $|\phi\ \mu \sim \tau_d, z)|$, can be found by evaluating equation (6.2) at $\mu \sim \tau_d$. (Recall that the pulse shifts back by $\sim$30% as a large phase wave approaches.) For fixed z, equation (6.3) shows that the peak of the phase wave occurs at

$$\mu = (z - z_o - \frac{r}{2})/\alpha'.$$

Thus, the peak of the phase wave reaches the peak of the pulse when

$$z - z_o = \alpha' \tau_d + \frac{r}{2}.$$

Thus

$$\Phi_{max} \approx |\phi(\mu \sim \tau_d, z - z_o \sim \alpha' \tau_d + \frac{r}{2})|$$

gives the maximum value of the phase wave in terms of α', β, r, and $\mathscr{P}_o$.

Finally, we notice that the "flip-flop" effect can be obtained from equation (6.2), if we let $r > 0$. When $0 < \beta < 180°$, then $S > 0$ and the denominator of the argument of equation (6.2) is always positive. Thus $0 < \phi < 180°$. Furthermore, as z increases so does S, so that the phase wave takes on the form

$$\phi(\mu, z) \approx \operatorname{arccot}\left(\frac{S}{\tan \beta/2}\right) \tag{6.6}$$

for large S. As S increases, ϕ decreases to zero and so the phase wave attenuates away.

However, when $180° < \beta < 360°$, then $\tan \beta/2 < 0$ and, for $z - z_o$ small enough, $S < 0$. Thus $0° < \phi < 180°$. However, as z increases so does S, and so S approaches zero. For S near zero Φ_{max} is near $180°$, and the numerator of the argument of equation (6.2) can be either

positive or negative depending on μ and z. Thus, ϕ can vary wildly over a small range. In this region, equation (6.2) is not valid. However, as z increases further, S becomes positive so that the denominator of the argument of equation (6.2) becomes negative and so $-180° < \phi < 0°$. Now, as z increases further, the phase wave again takes on the form of equation (6.6) and attenuates away. As we discuss in Appendix B, for $\beta \gtrsim 360°$ equation (6.2) is only valid for z large enough that the "flip-flop" has already occurred.

CHAPTER 7

STOCHASTICS

In the previous chapters, we have satisfactorily accounted for two of the four striking properties of the fluctuations in energy — the unidirectional character of the energy fluctuations and also the weak dependence of the fluctuations on the magnitude of the stochastic boundary condition $\mathscr{P}_o(z)$. The primary goal of this chapter is to quantify the remaining two effects, namely, the episodic nature of the fluctuations and their non-Gaussian character. First, we will show their episodic behavior by estimating the number of phase waves that one expects to see over a given length of amplifier. Second, we will determine a probability distribution function for the energy that we predict would be observed experimentally.

Probability Density Function for the Phase Wave

We consider the boundary condition $\mathscr{P}_o(z)$ as a stochastic variable and derive analytically a probability density function for the phase wave ϕ at the leading edge of the pulse. This function will be used both to estimate the number of phase waves one expects to observe and to determine the energy distribution.

Let us fix a point (μ,z) and study the stochastic variable $\phi(\mu,z)$. That is, we fix a distance, z, into the amplifier, fix a time, μ and then, for each "sweep" (i.e., for each realization of the stochastic boundary condition $\mathscr{P}_o(z)$), we observe the phase $\phi(\mu,z)$, at this point. Thus, along with $\phi(\mu,z)$, we have a probability density function, $P\{|\phi(\mu,z)|\}$, which is an ensemble average over the boundary data.

We will find, analytically, this probability density function in the linear region of the Maxwell-Bloch equations. However, all the striking features of the fluctuations occur for the phase wave near the peak of the pulse. Thus, we would like to evaluate the probability density function $P\{|\phi(\mu,z)|\}$, for $\mu \sim \tau_d$. Since numerical comparisons show that the analytical expression for the phase wave is valid, to within $\sim$10%, up to the peak of the pulse, we assume that $P\{|\phi(\mu \sim\tau_d,z)|\}$ is also accurate to within $\sim$10% at the peak of the pulse, even though the actual analysis only guarantees its accuracy at the leading edge of the pulse.

Specifically, we let $\mathscr{P}_o(z)$ be a stochastic variable with mean zero and delta correlation (see equation (4.1)), and we fix (μ,z) with μ at the leading edge of the pulse. Then $\mathscr{E}(\mu,z)$ and $\mathscr{P}(\mu,z)$ are complex

Gaussian stochastic processes as can be seen from the following argument. As discussed in Appendix A, $\mathscr{P}_o(z)$ can be considered the limit of the discrete Gaussian stochastic process $\mathscr{P}_o^{(\Delta z)}(z)$ as $\Delta z \to 0$, where

$$\langle \mathscr{P}_o^{(\Delta z)}(z) \rangle = 0$$

$$\langle \mathscr{P}_o^{(\Delta z)}(z)\, \mathscr{P}_o^{(\Delta z)*}(z') \rangle$$

$$= \begin{cases} \dfrac{\bar{\mathscr{P}}_o^2}{\Delta z} & \text{if } z,\ z' \in [(k-1)\Delta z, k\Delta z) \text{ for some} \\ & k = 1, 2, 3, \ldots \\ 0 & \text{otherwise} \end{cases}$$

and $\langle \cdot \rangle$ denotes the ensemble average. Now, solving the linearized Maxwell-Bloch equations, equation (6.1), we obtain (see Appendix B, equation (b.2))

$$\mathscr{E}(\mu,z) = \alpha' e^{-\mu} \int_0^z e^{-(z-x)} I_o(2\sqrt{\alpha'\mu(z-x)})\, \mathscr{P}_o(x)\,dx$$

$$\mathscr{P}(\mu,z) = e^{-\mu}\, \mathscr{P}_o(z) + \sqrt{\alpha'\mu} e^{-\mu} \int_0^z e^{-(z-x)} \frac{I_1(2\sqrt{\alpha'\mu(z-x)})}{\sqrt{z-x}}\, \mathscr{P}_o(x)\,dx. \tag{7.1}$$

Since integrals of Gaussian processes are still Gaussian (Miller 1974, Chapter 4), $\mathscr{E}^{(\Delta z)}(\mu,z)$ and $\mathscr{P}^{(\Delta z)}(\mu,z)$ are Gaussian. As $\Delta z \to 0$ the variances of $\mathscr{E}^{(\Delta z)}$ and

$\mathscr{P}^{(\Delta z)}$ remain finite. Thus $\mathscr{E}(\mu,z)$ and $\mathscr{P}(\mu,z)$ are complex Gausian Processes.

From Miller (1974) we find a formula for the joint probability density function of $\mathscr{E}$ and $\mathscr{P}$ in polar coordinates, $f(|\mathscr{E}|,\theta_{\mathscr{E}},|\mathscr{P}|,\theta_{\mathscr{P}})$. Then the joint density function of their phases, $g(\theta_{\mathscr{E}},\theta_{\mathscr{P}})$ is

$$g(\theta_{\mathscr{E}},\theta_{\mathscr{P}}) = \int_0^\infty\int_0^\infty f(|\mathscr{E}|,\theta_{\mathscr{E}},|\mathscr{P}|,\theta_{\mathscr{P}})\,d|\mathscr{E}|\,d|\mathscr{P}|$$

$$= \begin{cases} \dfrac{1-A^2}{4\pi}\,\dfrac{\sqrt{1-A^2\cos^2\phi}+A\cos\phi\,\arccos(A\cos\phi)}{(1-A^2\cos^2\phi)^{3/2}} & \\ \qquad\qquad \text{for } \theta_{\mathscr{E}},\ \theta_{\mathscr{P}} \in (-\pi,\pi) & \\ 0 \qquad\qquad \text{otherwise} & \end{cases} \tag{7.2}$$

where, as usual, $\phi = \theta_{\mathscr{P}} - \theta_{\mathscr{E}}$, and A is defined as

$$A(\mu,z) = \frac{\langle \mathscr{E}(\mu,z)\,\mathscr{P}^*(\mu,z)\rangle}{\sqrt{\langle|\mathscr{E}(\mu,z)|^2\rangle\langle|\mathscr{P}(\mu,z)|^2\rangle}} \tag{7.3}$$

Note that $g(\theta_{\mathscr{E}},\theta_{\mathscr{P}})$ is a function only of ϕ, so the probability density function of ϕ, $P\{\phi\}$ is $2\pi g(\theta_{\mathscr{E}},\theta_{\mathscr{P}})$. Thus

$$P\{|\phi(\mu,z)| = \xi\} = \frac{1-A^2}{\pi}\,\frac{\sqrt{1-A^2\cos^2\xi}+A\cos\xi\,\arccos(A\cos\xi)}{(1-A^2\cos^2\xi)^{3/2}} \tag{7.4}$$

Later we will also need the probability of observing an absolute phase $|\phi(\mu,z)|$ greater than ξ, $P\{|\phi(\mu,z)| \geq \xi\}$. This probability is

$$P\{|\phi| \geq \xi\} = \int_{\xi}^{\pi} P\{|\phi| = \xi\} d\xi \tag{7.5}$$

$$= 1 - \frac{\xi}{\pi} - \frac{A \sin \xi}{\sqrt{1-A^2\cos^2\xi}}\left(1 - \frac{\arccos(A \cos \xi)}{\pi}\right).$$

Equation (7.2) is valid for $\mathscr{E}$ and $\mathscr{P}$ as long as they are complex Gaussian processes with mean zero. However, to evaluate the expectations in equation (7.3), we will need to use equation (7.1), the solutions of the linearized Maxwell-Bloch equations. We assume that μ is large enough (but still in the linear region) so that the $e^{-\mu}\mathscr{P}_o(z)$ term in equation (7.1b) can be neglected. We also assume that $z >> 1$ so that we are in the power-balance region where the SSPs can form. Then, inserting $\mathscr{E}$ and $\mathscr{P}$, as given in equation (7.1), into equation (7.3) yields

$$A = \frac{e^{\alpha'\mu}I_o(\alpha'\mu)-1}{\sqrt{2\alpha'\mu e^{\alpha'\mu}I_o(\alpha'\mu)\{e^{\alpha'\mu}(I_o(\alpha'\mu)-I_1(\alpha'\mu))-1\}}}$$

$$+ O(e^{-\sqrt{z}}) \tag{7.6}$$

where I_o and I_1 are Bessel functions with imaginary

arguments. Notice that A is independent of z for $z >> 1$, and so the probability density function, $P\{|\phi(\mu,z)|\}$, is only a function of μ. We will denote this by $P\{|\phi(\mu)|\}$. The analytical expression $P\{|\phi(\mu)|\}$, with A as given in equation (7.6), has been compared with numerical computations for μ at the leading edge of the pulse and found to agree at the 97% confidence level.

Recall that we are actually interested in the probability density function at the peak of the pulse, $P\{|\phi(\mu \sim \tau_d)|\}$, since the phase waves cause all of the unusual fluctuations there. Also recall our assumption from numerical comparisons $P\{|\phi(\mu \sim \tau_d)|\}$ is valid, to within $\sim$10%, at the peak of the pulse. Thus to calculate $P\{|\phi(\mu \sim \tau_d)|\}$ we can use equation (7.5) where A is given in equation (7.6). In Figure 7.1a we graph $P\{|\phi(\mu \sim \tau_d)| = \xi\}$ versus ξ using the same parameters as in Figure 4.1, namely $\alpha' = 2$ and $\overline{\mathcal{P}_o} = 10^{-6}$. We also mention that A can be simplified near the peak of the pulse to

$$A(\mu) = 1 - \frac{1}{8\alpha'\mu} + O((\alpha'\mu)^{-2}).$$

Episodic Character of the Fluctuations

Let us turn our attention to the episodic character of the energy and peak power fluctuations. Since one energy

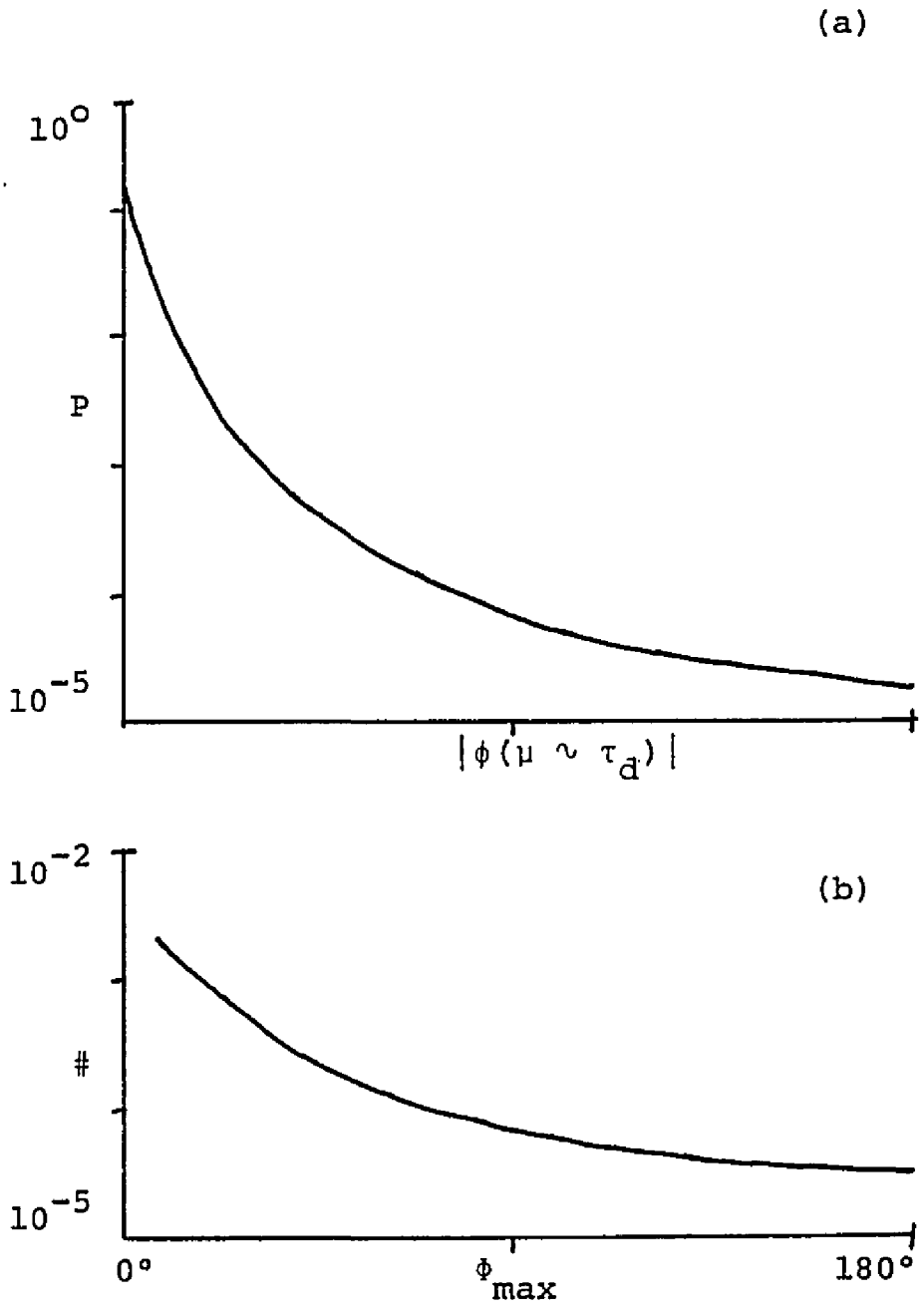

Figure 7.1. Semilog graph of $P\{|\phi(\mu \sim \tau_d)|\}$ and $\#\{\Phi_{max}\}$.

and power fluctuations corresponds to one phase wave passing the peak of the pulse, we begin by estimating the number of phase waves per unit length. Thus, we will calculate $\#\{\Phi_{max} = \rho\}$, the number of phase waves per unit length whose maximum absolute height at the peak of the pulse is ρ. (Recall that Φ_{max} is defined by

$$\Phi_{max} = \max_{z} |\phi(\mu \sim \tau_d, z)|$$

where z goes over an individual phase wave.)

In order to estimate the number of phase waves per unit length, let us first consider a thought experiment. Let us follow the "sweep" down the amplifier, looking near the peak of the pulse. We will observe the magnitude of the phase wave and plot it, $|\phi(\mu \sim \tau_d, z)|$, as a function of z. (Of course, we do not begin looking at the phase until we are in the power balance region.) In Figure 7.2 we have graphed a typical result of our thought experiment. In Figure 7.2a we plot the complete pulse, showing the phase waves (the solid black shapes) from their formation in the stochastic boundary condition through their disappearance once they have passed the peak of the pulse. In Figure 7.2b we graph the phase that we would see in our thought experiment if we were sitting at $\mu \sim \tau_d$ in Figure 7.2a. To

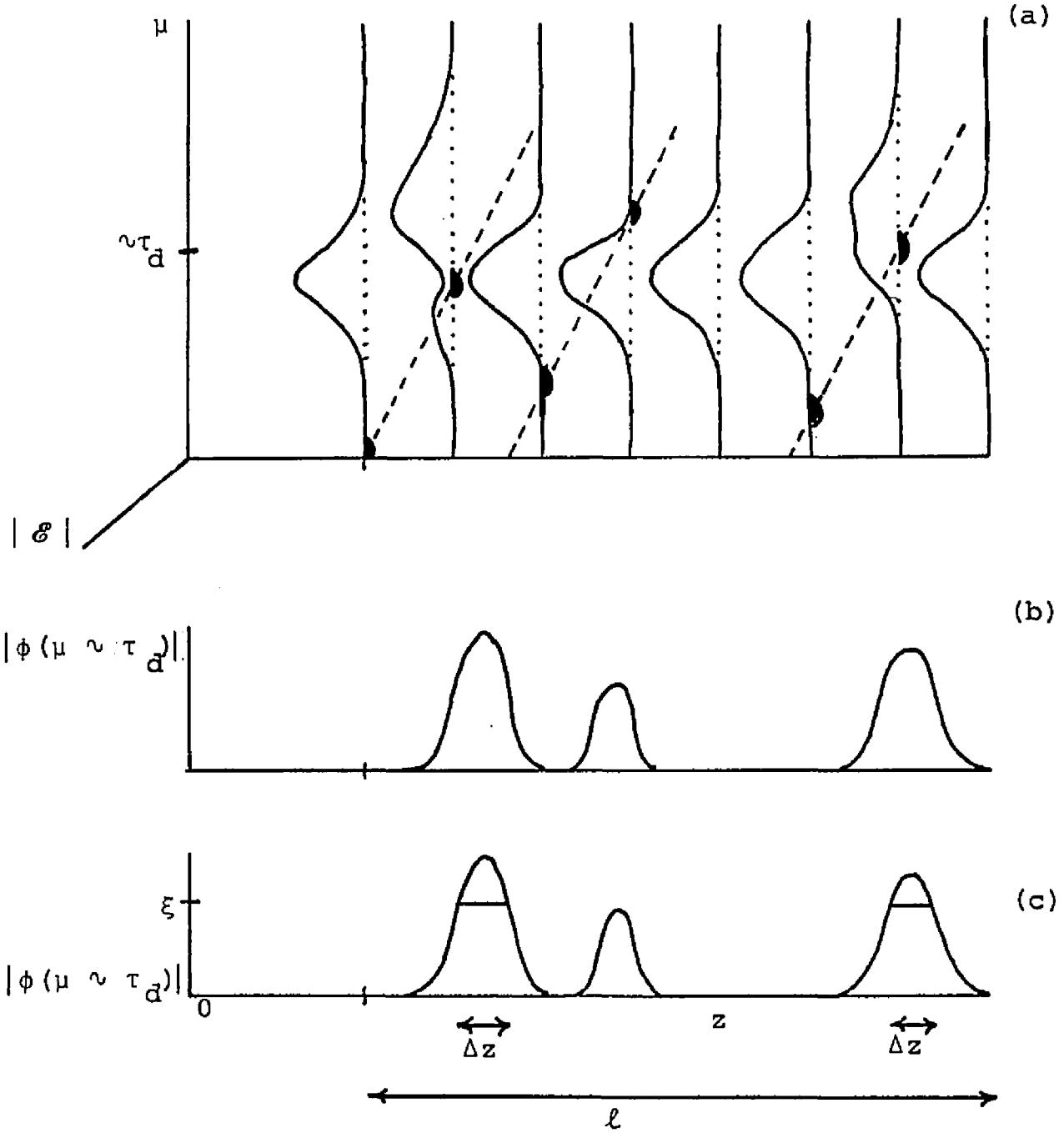

Figure 7.2. Typical graph of the thought experiment. In (a) the entire electric field, $|\mathcal{E}|$, is graphed, in (b) the phase, $|\phi|$, that the observer at $\mu \sim \tau_d$ would see, and in (c) the length that $|\phi| > \xi$.

estimate the number of phase waves per unit length with $\phi_{max} = \rho$, it is merely necessary to count the number of maxima at ρ in Figure 7.2b and divide by the total length, ℓ.

With this thought experiment firmly in mind, let us estimate the number of phase waves per unit length analytically. To do so, we will use the probability distribution function $P\{|\phi(\mu \sim \tau_d)| \geq \xi\}$ equation (7.5), which was determined analytically in the last section. Recall that this probability distribution was calculated by taking an ensemble average over the boundary data $\mathscr{P}_o(z)$. To agree with our thought experiment, we will convert this ensemble average to an average over z of $|\phi(\mu \sim \tau_d, z)|$. To calculate $P\{|\phi(\mu \sim \tau_d)| \geq \xi\}$, averaging over z instead of over $\mathscr{P}_o(z)$, let us return to Figure 7.2, which is the phase we observe as we travel down the amplifier. To estimate the probability of seeing a phase whose absolute value is greater than ξ, we merely find the length, Δz, that the phase is greater than ξ and divide by the total length, ℓ. That is,

$$P\{|\phi(\mu \sim \tau_d)| \geq \xi\} = \lim_{\ell \to \infty} \frac{\Delta z}{\ell} = \lim_{\ell \to \infty} \frac{\sum \Delta z_{\pm}}{\ell} \qquad (7.7)$$

(see Figure 7.2c).

(In this replacement of ensemble averages with space averages, we have not merely assumed ergodicity. This is because $\mathscr{E}(\mu,z)$ and $\mathscr{P}(\mu,z)$ only depend on a portion of the boundary data, that is, $\mathscr{E}$ and $\mathscr{P}$ only depend upon $\mathscr{P}_o(x)$ for x belonging to a small interval $z - z_D \leq x \leq z$. This fact can be seen in the solutions of the linearized Maxwell-Bloch equations, equation (7.1), since the integrands contain the term $\exp\{ -(z - x) \}$. Because of this exponential decay, it is possible to define a distance z_D beyond which the integrands make a negligable contribution to the integrals. This small interval amounts to a small domain of dependence over which $\mathscr{P}_o(x)$ influences $\mathscr{E}(\mu,z)$ and $\mathscr{P}(\mu,z)$. Returning to the point of this paragraph, we can thus replace ensemble averages over $\mathscr{P}_o(x)$ by averages over z (as long as our averages are over many of these domains of dependence). Said differently, the small width of this domain of dependence allows us to view long amplifier lengths as consisting of many independent experiments. With this viewpoint, ensemble averages can be effected by averages over z.)

In order to estimate the number of phase waves per unit length, $\#\{\Phi_{max} = \rho\}$, we will relate this quantity to $P\{|\phi(\mu \sim \tau_d)| \geq \xi\}$ as defined in equation (7.7), i.e.,

$$P\{|\phi| \geq \xi\} = \lim_{\ell \to \infty} \frac{\Delta z}{\ell}.$$

First, we introduce a function $h(\xi,\rho)$. To understand this function, let us again return to our thought experiment where we plot $|\phi(\mu \sim \tau_d, z)|$ versus z. In this plot, given a phase wave with maximum value ρ, $h(\xi,\rho)$ is the width of the phase wave at the value ξ, where $0 \leq \xi \leq \rho$ (see Figure 7.3).

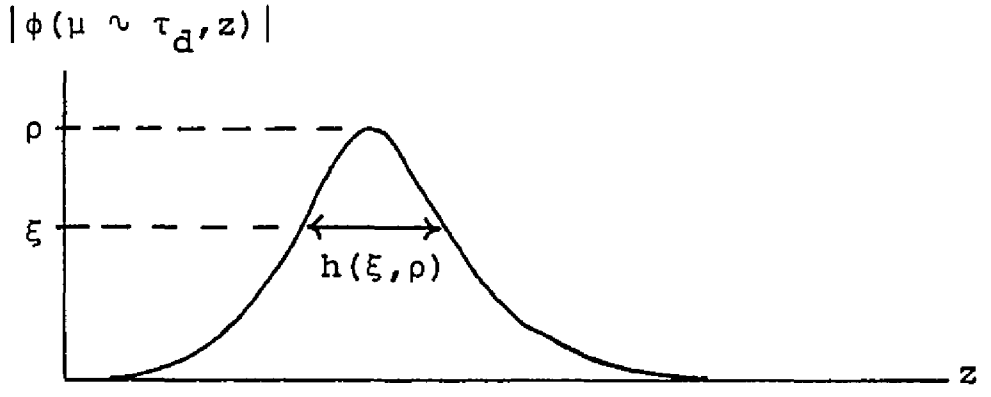

Figure 7.3. $h(\xi,\rho)$.

(From numerical computations the shape of a phase wave, near the peak of the pulse, is dependent mainly on ρ, the gain α', and the location of the peak, τ_d. It is largely independent of the parameters which actually form the phase

wave, namely, the phase shift in $\mathcal{P}_o(z)$, β, and the length over which the phase shifts, r. Thus h can be calculated without knowing how the phase wave was formed from the stochastic boundary data.)

With all these ingredients, we can now find an equation relating $\#\{\Phi_{max} = \rho\}$ to $P\{|\phi(\mu \sim \tau_d)| \geq \xi\}$. So fix ξ and ρ and again refer to our plot of $|\phi(\mu \sim \tau_d, z)|$ versus z. The distance that the phase, $|\phi|$, is greater than ξ, due to one phase wave with maximum height ρ, is $h(\xi,\rho)$. Thus, the distance per unit length (or the fraction of length) that the phase, $|\phi|$, is greater than ξ, due to all the phase waves with maximum height ρ, is

$$h(\xi,\rho)\#\{\Phi_{max} = \rho\},$$

and the total distance per unit length that $|\phi| > \xi$, due to all phase waves, is the sum over all phase waves with maximum height greater than ξ, i.e.,

$$\int_{\xi}^{\pi} h(\xi,\rho)\#\{\Phi_{max} = \rho\}d\rho. \tag{7.8}$$

However, as we mentioned previously, $P\{|\phi(\mu \sim \tau_d)| \geq \xi\}$ is the length, Δz that the phase, $|\phi|$, is greater than ξ divided by the total length ℓ (see equation (7.7)). But

this is exactly what we have calculated in equation (7.8). Thus, we have our relation between $\#\{\Phi_{max} = \rho\}$ and $P\{|\phi(\mu \sim \tau_d)| \geq \xi\}$, namely

$$\int_{\xi}^{\pi} h(\xi,\rho)\#\{\Phi_{max} = \rho\}d\rho \tag{7.9}$$

$$= P\{|\phi(\mu \sim \tau_d)| \geq \xi\} \quad \text{for all} \quad \xi \in (0,\pi).$$

Once we know h, the width of a phase wave, we can solve this ingegral equation (at least numerically) to obtain $\#$, the number of phase waves per unit length.

To calculate h we use the analytical expression for the phase wave, equation (6.2), and let $r = 0$ since the phase waves all have approximately the same shape by the time they arrive at the peak of the pulse. Given a phase wave with maximum value ρ, we find the width at the value ξ (in μ for fixed z) by using equation (6.2). To convert this width to a width in z for fixed μ, we use the fact that the phase wave is slowly varying. Thus we can use the speed of the phase wave, which is α' (see equation (6.4)), to convert from a temporal width to a spatial length and obtain

$$h(\xi,\rho) \approx \sqrt{\frac{2 \sin (\rho-\xi)}{\sin \xi(1-\cos \rho)}} \tag{7.10}$$

Now we can solve equation (7.9) numerically for $\#\{\Phi_{max} = \rho\}$ with h as given in equation (7.10). In Figure 7.1b we solve for $\#$ using the same parameters as in Figure 4.1. The curve is truncated at $\Phi_{max} = 10°$. (Below this value, our approximation to $\#\{\Phi_{max}\}$ goes negative. This inaccuracy is due to the fact that the analytical expression for the phase wave, equation (6.2), gives too large a value out in the wings of the phase wave, and so h, as given in equation (7.10), is too large. Also, small phase waves overlap and are not episodic far away from the region of maximum energy loss. We expect that our choice of h will tend to undercount the small phase waves. We will see below that this is the case.)

We note, from Figure 5.11a, that for $\alpha' = 2$ the phase waves with $\Phi_{max} \geq 20°$ give maximum excursions in energy of more than 10% (i.e., $\mathcal{T}_{min}/\mathcal{T}_{sc} < .9$ in Figure 4.1). We integrate $\#\{\Phi_{max} = \rho\}$ from 20° to 180° and multiply by a distance of 160 to predict that there should be three such excursions (there are four in Figure 4.1a). If we integrate from the cutoff at 10% (3% energy fluctuations) to 20%, we find that there should be two more fluctuations between 3% and 10% (there are five). (Note that one of the fluctuations in Figure 4.1a is less than 3%.) As expected, then, we find the estimate of the number of small fluctuations is somewhat low. (Heuristically, we can

improve our expression for h by replacing the $\sin \xi$ term in the denominator of equation (7.10) by $\sin \xi + .01(\pi - \xi)$ so that h remains bounded as $\xi \to 0$. This replacement raises the number of phase waves to four for energy fluctuations greater than 10% and to three the number of energy fluctuations between 3% and 10%.)

We have just quantified the episodic character of the phase waves and, thus, of the energy and peak power fluctuations. However, we have also quantified another unusual feature of Figure 4.1a. Recall that $1 - \mathcal{T}_{min}/\mathcal{T}_{sc}$ is the magnitude of one energy fluctuation. For Gaussian fluctuations small fluctuations should occur much more frequently than large fluctuations. However in Figure 4.1a we see that the fluctuations whose magnitudes are between 3% and 20% all occur with about the same frequency. This can now be understood from Figures 5.11 and 6.2. The number of large phase waves, at a given Φ_{max}, is small, but all large phase waves correspond to roughly the same energy. The number of small phase waves, at a given Φ_{max}, is large, but small phase waves correspond to a wide range of energies. Hence, the number of phase waves of a given size is nearly constant.

Energy Distribution

Here, we determine the energy distribution that we predict would be observed at the output of the laser. Recall that we have found the probability density function for observing a given phase, ξ, at the peak of the pulse $P\{|\phi(\mu \sim \tau_d)| = \xi\}$, and from Chapter 5 that the energy fluctuations depend adiabatically on the value of the phase wave at the peak of the pulse. Thus we need merely to convert the probability density function at the peak of the pulse into an energy distribution function. As discussed in Chapter 5, that is precisely what Figure 5.11a does when we let the variable on the ordinate be $\mathscr{T}(z)/\mathscr{T}_{sc}$ and the variable on the abscissa be $|\phi(\mu \sim \tau_d, z)|$. Thus, combining equation (7.4), the expression for the probability density function of the phase, with Figure 5.11a, the relation between the phase and the energy, we obtain the energy density function $P\{\mathscr{T}/\mathscr{T}_{sc}\}$. We have calculated this energy density using the same parameters as Figure 4.1 and graphed it in Figure 7.4. We also show a histogram constructed from the numerical data in Figure 4.1a. In view of the fact that the analysis is, by this point, only accurate to $\sim$20% and that the numerical histogram is made up of only ten statistically independent events, the close agreement of these two curves is somewhat fortuitous. We are, nonetheless, justified in

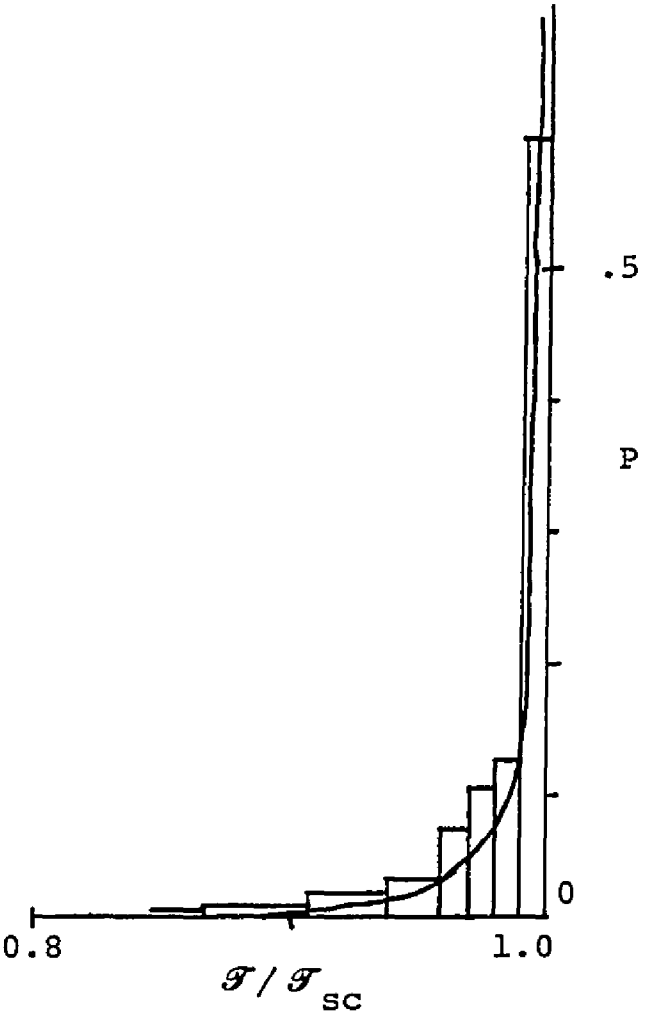

Figure 7.4. Probability of observing a given energy in the output of the amplifier (graph) and the corresponding histogram from Figure 4.1a.

concluding that this method gives a satisfactory prediction of the energy fluctuations.

The energy distribution we have just calculated could have been calculated by continuing the arguments of the previous section. However the energy has the fortuitous property that it is adiabatic. This has allowed us to present the energy distribution by the simpler arguments of this section. As for the power distribution, since the peak power fluctuations are not adiabatic, we would need to use the arguments of the previous section to find the power distribution. We would have to guess some characteristic shape for the power fluctuations and deduce the probability of a given power fluctuation from the number of power fluctuations of a given size. The situation would be made more complicated by the smaller fluctuations arising out of the jitter in $\mathscr{P}_o(z)$ due to amplitude fluctuations in the initial noise (see Chapter 4 and Figure 5.1). While these are statistically independent of the phase changes in the linear region, they are superceded by the phase wave effects in the nonlinear region. For these reasons, we have chosen not to analyze the power in detail.

CHAPTER 8

SUMMARY

In conclusion, in the superradiant regime of the swept-gain amplifier we have seen that there are macroscopic fluctuations in energy and peak power which are unlike normal laser fluctuations. In particular, our fluctuations are (1) macroscopic, (2) unidirectional, (3) episodic, and (4) weakly dependent on the standard deviation of $\mathscr{P}_o(z)$. We have shown that our fluctuations originate in fluctuations in the phase of the stochastic $\mathscr{P}_o(z)$ (i.e., quantum mechanical spontaneous emission). We have shown that these fluctions in the phase of $\mathscr{P}_o(z)$ generate phase waves which travel through the pulse and directly cause all of the effects described above. And, finally, we have plotted an energy distribution function that we predict would be observed in the output of such an amplifier.

Although no experiment, to date, has succeeded in reproducing the exact conditions that we have assumed for our calculations, we emphasize that our method of analysis should be directly applicable to other problems in which superradiant dynamics play an important role. Two physical problems come to mind. The first is the swept-gain

experiments in the far infrared (Ehrlich et al.). In the nonlinear region of this swept-gain device, there are Raman processes associated with the three-level dynamics. Thus, our calculations would have to be modified to include three-level (rather than two-level) quantum mechanics. The second case is Dicke superradiance, which was discussed briefly in Chapter 4. The experiments in Dicke superradiance (MacGillivray and Feld p. 1; Gibbs p. 61; Vrehen p. 79; Rosenberger, Petuchowsky, and DeTemple p. 15 in Bowden et al. 1977) are somewhat more advanced than the far infrared swept-gain experiments. (In that regard, we note that the fluctuations we predict are similar to those in a malfunctioning apparatus so that the experimental conditions must be well controlled.) The linear region of the Dicke problem has a very similar analytic form to the case we deal with here. The main differences are that one has two fields travelling in opposite directions and that one analyzes ensemble averages in the polarization phase at fixed time. In any case, the analytical methods which we have developed in this dissertation could certainly be extended to include these other physical situations.

APPENDIX A

THE NUMERICAL CODE

The numerical code described here solves the fully nonlinear Maxwell-Bloch equations, equation (3.2). It does this by solving the system of ordinary differential equations

$$\frac{\partial}{\partial \mu}\mathcal{P} = \mathcal{E}\, n - \mathcal{P}$$

$$\frac{\partial}{\partial \mu} n = -\mathrm{Re}(\mathcal{E}\,\mathcal{P}^*) \tag{A.1}$$

where $\mathcal{E}$ is calculated by

$$\mathcal{E}(\mu,z) = e^{z_1 - z}\left(\mathcal{E}(\mu,z) + \alpha' \int_{z_1}^{z} e^{x}\,\mathcal{P}(\mu,x)\,dx\right). \tag{A.2}$$

All the methods used in this code are fourth order. At $z = 0$ equation (A.1) is solved by a Runge-Kutta method (Abramowitz and Stegun 1972, p. 896, 25.5.10). For $z > 0$ Adams-Bashforth predictor-corrector is used (Abramowitz and Stegun 1972, p. 896, 25.5.4 and 25.5.5). To calculate the integral in equation (A.2) a Lagrange integration method is used (Abramowitz and Stegun 1972, p. 915). And a finite difference method is used to begin these methods. The code

used to generate Figure 4.1 is a second order version of the above methods and was written by Frederic A. Hopf.

In all the stochastic numerical work $\mathscr{P}_o(z)$, with mean zero and delta correlation, was replaced by a discrete Gaussian stochastic variable, $\mathscr{P}_o^{(\Delta z)}(z)$, where

$$\langle \mathscr{P}_o^{(\Delta z)}(z) \rangle = 0$$

$$\langle \mathscr{P}_o^{(\Delta z)}(z)\, \mathscr{P}_o^{(\Delta z)*}(z') \rangle = \begin{cases} \dfrac{\bar{\mathscr{P}}_o^2}{\Delta z} & \text{if } z,\ z' \in [(k-1)\Delta z, k\Delta z) \\ & \text{for some } k = 1, 2, 3, \ldots \\ 0 & \text{otherwise.} \end{cases}$$

z was typically chosen so that the length z from a phase wave forming to its reaching the peak of the pulse was divided into a few thousand intervals on the z-axis.

APPENDIX B

THE ANALYTICAL EXPRESSION FOR THE PHASE WAVE

As mentioned previously, the Maxwell-Bloch equations are linear at the leading edge of the pulse $(0 \leq \mu \lesssim \tau_d - \tau_p)$ where $|\mathscr{E}\mathscr{P}| << 1$ so $n \approx +1$. In the linear regime the Maxwell-Bloch equations, equation (3.2), reduce to

$$\frac{\partial}{\partial \mu} \mathscr{P} = \mathscr{E} - \mathscr{P}$$

$$\frac{\partial}{\partial z} \mathscr{E} = \alpha' \mathscr{P} - \mathscr{E}$$

as given in equation (6.1). The solutions of these equations can be found either by using Laplace transforms or by noting that this is a Riemann problem (see Hopf et al. 1976). In either case the solutions are

$$\mathscr{E}(\mu,z) = \alpha' e^{-\mu} \int_0^z e^{-(z-x)} I_o(2\sqrt{\alpha' \mu (z-x)})\, \mathscr{P}_o(x) + e^{-z}\, \mathscr{E}(\mu,0) + \sqrt{\alpha' z} e^{-z} \int_0^\mu e^{-(\mu-\nu)} \frac{I_1(2\sqrt{\alpha' z(\mu-\nu)})}{\sqrt{\mu-\nu}}\, \mathscr{E}(\nu,0)\, d\nu \tag{B.1}$$

$$\mathscr{P}(\mu,z) = \sqrt{\alpha'\mu}e^{-\mu}\int_0^z e^{-(z-x)}\frac{I_1(2\sqrt{\alpha'\mu(z-x)})}{\sqrt{z-x}}\mathscr{P}_o(x) + e^{-\mu}\mathscr{P}_o(z)$$

$$+ e^{-z}\int_0^\mu e^{-(\mu-\nu)}I_o(2\sqrt{\alpha'z(\mu-\nu)})\,\mathscr{E}(\nu,0)d\nu,$$

where I_o and I_1 are Bessel functions with imaginary arguments. Here the SSP solution, corresponding to $\mathscr{P}_o(z) \equiv \mathscr{P}_o$, is

$$\mathscr{P}_{SSP,linear}(\mu,z) = \mathscr{P}_o e^{(\alpha'-1)\mu}$$

$$\mathscr{E}_{SSP,linear}(\mu,z) = \alpha'\mathscr{P}_{SSP,linear}(\mu,z).$$

To see for what values of μ this linear SSP is a good approximation to the nonlinear SSP, let us compare the two. The nonlinear SSP, $\mathscr{E}_{SSP,nonlinear}$, given in equation (3.6c), can be rewritten as

$$\mathscr{E}_{SSP,nonlinear}(\mu) = \alpha'|\mathscr{P}_o|\frac{e^{(\alpha'-1)\mu}}{1+[\frac{|\mathscr{P}_o|}{2(1-\frac{1}{\alpha'})}e^{(\alpha'-1)\mu}]^2}.$$

Thus if

$$[\frac{|\mathscr{P}_o|}{2(1-\frac{1}{\alpha'})}e^{(\alpha'-1)\mu}]^2 < \epsilon \qquad (B.2)$$

then

$$1 < \frac{\mathcal{E}_{SSP,linear}(\mu)}{\mathcal{E}_{SSP,nonlinear}(\mu)} \leq 1 + \epsilon.$$

Now equation (B.2) gives

$$\mu \leq \frac{1}{\alpha'-1}\left[\ell n 2\left(\frac{1-\frac{1}{\alpha'}}{|\mathcal{P}_o|}\right) - \frac{1}{2}\ell n\frac{1}{\epsilon}\right] = \tau_d - \frac{1}{2}\frac{1}{\alpha'-1}\ell n\frac{1}{\epsilon}.$$

where τ_d is the location of the peak of the nonlinear SSP. Thus

$$\frac{\mu}{\tau_d} \leq 1 - \frac{1}{2}\frac{1}{\alpha'-1}\frac{\ell n\ 1/\epsilon}{\tau_d}.$$

For example, let $\epsilon = .01$. If $\mathcal{P}_o = 10^{-4}$, then for all $\alpha' \geq 2$, $\frac{\mu}{\tau_d} \lesssim .75$.

To obtain the analytical expression for the phase wave, equation (6.2), let us concentrate on equation (B.1) and find $\mathcal{E}(\mu,z)$. A similar argument works for $\mathcal{P}(\mu,z)$. First, our boundary conditions are

$$\mathcal{P}_o(z) = \begin{cases} \mathcal{P}_o e^{i\beta\frac{z}{r}} & \text{for } 0 \leq z \leq r \\ \mathcal{P}_o e^{i\beta} & \text{for } r < z \end{cases} \qquad \text{(B.3)}$$

$$\mathcal{E}(\mu,0) = \mathcal{E}_{SSP,linear}(\mu,0) = \alpha'\,\mathcal{P}_o e^{(\alpha'-1)\mu}.$$

(We could, instead, let $\mathcal{E}(\mu,0) = 0$, and $z_o >> 1$ so that a SSP would have formed. However, we choose to insert the SSP directly into the boundary condition and then change the boundary polarization immediately.)

Once we have inserted the boundary conditions, equation (B.3), into equation (B.1), then it becomes necessary to evaluate the integrals. The main concern of this appendix is this integration. To begin, we assume that μ and z are large enough so that $I_o(y)$ and $I_1(y)$ can be replaced by

$$\frac{e^y}{\sqrt{2\pi y}}.$$

(From numerical computations of the integrals themselves, this replacement gives 1 - 3% errors in the integrals for $z >> 0$, $0 << \mu \lesssim \tau_d - \tau_p$). Thus, the only regime in which this replacement is not valid is where the phase wave is forming. By the time the phase wave has attained its characteristic shape, as it has in the figures in Chapter 5, our replacement is valid (see Figure 6.1 for further confirmation).

Then, equation (B.1) gives

$$\mathcal{E}(\mu,z) = \alpha' e^{-\mu}\int_0^r e^{-(z-x)}\,\frac{e^{2\sqrt{\alpha'\mu(z-x)}}}{\sqrt{4\pi\,\sqrt{\alpha'\mu(z-x)}}}\,\mathcal{P}_o e^{i\beta\frac{x}{r}}dx$$

$$+\ \alpha' e^{-\mu}\int_r^z e^{-(z-x)}\,\frac{e^{2\sqrt{\alpha'\mu(z-x)}}}{\sqrt{4\pi\,\sqrt{\alpha'\mu(z-x)}}}\,\mathcal{P}_o e^{i\beta}dx \qquad \text{(B.4)}$$

$$+\ \alpha'\,\mathcal{P}_o e^{(\alpha'-1)\mu}e^{-z}$$

$$+\ \sqrt{\alpha' z}e^{-z}\int_0^\mu \frac{e^{-(\mu-\nu)}}{\sqrt{\mu-\nu}}\,\frac{e^{2\sqrt{\alpha' z(\mu-\nu)}}}{\sqrt{4\pi\,\sqrt{\alpha'\mu(z-x)}}}\alpha'\,\mathcal{P}_o e^{(\alpha'-1)\nu}d\nu$$

(Note that the singularities in the integrals are no problem since they are integrable singularities.) These integrals will be evaluated by two distinct methods - lowest order expansions and the method of steepest descent. In order to use lowest order expansions we will need $\frac{r}{z} << 1$ and so we will require this throughout. To begin these methods let us separate the integrals out further:

$$\mathcal{E}(\mu,z) = \mathcal{P}_o\,\frac{\alpha'}{2\sqrt{\pi}}\,\frac{e^{-\mu}}{(\alpha'\mu)^{1/4}}\int_0^r e^{-(z-x)}\,\frac{e^{2\sqrt{\alpha'\mu(z-x)}}\,i\beta\frac{x}{r}}{(z-x)^{1/4}}dx \qquad \text{(B.5)}$$

$$+\ \mathcal{P}_o e^{i\beta}\,\frac{\alpha'}{2\sqrt{\pi}}\,\frac{e^{-\mu}}{(\alpha'\mu)^{1/4}}\left(\int_r^{\rho_1} + \int_{\rho_1}^z\right)e^{-(z-x)}\,\frac{e^{2\sqrt{\alpha'\mu(z-x)}}}{(z-x)^{1/4}}dx$$

$$+\ \alpha'\,\mathcal{P}_o e^{(\alpha'-1)\mu}e^{-z} +$$

$$+ \mathcal{P}_o \frac{\alpha'}{2\sqrt{\pi}}(\alpha' z)^{1/4} e^{-z} \left(\int_0^{\rho_2} + \int_{\rho_2}^{\mu}\right)$$

$$\cdot e^{-(\mu-z)} \frac{e^{2\sqrt{\alpha' z(\mu-\nu)}}}{(\mu-\nu)^{3/4}} e^{(\alpha'-1)\nu} d\nu$$

where ρ_1 and ρ_2 will be defined later but satisfy

$$\frac{\rho_1}{z} << 1, \qquad \frac{\rho_2}{\mu} << 1.$$

Now let us begin to evaluate these integrals. Let us begin by evaluating

$$\int_a^b e^{-(z-x)} \frac{e^{2\sqrt{\alpha' \mu(z-x)}}}{(z-x)^{1/4}} e^{icx} dx \tag{B.6}$$

which is the first integral in equation (B.5) for $a = 0$, $b = r$, and $c = \frac{\beta}{r}$. It is also the third integral for $a = r$, $b = \rho_1$, and $c = 0$. We have, in either case,

$$\frac{a}{z} << 1, \qquad \frac{b}{z} << 1.$$

This integral will be evaluated by lowest order expansion using the fact that $\frac{x}{z} << 1$ for $a \leq x \leq b$. Thus, equation (B.6) can be rewritten as

$$\frac{e^{-z}}{z^{1/4}}\int_a^b e^{(1+ic)x}\,\frac{e^{2\sqrt{\alpha'\mu z(1-\frac{x}{z})}}}{(1-\frac{x}{z})^{1/4}}dx.$$

Taking the first order expansions for $1-\frac{x}{z}$ we obtain

$$\frac{e^{-z}}{z^{1/4}}\int_a^b e^{(1+ic)x}e^{2\sqrt{\alpha'\mu z}(1-\frac{x}{2z})}(1+\frac{x}{4z})dx \qquad (B.7)$$

which is

$$\frac{e^{-z}e^{2\sqrt{\alpha'\mu z}}}{z^{1/4}}\int_a^b e^{(1+ic-\sqrt{\frac{\alpha'\mu}{z}})x}(1+\frac{x}{4z})dx.$$

Now to evaluate this integral to lowest order, neglect the $x/4z$ in the integrand. Then we obtain

$$\frac{e^{-z}e^{2\sqrt{\alpha'\mu z}}}{z^{1/4}}\,\frac{e^{(1+ic-\sqrt{\frac{\alpha'\mu}{z}})b}-e^{(1+ic-\sqrt{\frac{\alpha'\mu}{z}})a}}{1+ic-\sqrt{\frac{\alpha'\mu}{z}}}. \qquad (B.8)$$

Now let us evaluate the integral

$$\int_{\rho_I^-}^{z} e^{-(z-x)}\,\frac{e^{2\sqrt{\alpha'\mu(z-x)}}}{(z-x)^{1/4}}dx \qquad (B.9)$$

which is the third integral in equation (B.5). This integral will be evaluated by steepest descent. Replacing x by $z-x$ in equation (B.9) we obtain

$$\int_0^{z-\rho_1} e^{-x} \frac{e^{2\sqrt{\alpha'\mu x}}}{x^{1/4}} dx.$$

This is, by completing the square in the exponent,

$$e^{\alpha'\mu} \int_0^{z-\rho_1} \frac{e^{-(\sqrt{x}-\sqrt{\alpha'\mu})^2}}{x^{1/4}} dx.$$

Letting $s = \sqrt{\frac{x}{\alpha'\mu}} - 1$ we obtain

$$2(\alpha'\mu)^{3/4} e^{\alpha'\mu} \int_{-1}^{\sqrt{\frac{z-\rho_1}{\alpha'\mu}} - 1} e^{-\alpha'\mu s^2} \sqrt{s+1}\, ds. \qquad \text{(B.10)}$$

In order to evaluate this integral by steepest descent, we need to know the upper limit. We will delay evaluating this integral until we know what the upper bound should be.

Now let us evaluate this fourth integral in equation (B.5), namely

$$\int_0^{\rho_1} e^{-(\mu-\nu)} \frac{e^{2\sqrt{\alpha' z(\mu-\nu)}}}{(\mu-\nu)^{3/4}} e^{(\alpha'-1)\nu} d\nu. \qquad \text{(B.11)}$$

Again we will use lowest order expansions since $\nu/\mu << 1$ for $0 \leq \nu \leq \rho_1$. Thus, we obtain, similar to a previous integral,

$$\frac{e^{-\mu}}{\mu^{3/4}}\int_0^{\rho_1} e^{\alpha'\nu}\,\frac{e^{2\sqrt{\alpha' z\mu(1-\nu/\mu)}}}{(1-\nu/\mu)^{3/4}}d\nu \approx e^{2\sqrt{\alpha'\mu z}}\,\frac{e^{-\mu}}{\mu^{3/4}}\int_0^{\rho_1} e^{\alpha'(1-\sqrt{\frac{z}{\alpha'\mu}})\nu}\,d\nu \tag{B.12}$$

$$= e^{2\sqrt{\alpha'\mu z}}\,\frac{e^{-\mu}}{\mu^{3/4}}\,\frac{e^{\alpha'(1-\sqrt{\frac{z}{\alpha'\mu}})\rho_1}-1}{\alpha'(1-\sqrt{\frac{z}{\alpha'\mu}})}$$

Our final integral is

$$\int_{\rho_2}^{\mu} e^{-(\mu-\nu)}\,\frac{e^{2\sqrt{\alpha' z(\mu-\nu)}}}{(\mu-\nu)^{3/4}}e^{(\alpha'-1)\nu}d\nu, \tag{B.13}$$

which will also be evaluated by steepest descent. First, let us replace ν by $\mu - \nu$ in equation (B.13) to obtain

$$e^{(\alpha'-1)\mu}\int_0^{\mu-\rho_2} e^{-\alpha'\nu}\,\frac{e^{2\sqrt{\alpha' z\nu}}}{\nu^{3/4}}d\nu$$

$$= e^{(\alpha'-1)\mu}e^{z}\int_0^{\mu-\rho_2}\frac{e^{-(\sqrt{\alpha'\nu}-\sqrt{z})^2}}{\nu^{3/4}}d\nu.$$

Letting $s = \sqrt{\frac{\alpha'\nu}{z}} - 1$ we obtain

$$e^{(\alpha'-1)\mu}e^{z}2(\tfrac{z}{\alpha'})^{1/4}\int_{-1}^{\sqrt{\frac{\alpha'(\mu-\rho_2)}{z}}}\frac{e^{-zs^2}}{\sqrt{s+1}}ds. \tag{B.14}$$

Again this integral cannot be evaluated until the upper limit is known.

Let us now substitute into equation (B.5) the integrals we have evaluated, equations (B.8) and (B.12), and

the steepest descent integrals which we have left to evaluate, equations (B.10) and (B.14) to obtain

$$\mathcal{E}(\mu,z) \approx \frac{\mathcal{P}_o \alpha'}{2\sqrt{\pi}} \frac{e^{-\mu} e^{2\sqrt{\alpha'\mu z}} e^{-z}}{(\alpha'\mu z)^{1/4}} \left[\frac{e^{(1+i\frac{\beta}{r} - \sqrt{\frac{\alpha'\mu}{z}})r} - 1}{1+i\frac{\beta}{r} - \sqrt{\frac{\alpha'\mu}{z}}} \right.$$

$$\left. + e^{i\beta} \frac{e^{(1-\sqrt{\frac{\alpha'\mu}{z}})\rho_1} - e^{(1-\sqrt{\frac{\alpha'\mu}{z}})r}}{1-\sqrt{\frac{\alpha'\mu}{z}}} \right] \qquad \text{(B.15)}$$

$$+ \frac{\mathcal{P}_o e^{i\beta} \alpha' \sqrt{\alpha'\mu}}{\sqrt{\pi}} e^{(\alpha'-1)\mu} \int_{-1}^{\sqrt{\frac{z-\rho_1}{\alpha'\mu}} - 1} e^{-\alpha'\mu s^2} \sqrt{s+1}\, ds$$

$$+ \alpha' \mathcal{P}_o e^{(\alpha'-1)\mu} e^{-z}$$

$$+ \frac{\mathcal{P}_o \alpha'}{2\sqrt{\pi}} \frac{z^{1/4}}{(\alpha'\mu)^{3/4}} e^{-z} e^{-\mu} e^{2\sqrt{\alpha'\mu z}} \frac{e^{\alpha'(1-\sqrt{\frac{z}{\alpha'\mu}})\rho_2} - 1}{1-\sqrt{\frac{z}{\alpha'\mu}}}$$

$$+ \frac{\mathcal{P}_o \alpha'}{\sqrt{\pi}} e^{(\alpha'-1)\mu} \sqrt{z} \int_{-1}^{\sqrt{\frac{\alpha'(\mu-\rho_2)}{z}} - 1} \frac{e^{-zs^2}}{\sqrt{s+1}} ds.$$

In order to determine the upper limits of the two integrals in equation (B.13), let us simplify the equation by setting $r = \rho_1 = \rho_2 = 0$. Then we obtain

$$\mathcal{E}(\mu,z) = \frac{\alpha' \mathcal{P}_o}{\sqrt{\pi}} e^{(\alpha'-1)\mu} [\sqrt{\pi} e^{-z} + e^{i\beta\sqrt{\alpha'\mu}} \int_{-1}^{\sqrt{\frac{z}{\alpha'\mu}} - 1}$$

$$\cdot e^{-\alpha\mu s^2} \sqrt{s+1}\, ds + \sqrt{z} \int_{-1}^{\sqrt{\frac{\alpha'\mu}{z}} - 1} \frac{e^{-zs^2}}{\sqrt{s+1}} ds]. \qquad (B.16)$$

Recall that the phase wave is largest when $\theta_{\mathcal{E}}$ and $\theta_{\mathcal{P}}$ are both changing rapidly, i.e., when $\theta_{\mathcal{E}}$ and $\theta_{\mathcal{P}}$ are near $\beta/2$ (see Figures 5.2 and 5.3). Notice in equation (B.16) that the first integral has phase β and the second integral has phase 0. Thus, for the phase of $\mathcal{E}$ to be near $\beta/2$, we want both integrals to have approximately the same magnitude. This requires that $\frac{\alpha'\mu}{z} \approx 1$.

Thus, let μ_o be fixed and let $z = \alpha'\mu_o$ so that z is fixed. We wish to find $\mathcal{E}(\mu,z)$ for μ near μ_o so let $\mu = \mu_o + \epsilon$ where $\frac{|\epsilon|}{\mu_o} << 1$. Now we only keep terms to order ϵ and r and ignore $O(\epsilon\frac{\epsilon}{\mu_o})$ and $O(r\frac{\epsilon}{\mu_o})$.

Let us return to the equation for $\mathcal{E}(\mu,z)$, equation (B.15). In order to carry out the two remaining integrals we would like the upper limit of integration to be zero. This is where the slopes of the argument of the exponents, $-\alpha\mu s^2$ and $-zs^2$, are zero. (This is indeed why ρ_1 and ρ_2 were inserted in equation (B.5).) Thus we require that $\rho_1 = -\alpha'\epsilon$, $\rho_2 = \epsilon$ and thus $\frac{|\rho_1|}{z} << 1$ and $\frac{|\rho_2|}{z} << 1$ as was assumed previously. Then our integrals can be evaluated as follows:

$$\int_{-1}^{0} e^{-\alpha'\mu_o s^2}\sqrt{s+1}\,ds = \frac{1}{2}\left(\sqrt{\frac{\pi}{\alpha'\mu_o}} - \frac{1}{2\alpha'\mu_o}\right) + O((\alpha'\mu_o)^{-3/2})$$

$$\int_{-1}^{0} \frac{e^{-\alpha'\mu_o s^2}}{\sqrt{s+1}}\,ds = \frac{1}{2}\left(\sqrt{\frac{\pi}{\alpha'\mu_o}} + \frac{1}{2\alpha'\mu_o}\right) + O((\alpha'\mu_o)^{-3/2}). \qquad (B.17)$$

Before substituting these expressions into equation (B.15), let us mention one final point. In all the terms where the integral has already been evaluated we have the term

$$e^{-\mu} e^{2\sqrt{\alpha'\mu z}} e^{-z} = e^{(\alpha'-1)\mu} e^{-(\sqrt{\alpha'\mu}-\sqrt{z})^2}.$$

Substituting in $z = \alpha'\mu_o$, $\mu = \mu_o + \epsilon$ we find that

$$e^{-(\sqrt{\alpha'\mu}-\sqrt{z})^2} \approx e^{-\frac{\alpha'}{4}\epsilon\left(\frac{\epsilon}{\mu_o}\right)}$$

and this will be ignored since it is of higher order than we are considering. Now, substituting equation (B.17) into equation (B.15) we obtain

$$\mathcal{G}(\mu,z) \approx \frac{\alpha'}{2} e^{(\alpha'-1)\mu}\left[e^{i\beta}\left(1 - \frac{1+2(r+\alpha'\epsilon)}{2\sqrt{\pi}\sqrt{\alpha'\mu_o}} + \frac{1}{\sqrt{\pi}\sqrt{\alpha'\mu_o}}\,\frac{e^{i\beta}-1}{i\beta/r}\right.\right.$$

$$\left.\left. + \left(1 + \frac{1+2\alpha'\epsilon}{2\sqrt{\pi}\sqrt{\alpha'\mu_o}}\right)\right] \mathcal{P}_o.$$

This can be written as

$$\mathcal{E}(\mu,z) = \mathcal{P}_o \frac{\alpha'}{2} e^{(\alpha'-1)\mu} e^{i\beta/2} [\{(2 - \frac{r}{\sqrt{\pi}\sqrt{\alpha'\mu}}) \cos \beta/2 + \frac{r}{\sqrt{\pi}\sqrt{\alpha'\mu}} \frac{\sin \beta/2}{\beta/2}\} - i(\frac{1+2\alpha'\epsilon+r}{\sqrt{\pi}\sqrt{\alpha'\mu}}) \sin \beta/2]. \tag{B.18}$$

Using the same techniques we find

$$\mathcal{P}(\mu,z) = \frac{\mathcal{P}_o}{2} e^{(\alpha'-1)\mu} e^{i\beta/2} [\{(2 - \frac{r}{\sqrt{\pi}\sqrt{\alpha'\mu}}) \cos \beta/2 + \frac{r}{\sqrt{\pi}\sqrt{\alpha'\mu}} \frac{\sin \beta/2}{\beta/2}\} - i(\frac{-1+2\alpha'\epsilon+r}{\sqrt{\pi}\sqrt{\alpha'\mu}}) \sin \beta/2]. \tag{B.19}$$

(Notice that the phase of $\mathcal{E}$ is $\beta/2$ when $1 + 2\alpha'\epsilon + r = 0$ and the phase of $\mathcal{P}$ is $\beta/2$ when $-1 + 2\alpha'\epsilon + r = 0$. Thus $\theta_{\mathcal{P}}$ lags behind $\theta_{\mathcal{E}}$ in time by $(r + 1)\alpha'$.)

Rewriting equation (B.18),

$$\frac{e^{-i\beta/2}\,\mathcal{E}(\mu,z)}{\frac{\alpha'\,\mathcal{P}_o}{2} e^{(\alpha'-1)\mu}} = (2 - \frac{r}{\sqrt{\pi}\sqrt{\alpha'\mu}}) \cos \beta/2 + \frac{r}{\sqrt{\pi}\sqrt{\alpha'\mu}} \frac{\sin \beta/2}{\beta/2} - i\frac{1+2\alpha'\epsilon+r}{\sqrt{\pi}\sqrt{\alpha'\mu}} \sin \beta/2, \tag{B.20}$$

we see that the phase of $e^{-\beta/2}\mathcal{E}$ is in $(-\frac{\pi}{2},\frac{\pi}{2})$ if the real part of equation (B.20) is positive. If the real part is negative then the phase will be in $(\frac{\pi}{2},\frac{3\pi}{2})$. Thus, the phase of $\mathcal{E}$ is

$$\theta_{\mathscr{E}} = \frac{\beta}{2} - \arctan\left(\frac{(1+2\alpha'\epsilon+r)\tan\ \beta/2}{2\sqrt{\pi}\sqrt{\alpha'\mu}-r+r\frac{\tan\ \beta/2}{\beta/2}}\right) \qquad (B.21)$$

if the real part of equation (B.20) is positive. If the real part is negative, we replace $\frac{\beta}{2}$ by $\frac{\beta}{2} + \pi$.

Concentrating on the phase of $\mathscr{E}$, equation (B.21), we note that $\theta_{\mathscr{E}}$ goes from $\frac{\beta}{2} + \frac{\pi}{2}$ to $\frac{\beta}{2} - \frac{\pi}{2}$ instead of from β to 0. Thus, out in the wings equation (B.21) is inaccurate. However we emphasize that, for small ϵ, it is a good approximation. From comparisons with the numerical computations, equation (B.21) is accurate to $\sim$2% for small ϵ. The phase of $\mathscr{P}$ is

$$\theta_{\mathscr{P}} = \frac{\beta}{2} - \arctan\left(\frac{(-1+2\alpha'\epsilon+r)\tan\ \beta/2}{2\sqrt{\pi}\sqrt{\alpha'\mu_o}-r+r\frac{\tan\ \beta/2}{\beta/2}}\right) \qquad (B.22)$$

If the real part of equation (B.20) is positive, and, again, π must be added if it is negative. Finally, to calculate the phase wave, $\phi = \theta_{\mathscr{P}} - \theta_{\mathscr{E}}$, we subtract equation (B.22) from equation (B.21) and obtain equation (6.2), where we let $z - z_o = \alpha'\mu_o$ and $\alpha'\epsilon = \alpha'(\mu - \mu_o) = \alpha'\mu - (z - z_o)$.

Although the analytical expressions for $\theta_{\mathscr{P}}$ and $\theta_{\mathscr{E}}$ are inaccurate for large ϵ, the analytical expression for ϕ, equation (6.2), is accurate for all ϵ. This occurs because the values of $\theta_{\mathscr{P}}$ and $\theta_{\mathscr{E}}$ are approaching $\frac{\beta}{2} \pm \frac{\pi}{2}$ out in the wings of the phase wave and so $\phi = \theta_{\mathscr{P}} - \theta_{\mathscr{E}}$

is near zero. Thus the errors are cancelling out. We emphasize that, although the absolute error is small out in the wings of the phase wave, the relative error is not. Thus the relative error of the analytical expression for the phase wave is $\sim 3\%$ in the main body of the pulse. Out in the wings the relative error is very large ($\sim 100\%$) although the absolute error is small ($\sim 3\%$ of the maximum height of the phase wave). This large relative error out in the wings will become important in Chapter 7.

Note in equation (6.2) that $\phi \equiv 0$ when $\beta = 360°$. This occurs both because the phase wave decreases rapidly once the "flip-flop" occurs and also because we have only considered lowest order effects. Thus we see that, for $\beta \gtrsim 360°$, equation (6.2) is only valid for z large enough that the "flip-flop" has already occurred. Although it is possible to keep higher order terms in the calculation of the phase wave, we emphasize that this would make the analytical expression for the phase wave completely unmanagable and would not significantly improve our results.

REFERENCES

Abramowitz, Milton, and Irene A. Stegun, Handbook of Mathematical Functions, Dover Publications, Inc., New York (1972).

Allen, L., and J. H. Eberly, Optical Resonance and Two-level Atoms, Wiley, New York (1975).

Arecchi, F. T., and R. Bonifacio, IEEE J. Quantum Elect. QE-1, 169 (1965).

Armstrong, J. A., and E. Courtens, IEEE J. Quantum Elect. QE-4, 411 (1968).

Armstrong, J. A., and E. Courtens, IEEE J. Quantum Elect. QE-5, 249 (1969).

Banfi, G., and R. Bonifacio, Phys. Rev. Lett. 33, 1259 (1974).

Bonifacio, R., F. A. Hopf, P. Meystre, and M. O. Scully, Phys. Rev. A 12, 2568 (1975).

Bonifacio, R., D. M. Kim, and M. O. Scully, Phys. Rev. 187, 441 (1969).

Bonifacio, R., P. Schwendimann, and F. Haake, Phys. Rev. A 4, 302, 854 (1971).

Bowden, C. M., D. W. Howgate, and H. R. Robl, ed., Co-operative Effects in Matter and Radiation, Plenum Press, New York (1977).

Degiorgio, V., Opt. Comm. 2, 362 (1971).

Dicke, R. H., Phys. Rev. 93, 99 (1954).

Ehrlich, J. J., C. M. Bowden, D. W. Howgate, G. H. Sehnick, A. T. Rosenberger, and T. A. DeTemple in Proceedings of the Fourth Rochester Conference on Coherence and Quantum Optics, ed. by L. Mandel and F. Wolf, Plenum Press, New York (1978).

Harvey, A. F., Coherent Light, Wiley, New York (1970).

Hopf, F. A., Ph. D. Dissertation, Yale University (1968).

Hopf, F. A., and P. Meystre, Phys. Rev. A 12, 2534 (1975).

Hopf, F., P. Meystre, and D. W. McLaughlin, Phys. Rev. A 13, 777 (1976).

Hopf, F. A., P. Meystre, M. O. Scully, and J. F. Seeley, Phys. Rev. Lett. 35, 511 (1975).

Hopf, F. A., and M. O. Scully, Phys. Rev. 179, 399 (1969).

Icsevgi, A., and W. E. Lamb, Jr., Phys. Rev. 185, 517 (1969).

Miller, K. S., Complex Stochastic Processes, Addison-Wesley, Reading, Mass. (1974).

Rehler, N., and J. H. Eberly, Phys. Rev. A 3, 1735 (1971).

Sargent, M., III, M. O. Scully, and W. E. Lamb, Jr., Laser Physics, Addison-Wesley, Reading, Mass. (1974).